Economic Geology, v. 120, no. 7, pp. 1605–1647

Economic Geology

BULLETIN OF THE SOCIETY OF ECONOMIC GEOLOGISTS

VOL. 120 November NO. 7

Microplate Solutions to Crustal Growth and Metal Endowment in Modern Back-Arc Basins and Ancient Greenstone Belts

Mark Hannington,[1,†] Alan Baxter,[1] Erin Bethell,[1] Christopher Galley,[1] Marc Fassbender,[1] Margaret Stewart,[2] Patrick Mercier-Langevin,[3,*] Anna Krätschell,[4] Sven Petersen,[4] and Philipp Brandl[4]

[1] *University of Ottawa, 25 Templeton St., Ottawa, Ontario K1N 6N5, Canada*

[2] *Mount Royal University, 4825 Mt. Royal Gate SW, Calgary, Alberta T3E 6K6, Canada*

[3] *Geological Survey of Canada, 490 rue de la Couronne, Quebec G1K 9A9, Canada*

[4] *GEOMAR Helmholtz Centre for Ocean Research Kiel, Wischhofstr. 1-3, 24148 Kiel, Germany*

Abstract

Ore formation throughout Earth's history has tracked major pulses of crustal growth. The spectacular endowment of some greenstone belts, in particular, has been linked to high heat flow and extensive Archean rifting. Three aspects were likely important: (1) greater numbers of plates required to dissipate the heat; (2) abundant crustal-scale transcurrent faults to accommodate plate growth; and (3) increased hydrothermal convection to cool the crust at the plate boundaries. Because the plates were smaller and more numerous than today, the total ridge length was greater, thus allowing for more efficient cooling of the newly formed crust. Mantle upwelling and rifting between microplate domains focused melts and fluids into well-mineralized corridors. This tectonic style is observed today at the Indo-Australian margin, providing clues to the crustal architecture of some well-endowed Archean terranes, such as the Abitibi greenstone belt in the Superior province of Canada.

Hot, thickened oceanic crust, like that of the modern Lau basin and North Fiji basin, has strong similarities to mineral-rich greenstone belts like the Abitibi in terms of structure, kinematics, and magmatic evolution. The majority of this crust formed during a basin-wide microplate "breakout" that occurred in response to the collision of Australia with the Ontong Java and Melanesian Border plateaus in the Late Miocene. Today, the back-arc basins contain some of the fastest growing crust on Earth and an extraordinary concentration of magmatic and hydrothermal activity. In the northern Lau basin, at least seven distinct microplates formed within the last 5 m.y., with crustal growth partitioned across numerous simultaneously active plate boundaries in a complex microplate mosaic. The plates are bound by active spreading centers, ridges, and shear zones that are continuously deforming in response to plate rotation. Basin opening is dominated by many short, slow-spreading segments between large-scale transcurrent fault zones, with a combined strike length of spreading centers greater than in any other back-arc basin in the western Pacific. Seismic sections to depths of at least 20 km show that the plate boundaries are broad zones of deformation characterized by overlapping spreading centers, ridge jumps, and extensional transforms. Increased crustal permeability occurs where multiple spreading centers intersect (i.e., at triple junctions) with enhanced magmatic and hydrothermal activity at the plate boundaries. Seismic velocities and volcanic geochemistry also show large variations in crustal composition between the plates, indicating that the back-arc region is far more complex than supposed in earlier models.

We suggest crustal growth and mineral endowment in some greenstone belts were similarly regulated by microplate formation. Because the microplates behave independently, often at great distances from the nearest subduction zone, their formation is akin to autochthonous growth in the Archean when subduction-zone processes were either absent or in their infancy. Compelling evidence of this architecture is now being revealed in the Abitibi greenstone belt by modeling of the Archean Moho topography.

Introduction

The geodynamic underpinnings of large-scale mineral systems and regional metal endowment are fundamentally linked to crustal growth (e.g., Huston et al., 2010, 2016). The

[†]Corresponding author: e-mail, Mark.Hannington@uottawa.ca

[*]Current address: Agnico Eagle Mines Limited, 145 King St. East, Toronto, Ontario M5C 2Y7, Canada.

ISSN 0361-0128; doi:10.5382/econgeo.5195; 43 p.

Submitted: September 24, 2024/Accepted: June 20, 2025

Digital appendices are available in the online Supplements section.

key concepts were formulated in the 1980s (e.g., Sawkins, 1984, 1990), with explicit connections eventually established between different types of mineral deposits and tectonic processes at plate boundaries (Groves and Bierlein, 2007; Wilkinson and Kesler, 2009; Cawood and Hawkesworth, 2015; Huston et al., 2023). However, correlating metallogenic events to specific plate dynamics has been challenging, even in the best-studied systems (e.g., Blundell, 2002; Craw et al., 2002; Garwin et al., 2005; Rowland and Simmons, 2012; among many others). One reason is that the models of crustal growth are often at a very broad scale, involving only the major plates—too large to be of much use in predicting the locations of ore deposits (e.g., Fig. 1). New research is providing a far more detailed view of the plate boundaries and presenting testable hypotheses about the relationship between mineral endowment and crustal growth in both modern and ancient settings. Within the last decade, growing numbers of microplates have been revealed in high-resolution digital elevation models (DEMs), both on land and in the oceans (e.g., Bird, 2003; Argus et al., 2011; Harrison, 2016; Hasterok et al., 2022; Li et al., 2018; Liu et al., 2023). Few anticipated the complexity of the microplate mosaics that are now recognized. One of the most important episodes of microplate formation is still occurring today along the sawtooth margin of the Indo-Australian plate (Fig. 2), where a new continent is emerging (Baldwin et al., 2012). Major Cenozoic (especially Neogene) collisions are massively affecting the crust in this region, causing a modern-day microplate breakout. It includes some of the fastest growing crust on Earth and is the location of an extraordinary concentration of mineral resources on land and in the sea (Garwin et al., 2005; Sillitoe, 2010).

In this paper, we examine the present-day oceanic microplate mosaic at the Indo-Australian margin and show (1) how pulses of crustal growth occur by accretion at sea-floor spreading centers during microplate breakouts, (2) how microplate structures become the pathways for melts and fluids, (3) the role of the mantle in microplate development, and (4) how these conditions can be recognized in ancient systems. The short duration of microplate formation (e.g., in some cases within the error bars of magnetic polarity reversals) requires that they be studied in a neotectonic framework where plate adjustments are still occurring and where it is still possible to correlate specific magmatic and hydrothermal events to active microplate evolution. This analysis starts with a geologic map where increments of crustal growth can be measured in terms of area-age relationships of different formations and assemblages. However, until recently, the best geologic maps of the oceans have been at scales of 1:25 million to 1:17 mil-

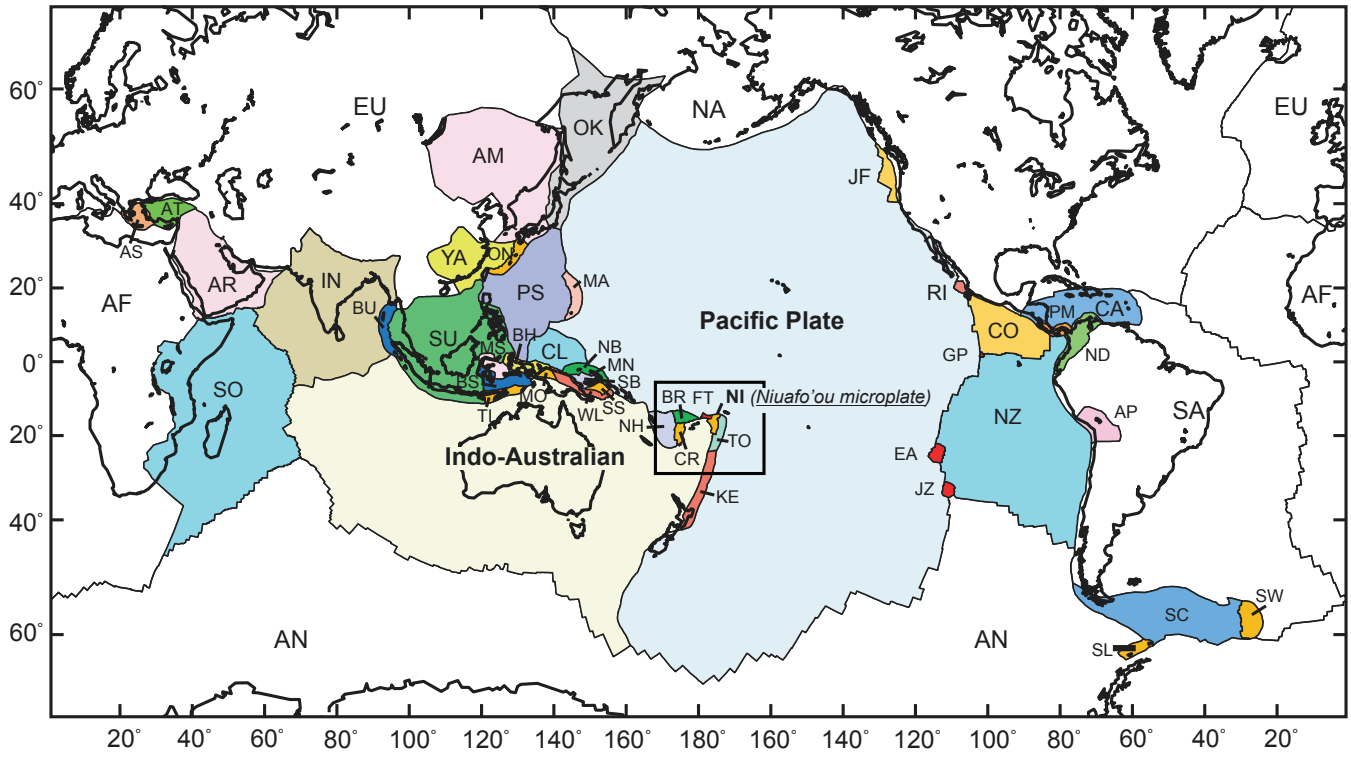

Fig. 1. Global distribution of tectonic plates modified from Bird (2003). The Bird model of 52 plates includes 35 located at the Indo-Australian margin. The study area (NI, Niuafo'ou microplate) is indicated. Minor and "micro"plates are shown in contrasting colors; major plates are not colored. Abbreviations: AF = Africa, AM = Amur, AN = Antarctica, AP = Altiplano, AR = Arabia, AS = Aegean Sea, AT = Anatolia, AU = Australia, BH = Birds Head, BR = Balmoral Reef, BS = Banda Sea, BU = Burma, CA = Caribbean, CL = Caroline, CO = Cocos, CR = Conway Reef, EA = Easter, EU = Eurasia, FT = Futuna, GP = Galapagos, IN = India, JF = Juan de Fuca, JZ = Juan Fernandez, KE = Kermadec, MA = Mariana, MN = Manus, MO = Maoke, MS = Molucca Sea, NA = North America, NB = North Bismarck, ND = North Andes, NH = New Hebrides, NI = Niuafo'ou, NZ = Nazca, OK = Okhotsk, ON = Okinawa, PA = Pacific, PM = Panama, PS = Philippine Sea, RI = Rivera, SA = South America, SB = South Bismarck, SC = Scotia, SL = Shetland, SO = Somalia, SS = Solomon Sea, SU = Sunda, SW = Sandwich, TI = Timor, TO = Tonga, WL = Woodlark, YA = Yangtze.

lion (e.g., Scheibner et al., 2013; Harris et al., 2014). They show large tectonic features, thousands of kilometers in size, but give a very limited view of microplates. At the same time, the most sophisticated geochronological information, derived from magnetic anomaly data (Mueller et al., 2016; Seton et al., 2020), provides only a patchwork of ages that are gridded at large intervals, thus only recording major tectonic events. This has meant considerable uncertainty about crustal growth where smaller plates dominate and where release of crustal fluids may happen in just a fraction of the resolvable time. These features can be studied in the active Lau back-arc basin, which is at the epicenter of runaway crustal growth at the Indo-Australian margin and bears a strong resemblance to some ancient greenstone belts. We compare this modern example to the Abitibi greenstone belt in the southern Superior province of Canada, which is the largest and best-preserved greenstone belt in the world. Although it remains a matter of debate whether modern-style tectonics figured in early Archean greenstone belts, processes such as plate fragmentation and microplate formation very likely played a role in controlling crustal permeability and heat flow regardless of the particular tectonic regime.

Crustal Growth and Mineral Endowment: A Role for Microplates

The major pulses of ore formation in Earth's history are directly linked to the supercontinent cycles (Barley and Groves, 1992; Groves and Bierlein, 2007; Cawood and Hawkesworth, 2015). However, the relationship to crustal growth is not always precisely known because the episodes of accretion may span hundreds of millions of years (e.g., Hawkesworth et al., 2013; Huston et al., 2014, 2016). This contrasts with the relatively short time scales of even the largest ore-forming systems. Most volcanogenic massive sulfide (VMS) deposits formed during peaks of crustal growth at 2700, 1900, and after 500 Ma (Fig. 3), but individual episodes of ore formation, even at a district scale, may have lasted only a few millions of years (e.g., Franklin et al., 2005; McNicoll et al., 2014). Predicting where and when the ore deposits formed depends on recognizing these relatively short pulses of growth within a much larger plate tectonic framework.

In the modern oceans, establishing the full extent of crustal growth and hydrothermal activity has depended on a rigorous accounting of the plate boundaries (Beaulieu et al., 2013). Hy-

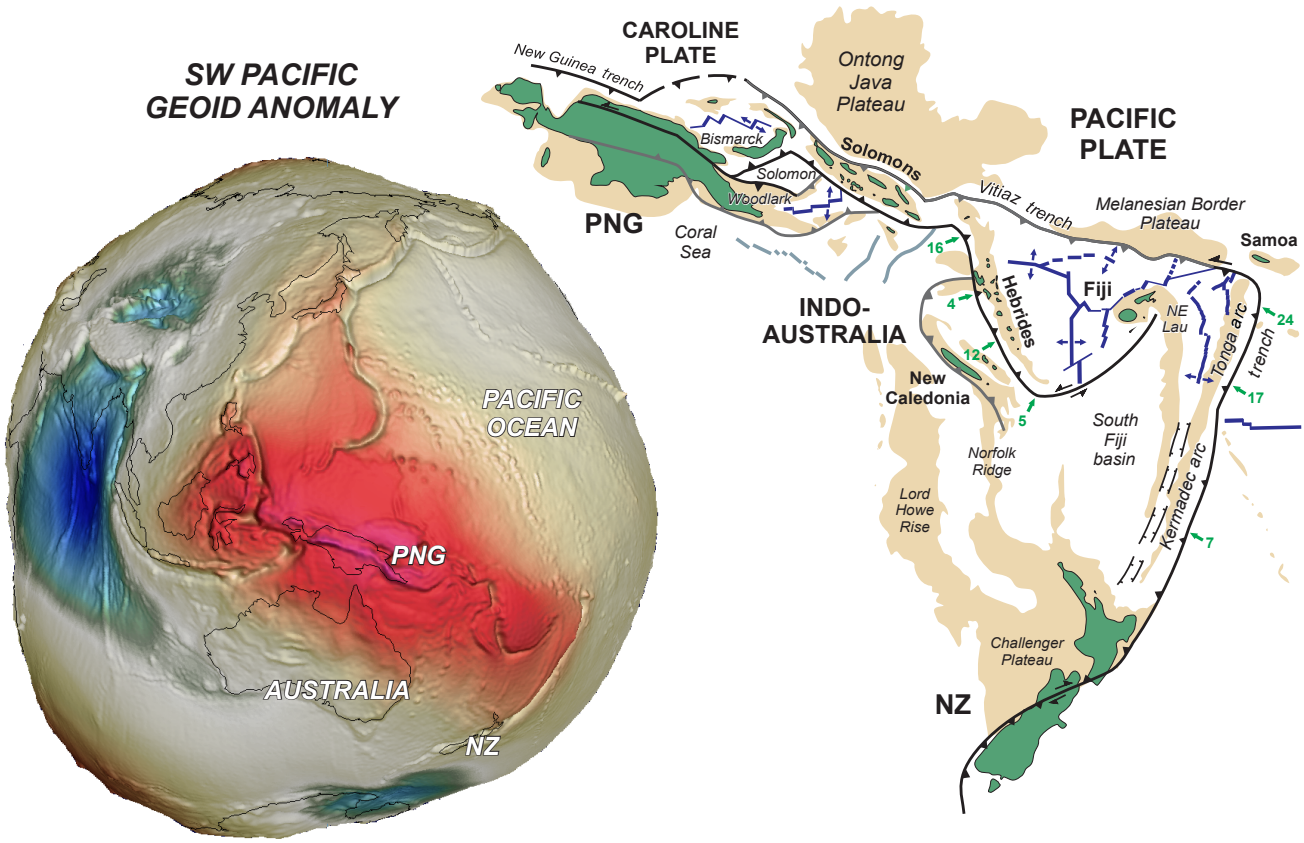

Fig. 2. Southwest Pacific geoid anomaly from the GRACE satellite gravity model of Barthelmes and Köhler (2012) and the Deutsches Geoforschungzentrum (GFZ) Potsdam International Centre for Global Earth Models (Ince et al., 2019). The geoid heights are calculated from the EIGEN-64 gravity field model. Colors represent height above and below the global ellipsoid (red, +88-m maximum; blue, –100-m maximum). The large positive anomaly at the boundary between the Pacific and Indo-Australian plates reflects anomalous crustal growth and high heat flow in this region. A simplified map shows the major tectonic features discussed in the text. Light brown (2,000-m isobath) corresponds to thickened crust, including possible continental crust (e.g., Mortimer et al., 2017). Blue lines are spreading centers; black and gray lines are active and inactive trenches. Green arrows show the motion of the Pacific Plate (cm/year). Abbreviations: NZ = New Zealand, PNG = Papua New Guinea.

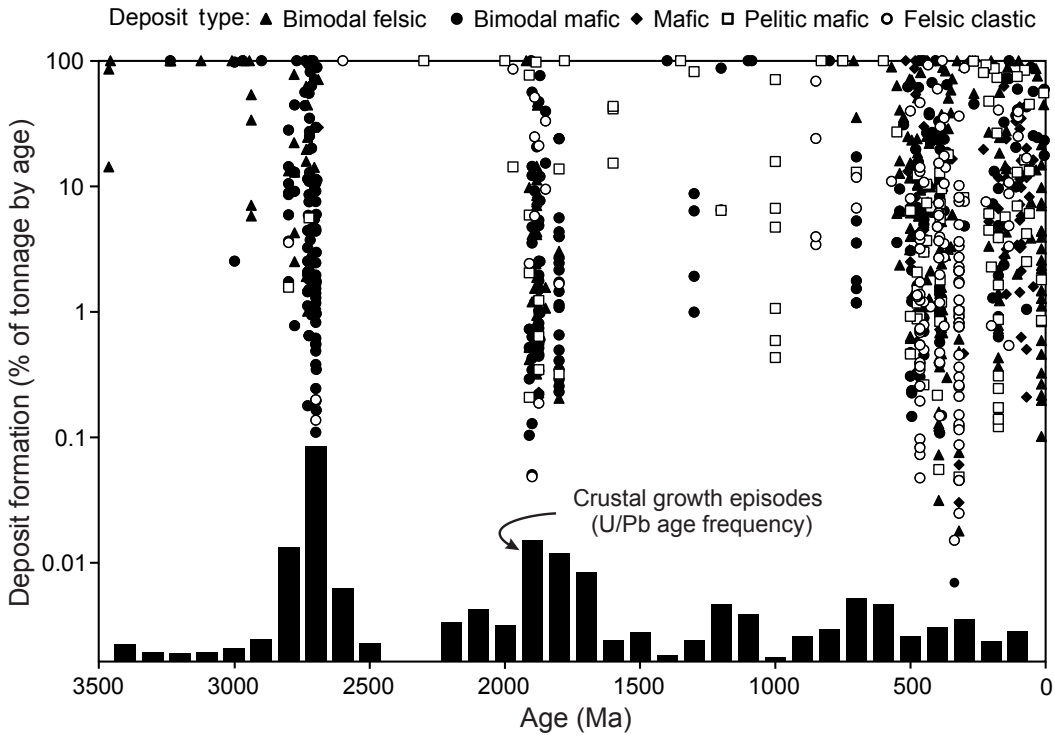

Fig. 3. Major episodes of formation of volcanogenic massive sulfide (VMS) deposits worldwide in comparison to crustal growth. The data points represent individual deposits plotted according to size (as a percentage of the total tonnage of VMS at each time interval). Age data and deposit tonnages are from Franklin et al. (2005), Mosier et al. (2009), and Huston et al. (2010). The different symbols refer to the classification of deposits by host rock type (see Barrie and Hannington, 1999). Crustal growth is represented by the frequency (not scaled) of zircon crystallization ages from Condie (1998). VMS formation was strongly correlated with pulses of crustal growth at roughly 2700, 1900, and after 500 Ma. However, most episodes of deposit formation occur at much shorter time scales of a few million years (compared to hundreds of m.y. for craton assembly: Condie et al., 2017; Huston et al., 2023).

drothermal convection is a fundamental process for removing the heat from newly formed oceanic crust (e.g., Lister, 1972, 1980), and so the majority of sea-floor hydrothermal vents occur at plate boundaries (Fig. 4). Likewise, ancient VMS deposits generally mark fossil rift systems that define the plate margins (e.g., Franklin et al., 2005). Because removal of heat at the plate boundaries is the major driver of ore formation, it stands to reason that the more plate boundaries there were, the more mineral deposits would have formed. This probably peaked in the Late Archean when high mantle geotherms would have required greater ridge lengths to dissipate the heat (e.g., Mallard et al., 2016). One solution to the effective removal of that heat is if the early Earth was covered by many small plates (e.g., Fig. 5). Smaller and more numerous plates equate to much greater total ridge length and therefore more efficient cooling of the crust. Significant pulses of crustal growth likely resulted from distributed extension across many plate boundaries that, on average, would have been spreading much more slowly than today (see below). Both conditions—greater ridge length and slow spreading—would have contributed to enhanced hydrothermal activity and mineral endowment as observed at modern ridges (Hannington et al., 2005, 2011).

Origins of Oceanic Microplates

At certain scales, accretion of new oceanic lithosphere at sea-floor spreading centers is a highly irregular process, involving propagation of ridges, ridge jumps, and transfer of crust from one plate to another (Hey, 1977; Searle and Escartin, 2013; Karson, 2017). New crust is commonly trapped between spreading centers, becoming increasingly deformed as the plates rotate and ridges propagate. The resulting microplates consist of new oceanic crust formed at the spreading centers as well as captured lithosphere from plate fragmentation (Mammerickx and Klitgord, 1982; Matthews et al., 2016). Examples of these processes at oceanic microplates are abundant throughout the eastern Pacific today (e.g., Easter Island, Juan Fernandez, Galapagos).

Bird (2003) defined microplates as small, mostly rigid areas of lithosphere that are located at major plate boundaries but behave as independent plates. In his compilation, the microplates have a maximum size of 1 million square kilometers (1,000 × 1,000 km), but plates of this size are almost always surrounded by much smaller plate fragments, some less than 100 km across. Conder and Wiens (2011) coined the term "nanoplate" to describe the smaller plate fragments (<100,000 km^2) and showed how they accommodate strain in complicated microplate systems. Whereas the boundaries of the major plates are mostly known from global seismicity, the microplates have been brought into focus by advances in satellite altimetry and derived gravity models (e.g., Sandwell et al., 2014; MacLeod et al., 2017).

Bird's (2003) model contains 52 plates (Fig. 1), but the numbers have been increasing. Argus et al. (2011) modeled

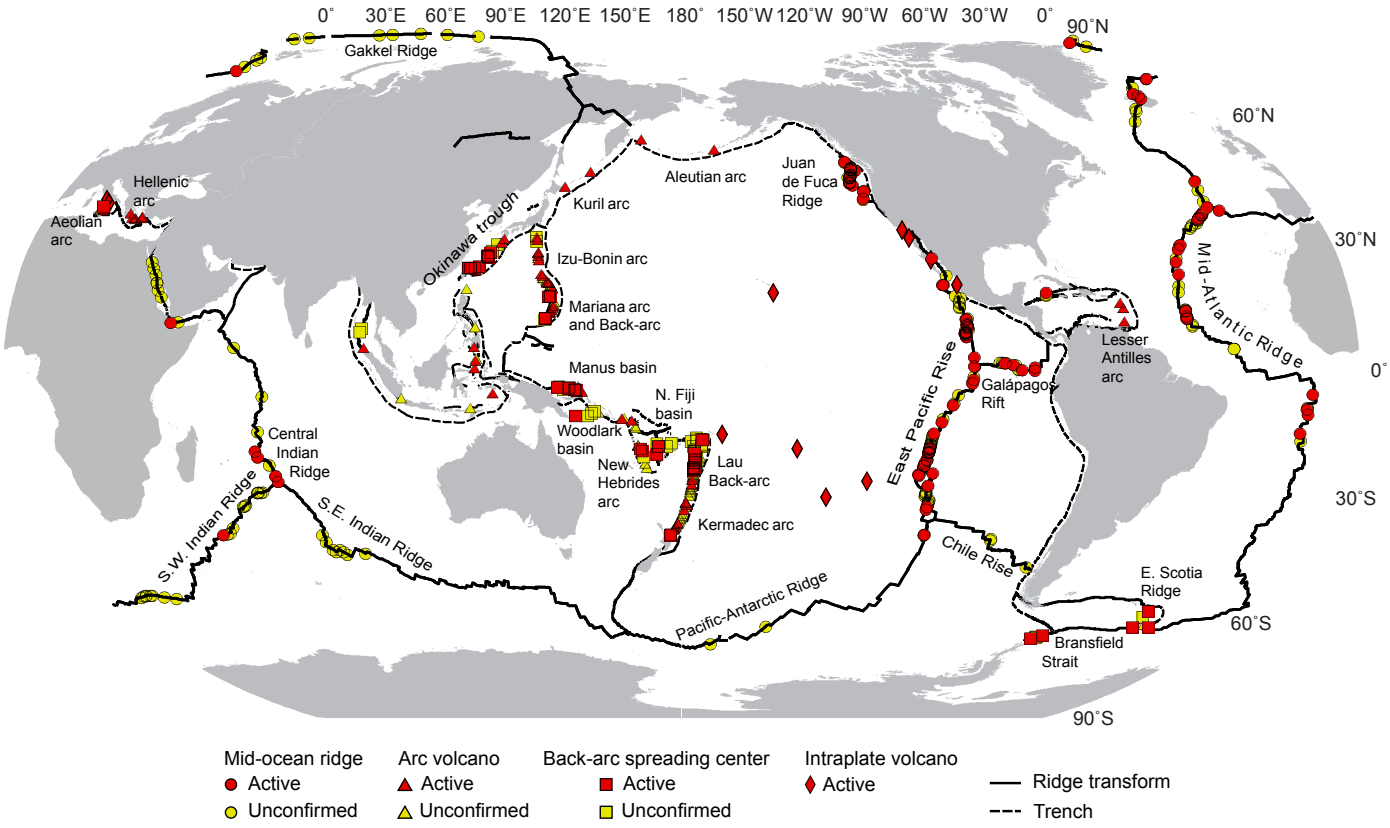

Fig. 4. Global distribution of modern sea-floor hydrothermal activity from Beaulieu et al. (2013), Beaulieu and Szafrański (2020), and the InterRidge database Ver 3.4 (www.interridge.org/irvents/). Seven hundred twenty sites are known globally: red symbols are confirmed sites, and yellow are inferred from remotely detected hydrothermal plumes. In almost every tectonic setting, the hydrothermal activity is restricted to the plate boundaries, including approximately 80,000 km of mid-ocean ridges and back-arc spreading centers. By comparison, an Archean Earth, with many more plates, could have had a total ridge length of ~500,000 km (e.g., Abbott and Menke, 1990) and many thousands of vent fields.

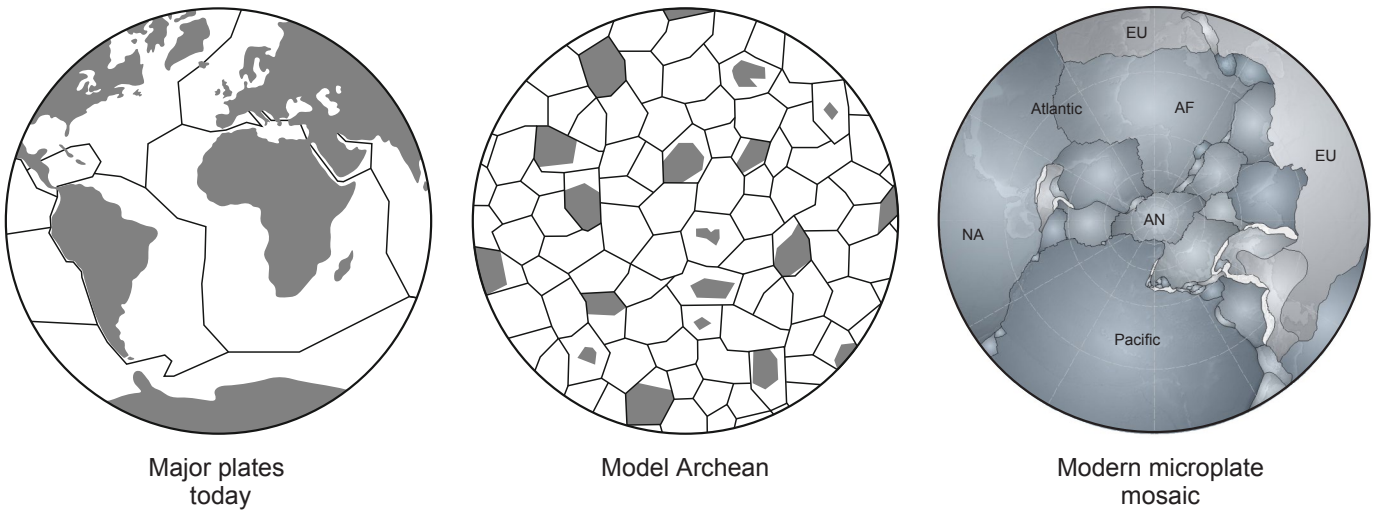

Fig. 5. Schematic illustration of a model Earth in the Archean with many more plates than today (from Martin and Pinti, 2011). To accommodate the high mantle geotherms, greater ridge lengths would have been required to dissipate the heat, resulting in smaller and more numerous plates. Microplate formation partitions heat across an increasing number of plate boundaries but may result in slower overall spreading rates (i.e., many short, slow-spreading segments rather than a few long, fast ridges; Pelletier et al., 1998). The image on the right shows the modern microplate mosaic at the Indo-Australian margin, displayed in an Antarctic polar stereographic projection.

56 plates, Harrison (2016) defined 159, and the compilation of Hasterok et al. (2022) contains 121, although most of the added plates are continental (e.g., Li et al., 2018; Liu et al., 2023). In the most recent global plate motion model, GPlates (www.gplates.org; see Mueller et al., 2016), there are now 435 closed polygons. These include both active microplates, with at least one boundary being an active spreading center, and structural blocks that lack evidence of recent crustal growth. Their numbers highlight the ubiquitous fragmentation of the upper crust, including the strong microplate fabric of the oceans.

A premise of modern plate tectonics is that the plates are rigid. However, detailed studies of today's oceanic microplates show that they are continuously deforming structures (Kreemer et al., 2014; Baxter et al., 2020). The deformation is caused by collisions, plate rotation, and reorganization of fault systems, often in response to stress relocation at distant plate margins (e.g., Collins, 2002; Wallace et al., 2005, 2009; Siddoway, 2010). Microplate mosaics are the dynamic substructure that accommodates the accumulated strain. For the most part, the deformation is concentrated in narrow domains at the edges of the plates (Kreemer et al., 2014; Mallard et al., 2016), which may include complex spreading networks, patchworks of orphaned crustal fragments, and shear zones. A common origin of microplates is reactivation of earlier extensional or compressional structures into free-slip boundaries (Matthews et al., 2016). These structures may be difficult to identify because of a lack of seismicity or distinctive bathymetric features marking the plate edges. However, vertical gravity gradient models have revealed large numbers of these cryptic boundaries, including complex networks of extinct spreading centers within older plates (Fig. 6; MacLeod et al., 2017).

Although most researchers recognize microplate breakouts as a consequence of changes in far-field stresses, some have argued that small-scale mantle convection (Faccenna et al., 2010) or more complex mantle-lithosphere interactions (Rey and Mueller, 2010; Mallard et al., 2016) are responsible. Mantle upwelling is commonly invoked (e.g., Mueller et al., 2001), although it is not always clear if microplate formation was caused by the rise of mantle into the plate boundaries or vice versa. Individual microplates may last for only a few million years before becoming incorporated into larger plates (Matthews et al., 2016), and some nanoplates have even shorter half-lives (Morra et al., 2013). In this way, microplate formation quickly approaches the time and space scales of melt and fluid release associated with ore formation. It also aligns with the concept of "tectonic switching" that is thought to have activated melt and fluid flow in large-scale mineral systems (e.g., Huston et al., 2016). Microplate formation is likely an important signal of these processes.

Introducing microplates into the geodynamic framework of a major plate boundary has a number of consequences (e.g., Badham and Halls, 1975; Coltice et al., 2012; Moresi et al., 2014). The plate fragmentation requires weakening of the lithosphere caused by melting and intrusion, reactivation of inherited structures, and stress concentration. Crustal thickness is likely a controlling factor, as the major structures generally scale with the thickness of the crust (e.g., Rowland et al., 2012) and thereby connect with discontinuities in the older, deeper basement. Strong asymmetries also typically develop, resulting in overlapping spreading centers, extensional transforms, and highly variable spreading rates. Here, we examine how microplate formation relates to crustal thickness, the nature of the crust just prior to plate fragmentation, the

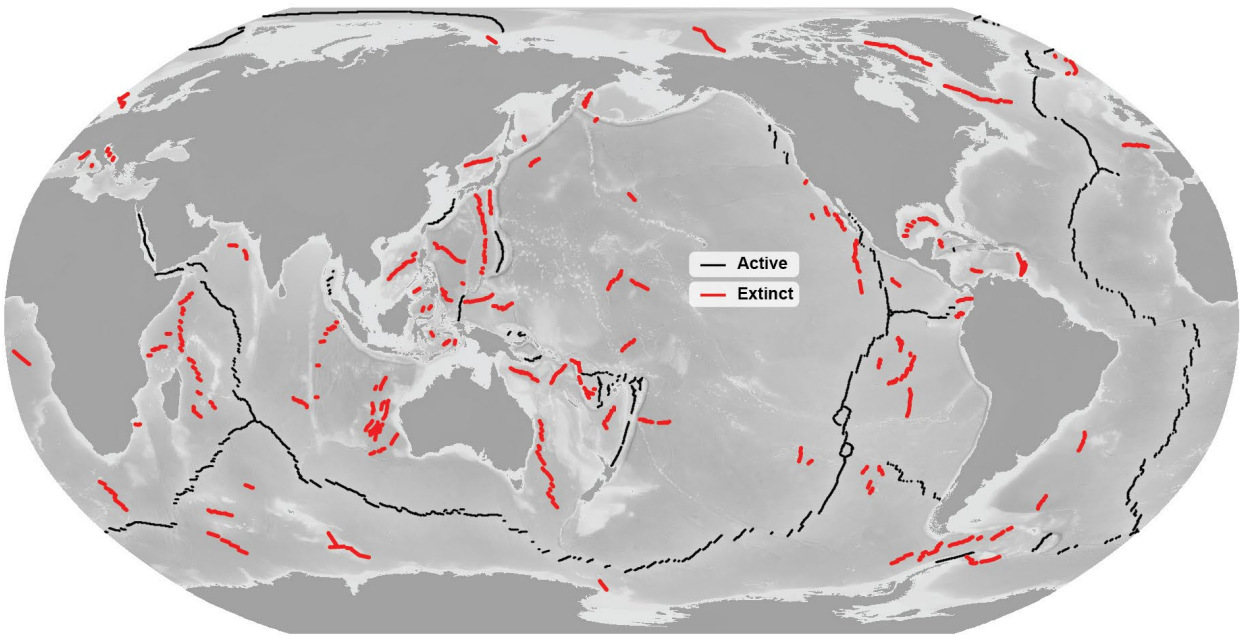

Fig. 6. Global vertical gravity gradient (VGG) grid of Sandwell et al. (2014), derived from CryoSat-2 and Jason-1 satellite altimetry (see text for description). Dark and light shading indicates steep positive and negative gradients in the gravity field corresponding to rises, depressions, and buried structures. Plate boundaries can be clearly seen in VGG, including extinct and buried ridges (modified after MacLeod et al., 2017). Fossil spreading centers shown as red lines total 42,000 km in strike length compared to active ridges in black. The large numbers of fossil spreading centers mark the boundaries of paleoplates (or plate fragments) that have been fused to younger plates.

different tectonic styles and links to basement structures, the composition of the microplate crust, and how microplates become part of larger plates.

The Miocene microplate breakout of the Indo-Australian margin

The northwest corner of the Indo-Australian margin comprises several large oceanic arc-back-arc systems and volcanic and sedimentary basins associated with westward subduction of the Pacific Plate (Ruellan and Lagabrielle, 2005; Schellart et al., 2006; Fig. 7). In the Middle to Late Miocene, the Ontong Java and Melanesian Border plateaus, large igneous provinces that formed in the central Pacific (Ratcliff et al., 1998), collided with the Australian margin and terminated Vitiaz subduction at ~12 Ma. This resulted in a large-scale subduction reversal (reestablishing in the New Hebrides), splitting of the former Vitiaz arc, and opening of the North Fiji and Lau basins (Ruellan et al., 2003; Ruellan and Lagabrielle, 2005; Seton et al., 2012; Martin, 2013). Microplate formation has since dominated the region. Owing to the structural complexity, and the fact that most of the resulting microplates are not yet part of Australia, it is not entirely clear where the boundary between the Indo-Australian and Pacific plates should be drawn (Ruellan and Lagabrielle, 2005; Lagabrielle et al., 1997).

The coevolution of the Lau and North Fiji basins fits the definition of a geologic province (e.g., Collot et al., 2011; Stewart et al., 2022), with a protracted, multistage tectonic history forming the building blocks of a Melanesian protocontinent, similar to the emerging continent Zealandia to the south (Mortimer et al., 2017). The entire region is characterized by thickened crust and the highest predicted mantle temperatures in the Pacific, which together offer the closest modern comparison to a hot Archean oceanic lithosphere (Fig. 8). In the Lau basin, in particular, seismic shear-wave velocities correspond to mantle temperatures of nearly 1,450°C (i.e., 150° to 200°C hotter than anywhere else in the western Pacific; Wiens et al., 2006). The high temperatures are thought to be related to an influx of mantle caused by the fast rollback of the Pacific Plate and also a lack of cooling by a shallow slab owing to the steepness of the subduction (Wiens et al., 2006).

This region also hosts some of the world's most important and youngest ore deposits, formed mainly within the last 5 m.y. They include at least three of the world's top 10 Cu and Au deposits and a number of other extraordinary mineral systems: Emperor in Fiji (epithermal Au), Panguna on Bougainville Island (porphyry Cu), Grasberg in Indonesia (porphyry Cu-Au), and Ladolam on Lihir Island (epithermal Au), to name a few. The first Cu-Au–rich massive sulfide deposits to be considered for sea-floor mining are also located in the Bismarck Sea, and submarine epithermal-style Au mineralization has been discovered offshore from Lihir. This remarkable concentration of metals owes its origin to well-established regional subduction zone processes, but the crucial connection to microplate tectonics is now also being established (e.g., Holm et al., 2016; Brandl et al., 2020).

Approaches and Methods

To investigate these features at a meaningful scale requires an unprecedented combination of technologies. The approach, including seismic reflection and refraction employed simultaneously with other geophysical and geochemical techniques, has been widely used to image craton boundaries in programs such as AuScope in Australia, Lithoprobe in Canada, Europrobe in Europe, and Metal Earth (e.g., Smith et al., 2023). This paper describes an application of this approach to the Indo-Australian margin in the Lau basin, directly comparable to crustal-scale geotraverses conducted on land (Fig. 9; Hannington et al., 2019). Except in the exploration for oil and gas, little coordinated research of this type has been carried out in the oceans. This project, which is an extension of Metal Earth, is aimed at the comparison of modern and ancient systems using the same integrated multiparameter geophysics, geochronology, and geochemistry. Readers familiar with Archean greenstone belts will recognize the nomenclature used in this comparison (provinces, subprovinces, and assemblages), which is applied here for the first time in a modern oceanic system.

After more than 50 research cruises since 1970, the Lau basin is one of the best-investigated regions of the deep ocean. The key geologic formations have been mapped based on crustal type, lithology, stratigraphic position, structure, magnetic character, spreading fabric, age, and sediment cover. This resulted in the first 1:1,000,000-scale compilation using techniques similar to those employed in remote predictive geologic mapping on land (Fig. 10; Stewart et al., 2022). The tipping point was the routine application of satellite altimetry (e.g., most recently the CryoSat-2 and Jason-1 missions: Sandwell et al., 2014; MacLeod et al., 2017) together with new scientific platforms for seabed mapping and sampling. These technologies have enabled recognition of many previously unidentifiable geologic features that are key parts of the microplate mosaic. The resolving power of satellite altimetry and gravity inversions is now at a point where features on the sea floor can be measured in kilometers rather than tens of kilometers, allowing critical structures to be identified. Previously unknown fabric has been revealed that clearly highlights the plate boundaries, and the corresponding structures have been verified with ship-based surveys.

In the northern Lau basin, Baxter et al. (2020) used global seismicity data (i.e., centroid moment tensors, CMTs) to identify major faults and their relative motions (Fig. 11A). Corresponding features on the sea floor were mapped from the vertical gravity gradient (VGG) with an average pixel size of ~5 km^2. Seamounts between 1 and 2 km in height were mapped throughout the study area, and buried structures (e.g., from spreading fabric; MacLeod et al., 2017) were also identified. The 2–arc-minute resolution Earth magnetic anomaly grid (EMAG2: Maus et al., 2009) was used to identify plate boundaries in areas where multibeam or other data were limited (Fig. 12). EMAG2 incorporates satellite, airborne, and marine magnetic measurements, compiled at a global scale, and can be used to identify regions of normal or reversed magnetic polarity that highlight spreading fabric and, locally, magmatic intrusions. Bouguer gravity anomalies from the Smith and Sandwell (1997) global gravity grid were used to help define assemblage boundaries outlined in Figure 10B. More detailed ship-based magnetic and gravity data from Hannington et al. (2019) were also employed (Fig. 13). From the global gravity grid and ship-based data, Galley et al. (2024) created the first well-constrained 3-D inversions of crustal thickness, which

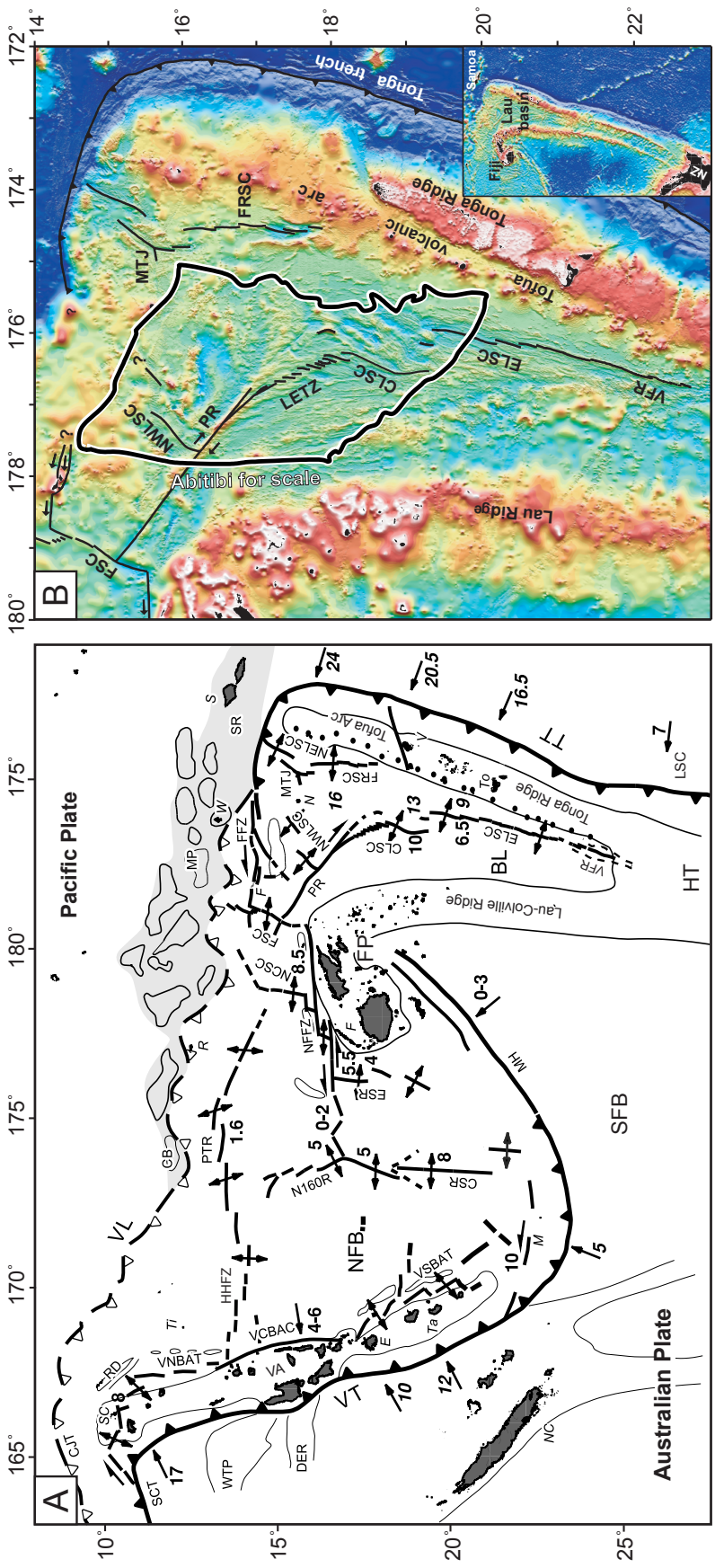

Fig. 7. (A) Kinematics of the Indo-Australian margin showing active spreading centers and spreading rates (cm/year) from magnetic chrons, as well as absolute plate motion vectors from GPS measurements (modified from Ruellan and Lagabrielle, 2005). The map shows a dense cluster of continuously deforming microplates and smaller plate fragments (about 30 in number). Thus, the boundary between the Indo-Australian and Pacific plates is a broad deformation zone rather than a sharp transition. The strain is accommodated by microplate rotation, translation, extension, and compression with limited static or rigid conditions. (B) Close-up of the northern Lau back-arc basin showing major structures that bound the emerging microplates (modified from Zellmer and Taylor, 2001). An outline of the Abitibi greenstone belt is shown for scale. Abbreviations: CB = Charlotte Bank, CJT = Cape Johnson Trough, CLSC = Central Lau spreading center, CSR = Central spreading ridge of the North Fiji basin, DER = D'Entrecasteaux Ridge, ELSC = Eastern Lau spreading center, ESR = Eastern spreading ridge of the North Fiji basin, FFZ = Futuna fracture zone, FP = Fiji Platform, FRSC = Fonualei rift and spreading center, FSC = Futuna spreading center, HHFZ = Hazel-Holme fracture zone, HT = Havre Trough, LSC = Louisville Seamount Chain, MH = Matthew-Hunter fracture zone, MP = Melanesian Plateau, MTJ = Mangatolu triple junction, N160 = N160° spreading ridge of the North Fiji basin, NCSC = North Cikobia spreading center, NELSC = Northeastern Lau basin spreading center, NFB = North Fiji basin, NFFZ = North Fiji fracture zone, NWLSC = Northwest Lau spreading center, OJP = Ontong Java Plateau, PR = Peggy Ridge, PTR = Pandora-Tripartite Ridge, RD = Duff Ridge, SCT = San Cristobal trench, SFB = South Fiji basin, SR = Samoa Ridge, TT = Tonga trench, VA = Vanuatu arc, VCBAC = Central Vanuatu back-arc compression, VFR = Valu Fa Ridge, VNBAT = Northern Vanuatu back-arc trough, VL = Vitiaz lineament, VSBAT = Southern Vanuatu back-arc trough, VT = Vanuatu trench, WTP = Western Torres Plateau. Islands in italics: E = Efate, F = Fiji, M = Mathew, NC = New Caledonia, N = Niuafo'ou, R = Rotuma, S = Samoa, SC = Santa Cruz, Ta = Tanna, Ti = Tikopia, To = Tonga Tapu, V = Vava, W = Wallis.

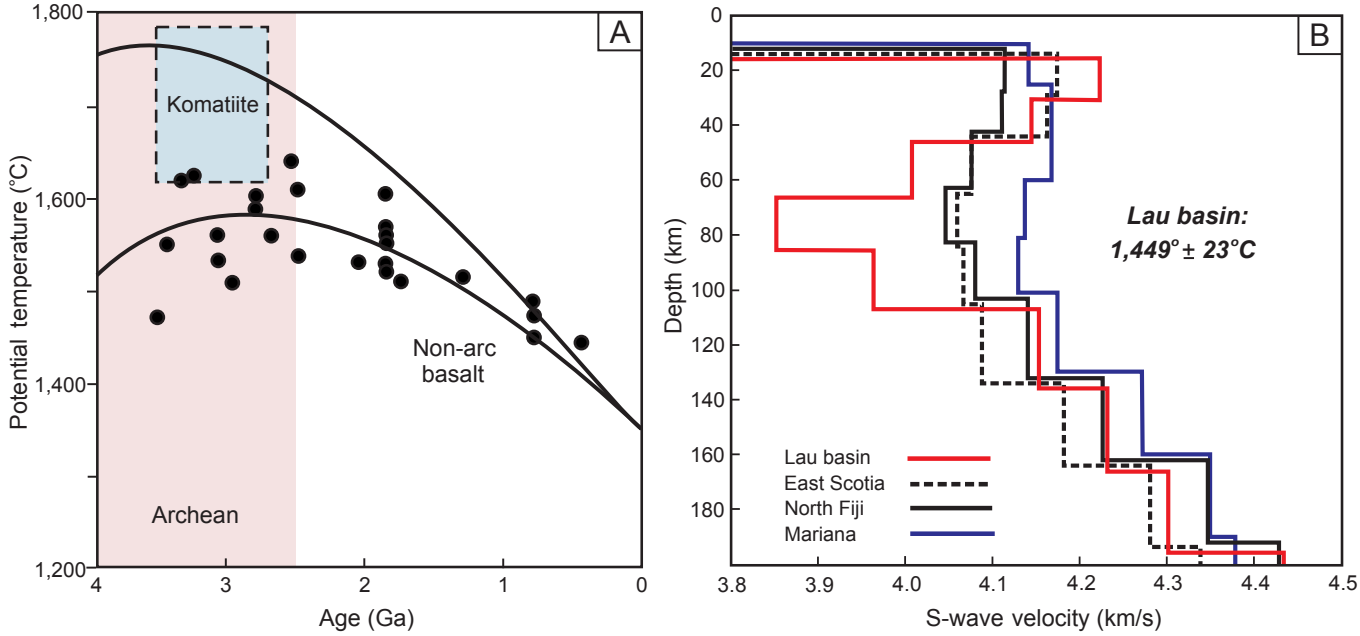

Fig. 8. (A) Example of predicted mantle potential temperatures for a range of thermal models in the Archean (curves from Korenaga, 2008a, b) and for petrological estimates from non-arc lavas (circles) and komatiites (shaded field) based on MgO content (modified from Herzberg et al., 2010). (B) Seismic shear-wave velocities of modern western Pacific back-arc basins from Wiens et al. (2006). Low shear-wave velocities at mantle depths in the Lau basin correspond to a mantle potential temperature of 1,449 ± 23°C, derived from a melting model, and concentrations of FeO and Na_2O in the corresponding melts. The Lau basin example may be the closest modern analog of a hot Archean mantle and is at least 100°C hotter than other back-arc basins in the region (see Wiens et al., 2006, for details).

clearly identify the rift structures and microplate architecture (Fig. 14).

These complementary data sets provided the framework for the first active-source seismic reflection and refraction studies in the northeast part of the basin (Hannington et al., 2019; Schmid et al., 2020). Previous seismic surveys had been conducted in the western half of the Lau basin as part of the site survey for Ocean Drilling Program (ODP) Leg 135 (Parson et al., 1994), and seismic tomography experiments were also carried out in the south (Zhao et al., 1997; Grevemeyer and Flüh, 2008; Contreras-Reyes et al., 2011; Dunn et al., 2013). However, most of the early seismic surveys focused on the volcanic front of the arc and the subduction zone rather than the back-arc basin. Prior to 2019, only one refraction line crossed the back-arc study area (Crawford et al., 2003). We conducted six transects across the arc-to-back-arc transition in the region of microplate formation (Fig. 9C), imaging the crust to a depth of 7 km in seismic reflection profiles and then 20 km in the refraction lines. The new seismic lines ranged from 100 to more than 300 km in length, crossing the entire central microplate of the basin. Magnetotelluric (MT) stations were also deployed for 40 days at the inferred microplate plate boundary (Franz et al., 2021). These combined data sets are unique in the oceans and directly comparable to the land-based transects of Metal Earth (Smith et al., 2023).

Geology of the Lau Basin

The study area is the most oceanic part of the Indo-Australian margin, far from the influence of any continental land mass. The Lau basin is bordered by the active Tofua volcanic arc in the east and the remnant Lau Ridge in the west. Opening of the basin started ~6 m.y. ago, initiated by rapid westward convergence of the Pacific Plate and retreat of the Tonga trench (Crawford et al., 2003; Zellmer and Taylor, 2001; Conder and Wiens, 2011; Sleeper and Martinez, 2016). Although the oldest rocks in the basin are Eocene (~40 m.y.-old basement of the Lau and Tonga Ridges), half of the basin formed by accretion of new back-arc crust in just the last 3 m.y. The basin fits the definition of a subprovince—a region with distinct lithological, stratigraphic, and structural characteristics belonging to a single tectonic system (Stewart et al., 2022)—and is dominated by a cluster of active microplates formed during the opening of the basin. The total strike length of active spreading centers exceeds that of any other arc-back-arc system in the western Pacific (e.g., Hasterok et al., 2022) and includes more than 80 hydrothermal vent sites (see InterRidge Vents Database, https://vents-data.interridge.org/; Fig. 9B; App. Table A1).

The Indo-Australian and Pacific plates at this location are the fastest converging plates in the oceans. Old Pacific lithosphere is approaching the Tonga trench at 165 mm/year at 22°S and 240 mm/year at 17°S (Ruellan and Lagabrielle, 2005). Regional tomographic images show the Pacific Plate subducting with dips of as much as 70° (Zhao et al., 2007). Because of an abrupt curvature of the trench caused by the collision with Ontong Java, the Pacific Plate is also torn through its entire lithospheric thickness at the northern edge of the Tonga platform (Millen and Hamburger, 1998; Bonnardot et al., 2007). The continuing westward motion of the plate is accommodated at the point of the slab tear by a large, left-lateral transform fault or STEP fault (subduction-transform edge propagator; Figs. 9, 11A; cf. Govers and Wortel, 2005).

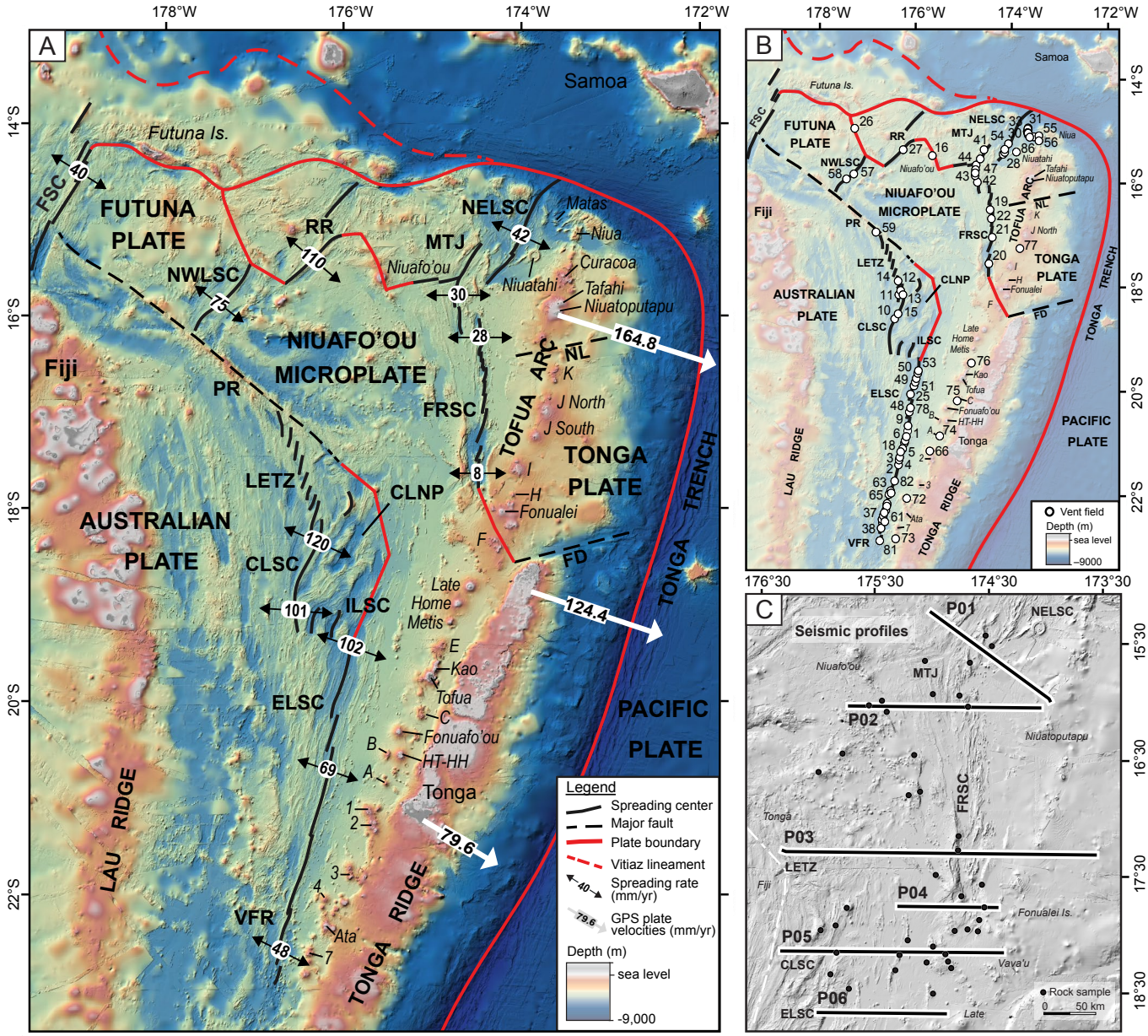

Fig. 9. Global multiresolution topography synthesis (GMRT version 3.6: Ryan et al., 2009) and kinematics of the northern Lau basin. Colors are water depth. (A) Current plate motions in the NE Lau basin from GPS velocities (white arrows) show the retreat of the Tonga plate relative to Australia. Full spreading rates (black arrows) are indicated for the Rochambeau rifts (RR) and the Northwest Lau spreading center (NWLSC) from Bird (2003); the Central Lau spreading center (CLSC), Fonualei rift and spreading center (FRSC), Eastern Lau spreading center (ELSC), Valu Fa Ridge (VFR), Mangatolu triple junction (MTJ) southern arm, and Northeast Lau spreading center (NELSC) from Sleeper and Martinez (2016); and the Futuna spreading center (FSC) from Pelletier et al. (2001). Active volcanoes (names and letter labels) are indicated in italics. Microplate boundaries are simplified from Conder and Wiens (2011) and Baxter et al. (2020). Other labeled features referenced in the text include the following: CLNP = Central Lau nanoplate, FD = Fonualei discontinuity, HT-HH = Hunga Tonga-Hunga Ha'apai, ILSC = Intermediate Lau spreading center, LETZ = Lau extensional transform zone, NL = Niuatoputapu lineament, PR = Peggy Ridge. (B) Distribution of known hydrothermal vents and sulfide deposits in the Lau-Tonga region, updated from the InterRidge database, version 3.4. Selected deposits and occurrences are numbered (see App. Table A1). (C) Locations of seismic reflection profiles across the eastern plate boundary of the Niuafo'ou microplate. Results of line P06 are discussed in the text; other profiles are described in Hannington et al. (2019).

There is evidence for an influx of Samoan mantle plume material through the slab tear (Turner and Hawkesworth, 1998; Bonnardot et al., 2007), but the precise geometry of the mantle flow is unknown. The Vitiaz lineament, which borders the north of the basin, is a relic of the former Vitiaz trench and is now a major deformation zone (e.g., Baxter et al., 2020). Transcurrent motion on the Vitiaz lineament continues as far west as the Futuna deformation zone and the Fiji transform. The rapid opening of the basin following the collision with Ontong Java has left a trail of spreading centers, failed rifts,

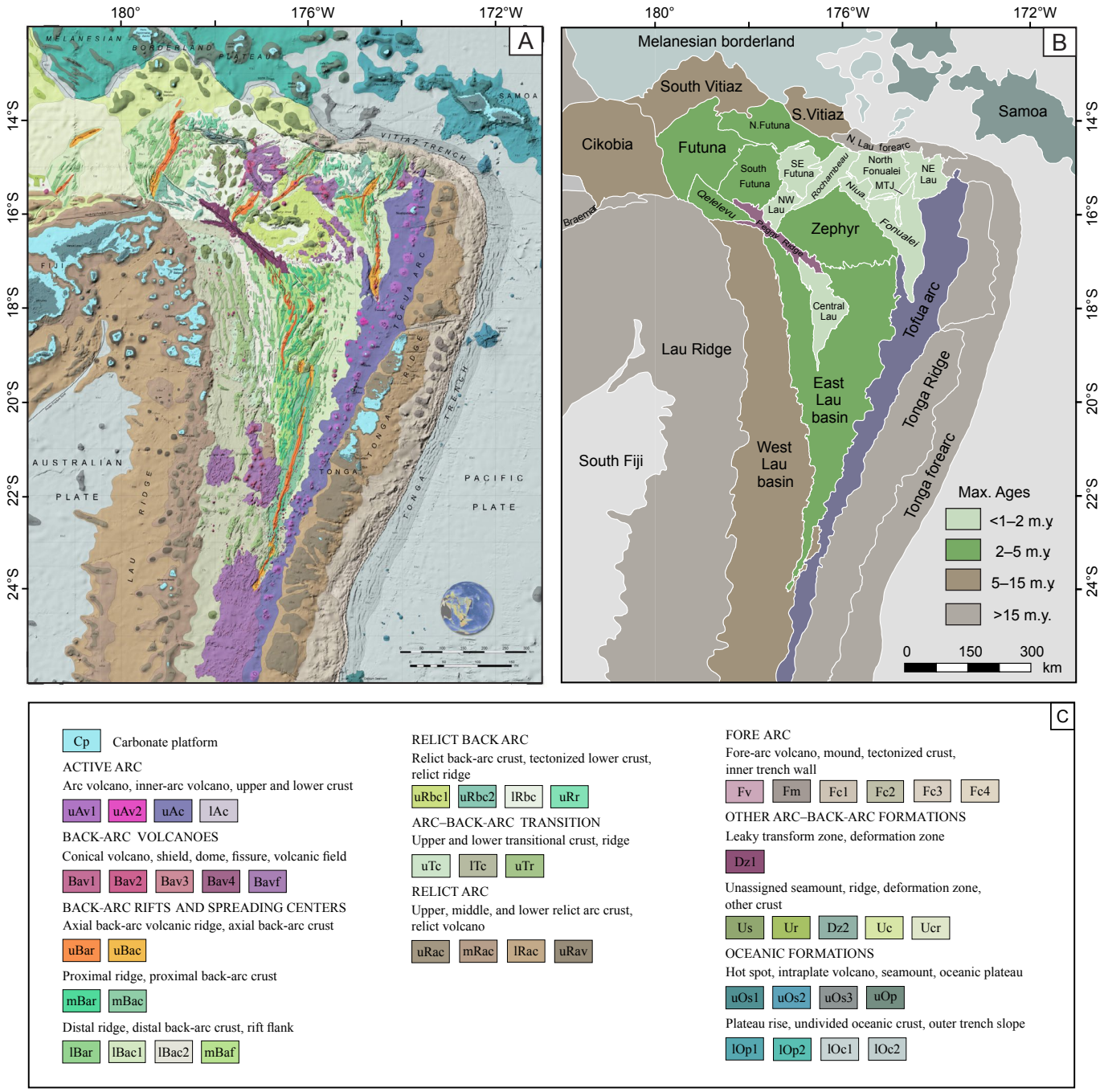

Fig. 10. (A) Geologic map of the Lau basin from Stewart et al. (2022) showing interpreted formation and assemblage-level units derived from regional magnetic, gravity, and seismic surveys together with high-resolution multibeam bathymetry. The complete map sheet at 1:1,000,000 scale with marginal notes is provided in the original reference and is available for download from https://doi.org/10.1130/GEOS.S.16869167. Labeled features referenced in the text include the following: CLSC = Central Lau spreading center, ELSC = Eastern Lau spreading center, FD = Fonualei discontinuity, FRSC = Fonualei rift and spreading center, FSC = Futuna spreading center, FTF = Futuna transform fault, ILSC = Intermediate Lau spreading center, LETZ = Lau extensional transform zone, MTJ = Mangatolu triple junction, NCSC = North Cikobia spreading center, NELSC = Northeast Lau spreading center, NL = Niuatoputapu lineament, NWLSC = Northwest Lau spreading center, QF = Qelelevu fault, RB = Rochambeau bank, RR = Rochambeau rifts, SEFVZ = Southeast Futuna volcanic zone, VFR = Valu Fa Ridge (and "ridges and knolls"), WCVZ = West Cikobia volcanic zone. (B) Assemblage map of the Lau basin. Assemblages are grouped according to lithology, inferred age, and tectonic and structural regime. See text for the descriptions. The oldest assemblages are shown in brown, in the external zones of the basin; the youngest are in pale green in the interior of the basin, altogether spanning a little over 15 m.y. of crustal growth. Ages are assigned according to magnetic chrons, where available, and from spreading ages where rates of extension are known (Stewart et al., 2022). The age relationships are broadly similar to the north volcanic zone and south volcanic zone divisions of the Abitibi greenstone belt (formerly referred to as "exterior" and "interior" zones). (C) Simplified legend of formations of the Lau basin (see Stewart et al., 2022, for details).

and microplates in its wake (Millen and Hamburger, 1998). Significant crustal-scale permeability resulting from the deformation likely explains an abundance of intraplate volcanoes and the numerous hydrothermal sites throughout the northern part of the basin (German et al., 2006; Kim et al., 2009; Baker et al., 2019; Fouquet et al., 2015; Konn et al., 2018). A regional plume-like $^{3}He/^{4}He$ anomaly in the northwest of the basin also highlights a significant mantle input that rivals the mantle helium anomaly of the East Pacific Rise (Lupton et al., 2012, 2015).

Sea-floor spreading in the Lau basin started in the north between 6 and 5.5 Ma, following splitting of the Vitiaz arc (Karig, 1970; Hawkins, 1995; Taylor et al., 1996). Basin opening quickly propagated ~700 km south, with asymmetric spreading toward the west resulting in the classic V shape of the basin (Fig. 9). Almost all of the original Cretaceous crust of the Vitiaz arc became part of the now relict Lau Ridge in the west. Arc volcanism continued along the Lau Ridge for at least several million years until about 2.5 Ma (Parson et al., 1992a; Hawkins and Allan, 1994), before stepping across the basin and reinitiating in the east, forming the currently active Tofua arc (Martinez and Taylor, 2006). Cores recovered during ODP Leg 135 (Bednarz and Schmincke, 1994; Clift and Dixon, 1994) confirm that the volcaniclastic sediments in the basin were derived first from a source in the west (Lau Ridge) and then from the east (Tofua arc). Magnetic reversals and rock samples also have a range of ages that do not increase linearly with distance from the center of the basin, as would be expected for a basin that was opening symmetrically. Instead, they indicate a more complex opening history involving multiple ridge jumps. Although arc magmatism stabilized in the east only about 1 m.y. ago (Hawkins, 1995), already the new arc is beginning to rift. Various models have been proposed for the asymmetric opening history, emphasizing different positions of the Euler pole for the earliest spreading (Pelletier et al., 2001; Zellmer and Taylor, 2001; Conder and Wiens, 2011; Sleeper and Martinez, 2016).

Until the 1980s, researchers recognized only one major spreading center (Hawkins, 1995; Taylor et al., 1996). Now, as many as 12 spreading segments have been identified, with individual lengths averaging ~100 km, and distributed across the full 600-km width of the basin (Fig. 11B). All of the spreading centers are currently active and are the defining features of the microplate network. They are generally very similar to mid-ocean ridges in terms of segmentation, volcanic architecture, and composition, with axial depths of 2,300 to 3,000 m below sea level. The main spreading centers are the Eastern Lau spreading center, the Central Lau spreading center, and the Lau extensional transform zone, with a short relay between the Central and Eastern Lau spreading centers. This geometry was first described from sidescan surveys (Parson et al., 1990) and has since been refined by analysis of regional magnetics, gravity, and additional sidescan data (Zellmer and Taylor, 2001; Martinez and Taylor, 2006; Sleeper and Martinez, 2014, 2016; Sleeper et al., 2016). Seismicity shows that extensional faulting is occurring at the northern and southern terminations of many of the spreading segments (Conder and Wiens, 2011; Baxter et al., 2020). However, focal mechanisms of the earthquakes indicate mostly strike-slip motion elsewhere, reflecting the rotation of the microplates between the spreading centers (e.g., Parson et al., 1990; Wetzel et al., 1993; Sleeper and Martinez, 2014; Baxter et al., 2020). The main spreading centers are now all propagating toward the south, but they have been advancing at different rates (from 120 to 320 mm/year; Pelletier et al., 1998; Zellmer and Taylor, 2001).

The Eastern Lau spreading center initiated in the north of the basin near 17°S at 5.5 to 5 Ma, shortly after splitting of the Vitiaz arc (Parson et al., 1992b; Hawkins, 1995; Clift et al., 1998; Martinez and Taylor, 2006; Martinez et al., 2006). The spreading rate is now 102 mm/year in the north, decreasing to 48 mm/year in the south at the Valu Fa Ridge. The northern segment is being overtaken by the southern Central Lau spreading center near 18°S, and in the south, the Valu Fa Ridge is propagating into the Tofua arc (Parson et al., 1990). A large area of intruded back-arc crust occurs where the Valu Fa Ridge first encounters the Tofua arc (so-called "ridges and knolls" of Ruellan et al., 2003; Fig. 10A), possibly representing the earliest magmatism associated with arc rifting. Earlier episodes of arc rifting and crustal growth are indicated by similar areas of inflated back-arc crust now located west of the Eastern Lau spreading center. The thickened crust is characterized by large positive Bouguer anomalies (Fig. 12B), consistent with the beginning of MORB-like magmatism before a stable spreading center was developed (Fujiwara et al., 2001; Martinez and Taylor, 2006).

Fig. 11. (A) Structure of the northern Lau basin based on lineaments and shallow seismicity from Baxter et al. (2020), with data from Parson et al. (1990), Wetzel et al. (1993), Conder and Wiens (2011), and Sleeper and Martinez (2014). Faults are classified according to the locations and sense of motion of 375 earthquakes (from the catalog of centroid moment tensors; CMTs). Different types of plate boundaries (spreading centers, transform faults, subduction zone faults, and other) are color coded. Uncertain boundaries inferred from seismicity are indicated as dashed lines, and several additional microplates may be present that are discussed in the text (e.g., Matas microplate). Transcurrent faulting is dominant throughout as a result of plate rotation, especially at major crustal-scale faults such as Peggy Ridge. Some structures are obscured by later volcanic centers, such as the Niuafo'ou Volcanic Complex and Mangatolu triple junction (MTJ), which overlap the boundary between the Niuafo'ou microplate and North Lau microplate, and the Southeast Futuna volcanic field, which almost completely covers the southwest portion of the Rochambeau microplate. (B) Interpreted microplate mosaic defined by spreading centers and transform fault boundaries (from west to east): Cikobia-Balmoral, Futuna, Rochambeau, North Lau, Northeast Lau, Niuafo'ou, Central Lau nanoplate, and North Tonga highlighted as semitransparent polygons in contrasting colors. Feature abbreviations: CFZ = Central Futuna deformation zone, FDZ = Futuna deformation zone, FSC = Futuna spreading center, FTZ = Fiji transform zone, MTJ = Mangatolu triple junction, NELSC = Northeast Lau spreading center, NWLSC = Northwest Lau spreading center, RR = Rochambeau rifts. Other abbreviations: RTF = ridge-trench-fault triple junction, STEP = subduction-transform edge propagator. (C) Relationship between interpreted microplates and mapped formations at 1:1,000,000. See Figure 10C for legend and abbreviations. The mapped structures corresponding to plate boundaries include back-arc spreading centers, ridge-transform boundaries, extensional transform zones, leaky transform faults, triple junction boundaries, overlapping spreading centers, intraplate volcanic fields, plume-driven spreading centers, central volcanic complexes, and arc rifts (described in the text).

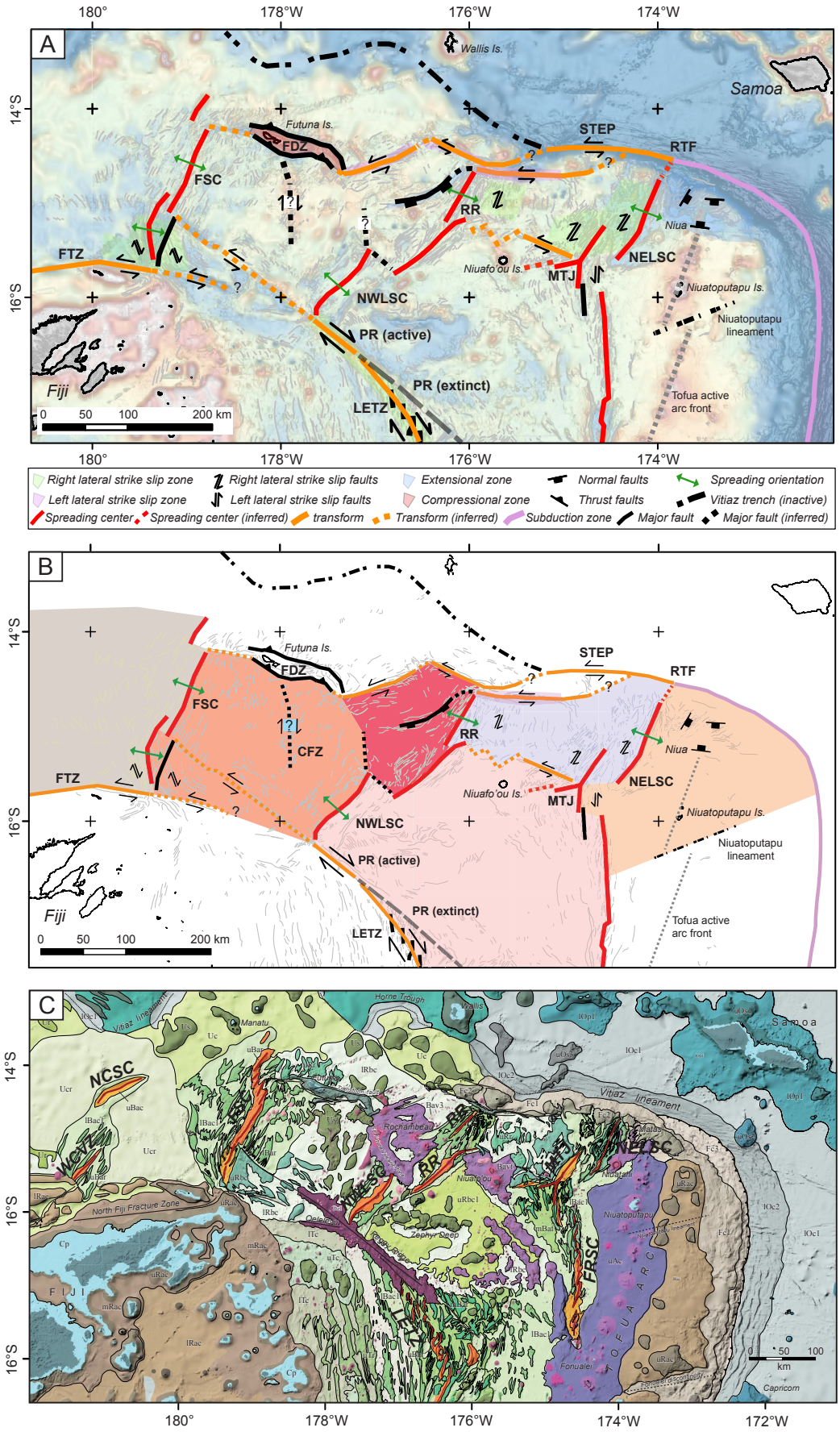

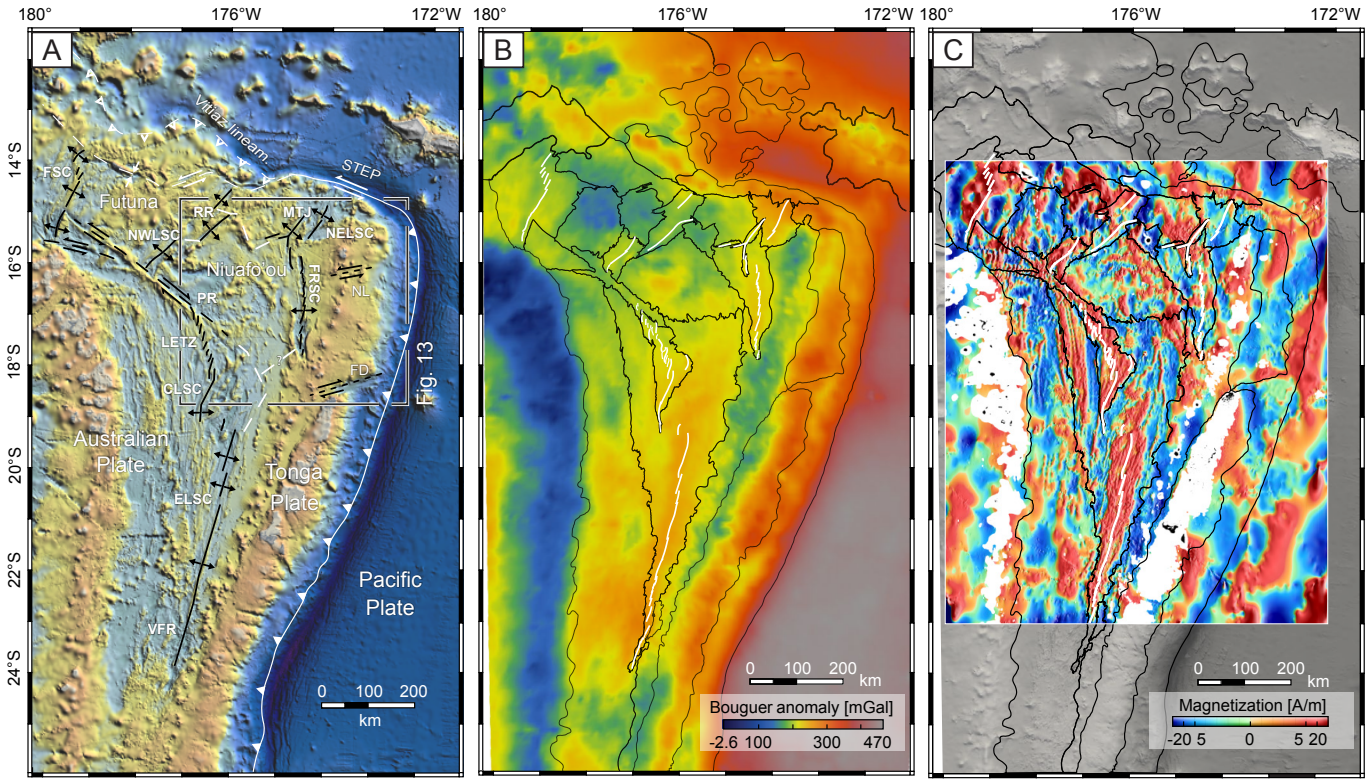

Fig. 12. (A) Location of the main study area with major structures of the northern Lau basin. Colors are water depth (see Fig. 9 for details). (B) Bouguer gravity anomalies from the Smith and Sandwell (1997) regional free-air gravity, calculated by subtracting the effect of bathymetry, sediments, and the seawater signal (Galley et al., 2024). The overlay shows the outline of the mapped assemblages (Fig. 10B), which correspond closely to the Bouguer gravity (see Fig. 16). Thin black lines are assemblage boundaries; white lines are spreading centers. In the West Lau basin, positive Bouguer anomalies are caused by voluminous eruptions and mafic intrusions such as the "ridges and knolls" described in the text. Bouguer highs at active spreading centers (e.g., Fonualei rift and spreading center [FRSC], Central Lau spreading center [CLSC], and Eastern Lau spreading center [ELSC]) correspond to thinned crust with dense mantle upwelling. Negative or low Bouguer anomalies correspond to thick crust (i.e., deep mantle) and less dense arc crust, such as at the Tofua arc and Lau Ridge. (C) Magnetic anomalies from the 2-arc-minute Earth Magnetic Anomaly Grid (EMAG2: Maus et al., 2009) incorporating satellite, airborne, and marine magnetic measurements. Areas of normal and reversed magnetic polarity (positive and negative anomalies) indicate the regional spreading from which spreading rates are calculated. Abbreviations: FD = Fonualei discontinuity, FSC = Futuna spreading center, LETZ = Lau extensional transform zone, MTJ = Mangatolu triple junction, NELSC = Northeast Lau spreading center, NL = Niuataputopu lineament, NWLSC = Northwest Lau spreading center, PR = Peggy Ridge, RR = Rochambeau rifts, VFR = Valu Fa Ridge.

The Central Lau spreading center is currently the main spreading center between 18° and 19.5°S, also with a maximum opening rate of 100 mm/year. Early workers interpreted the Central Lau spreading center to have formed at 1.5 Ma (Parson and Hawkins, 1994); however, more detailed magnetic studies suggest it may be as young as 0.78 Ma, corresponding to the Bruhnes-Matuyama magnetic reversal (Sleeper and Martinez, 2016). In the north, the Central Lau spreading center abuts the Peggy Ridge transform and is connected to Peggy Ridge via a series of short en echelon axial volcanic ridges belonging to the Lau extenstional transform zone (Sleeper and Martinez, 2014, 2016; Sleeper et al., 2016). Peggy Ridge is a long-lived transcrustal boundary between the Central Lau spreading center in the south and the younger, active back-arc spreading centers in the north of the basin. Since at least 3 Ma, Peggy Ridge has accommodated significant opening of the Lau basin (i.e., ~600 km of differential movement at latitude 15°S). The fault is magmatically active in its central part, referred to as a "leaky transform," which accounts for its ridge-like morphology.

Three additional spreading centers of different ages occur in the northeast of the basin: the Mangatolu triple junction, the Northeast Lau spreading center, and the Fonualei rift and spreading center. The Mangatolu triple junction appears to have only one dominant spreading segment along its northeast arm, which is opening at 30 mm/year. The Fonualei rift is the youngest spreading center and is propagating southward into the northern Tofua arc, similar to the Valu Fa Ridge in the south. Based on a reinterpretation of the sea-floor magnetization patterns and ridge morphology, Sleeper and Martinez (2016) suggested only slow spreading at the Fonualei rift (from 28 mm/year to as little as 8 mm/year; see below). Immediately south of the propagating tip of the Fonualei rift, magmatism in advance of the rift has inflated the crust, similar to the ridges and knolls of the Valu Fa Ridge. North of the Fonualei rift and Mangatolu triple junction, another spreading center (Northeast Lau spreading center) is opening at 42 mm/year and propagating northward into old crust of the former Vitiaz arc (Anderson et al., 2021). One interpretation is that the Northeast Lau spreading center and Fonualei rift will eventually connect

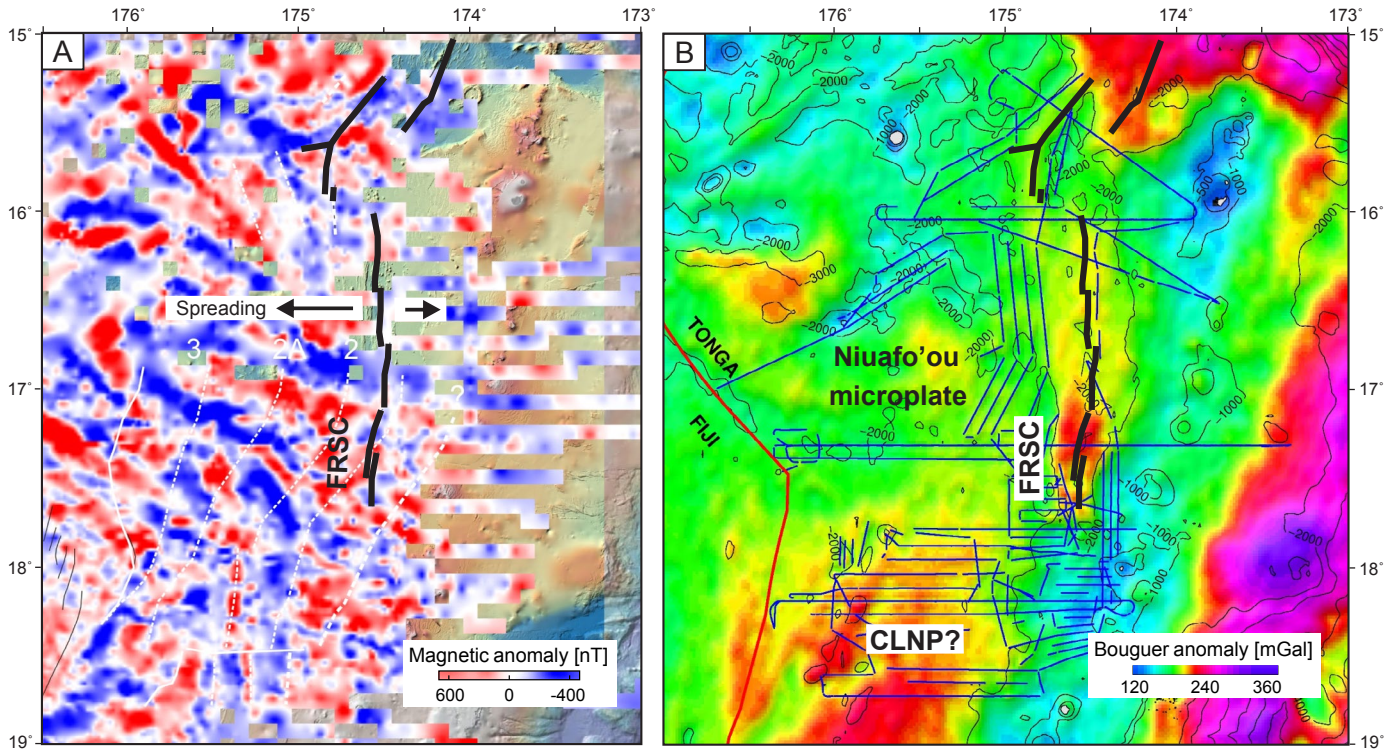

Fig. 13. Ship-based magnetics and gravity, showing the structural fabric of the Niuafo'ou microplate adjacent to the Fonualei rift and spreading center (FRSC) plate boundary. The data were collected with a towed magnetometer and a gravimeter installed in the vessel, which continuously records the gravity field. Details of the surveys and processing are in Hannington et al. (2019). (A) Magnetic anomaly map processed by Barckhausen et al. (2019) and combined with aeromagnetic data. At this resolution, the magnetic fabric is characterized by a discontinuous pattern of magnetization that is highly asymmetric and oblique to the east-west accretion at the FRSC, reflecting the strong influence of plate rotation. Black lines show the trace of the FRSC and Mangatolu triple junction (MTJ) rifts. White dashed lines are the expected locations of magnetic reversals for more regular basin opening. (B) Bouguer gravity map from SO-267 shipboard data processed by Heyde et al. (2019) and merged with data from satellite altimetry (Sandwell and Smith, 2009). A strong positive Bouguer anomaly under the FRSC corresponds to the interpreted mantle upwelling associated with the rift. The positive Bouguer anomalies in the area of the Central Lau nanoplate (CLNP; Fig. 9A) appear to mark the emerging southern boundary of the Niuafo'ou microplate (see text for discussion). Blue lines are ship tracks, and black contours are depth below sea level in meters.

near the Mantaolu triple junction and form a new triple junction and plate boundary (Baxter et al., 2020).

Several other spreading centers occur in the northwest of the basin, including the Northwest Lau spreading center and the Futuna spreading center (Parson and Tiffin, 1993; Pelletier et al., 2001), which are partly obscured by several large volcanic flow fields. The Northwest Lau spreading center is a prominent volcanic ridge, ~100 km long and >500 m high, with two large summit calderas (Arculus, 2008). It is truncated by the Peggy Ridge in the south and partially overlaps the Rochambeau rifts in the north. The Northwest Lau spreading center is spreading at 75 mm/year; the main Rochambeau rift is spreading at 110 mm/year (Lupton et al., 2012). The Rochambeau rift also has a prominent axial volcanic high and large summit caldera (Lobster caldera). A smaller en echelon rift to the northwest lacks an axial high but is floored by young back-arc crust. The largest and oldest spreading center is the Futuna spreading center, which is nearly 215 km long and 800 m high. It is spreading at about 40 mm/year, and the southern end may be propagating into the Fiji platform, although the connection to the North Fiji fracture zone is unclear.

The combined spreading at these centers has resulted in expansion of the basin by nearly 170 mm/yr, which matches the measured GPS velocity of the retreating arc (164.8 mm/yr: Bevis et al., 1995; Fig. 7). Although discrete segments have much lower spreading rates (an average of only 47 mm/year across the basin), together they contribute the same amount of crustal growth as some of the fastest spreading mid-ocean ridges, such as the Southern East Pacific Rise. The crust is also thicker (8–9 vs. 6–7 km at the East Pacific Rise: Turner et al., 1999; Crawford et al., 2003), resulting in even greater volumes being produced. This style of back-arc basin opening, involving widely distributed extension, is now considered to be a dominant pattern of crustal accretion in other large back-arc systems (e.g., Martinez et al., 2018). To accommodate the opening, the required displacement along the Peggy Ridge transform has been as much as 100 km per million years.

The compositions of dredged volcanic rocks throughout the basin include basalt to rhyolite and boninitic to alkaline lavas, locally within tens of km of each other and indicating highly variable melting conditions (Falloon et al., 2007; Harmon and Blackman, 2010; Resing et al., 2011; Escrig et al., 2012; Haase et al., 2022; Fassbender et al., 2023, 2024). The magmatic diversity resembles that of other propagating rifts in the oceans (e.g., Ishizuka et al., 2010; Regelous et al., 2014), but the reason for the close juxtaposition of different

volcanic suites is still uncertain. Several major volcanic centers are thought to be sites of mantle upwelling (Turner and Hawkesworth, 1998), in particular where plate boundaries are marked by large volcanic flow fields or shield volcanoes (e.g., southeast Futuna volcanic field and the Niuafo'ou volcano) and triple junctions (e.g., at the Mangatolu triple junction). These aspects are discussed further below.

Hydrothermal mineralization was first reported in the Lau basin in 1975 from a single dredge on Peggy Ridge (Bertine and Keene, 1975). In 1986, sulfide chimneys were recovered from the north arm of the Mangaolu triple junction (Hawkins and Helu, 1986), and Fe-Mn crusts and sulfide-impregnated lavas were reported from the Valu Fa Ridge (von Stackelberg et al., 1985). Hydrothermal venting was discovered first in 1987 at the southern Valu Fa Ridge (von Stackelberg et al., 1987, 1990), and eventually sulfide deposits and hydrothermal vents were located along all segments of the Valu Fa Ridge and Eastern Lau spreading center (Fig. 9B). At the same time, Russian researchers made several new discoveries in the Mangatolu triple junction area and on the Central Lau spreading center (Lisitsyn et al., 1992; Bortnikov et al., 1993). The large numbers of hydrothermal plume sites and areas of high-temperature venting now identified (Fouquet et al., 1993; Herzig et al., 1993; Baker et al., 2006, 2011; German et al., 2006; Arculus, 2008, 2009; Embley et al., 2009; Kim et al., 2009; Evans et al., 2017; Konn et al., 2016; Fouquet et al., 2018) make the Lau basin one of the most hydrothermally active places in the oceans.

Formations and assemblages

Stewart et al. (2022) provided the first detailed description of the crustal makeup of the Lau basin. Formation-level geologic units (Fig. 10C) were identified at scales of 1:100,000 to 1:200,000 and then grouped by age and origin into 25 assemblages assigned to different episodes and locations of crustal growth (Fig. 10B). The different assemblage types include (by area) crust of the active volcanic arc (7%) and fore-arc (9%), relict arc crust that is no longer active (38%), back-arc rifts and spreading centers (20%), transitional arc-back-arc crust (13%), relict back-arc crust (8%), and undivided crust (5%), plus intraplate volcanoes and carbonate platforms. The crustal growth is quantified in terms of area-age relationships of the different assemblages (Table 1); the oldest and most expan-

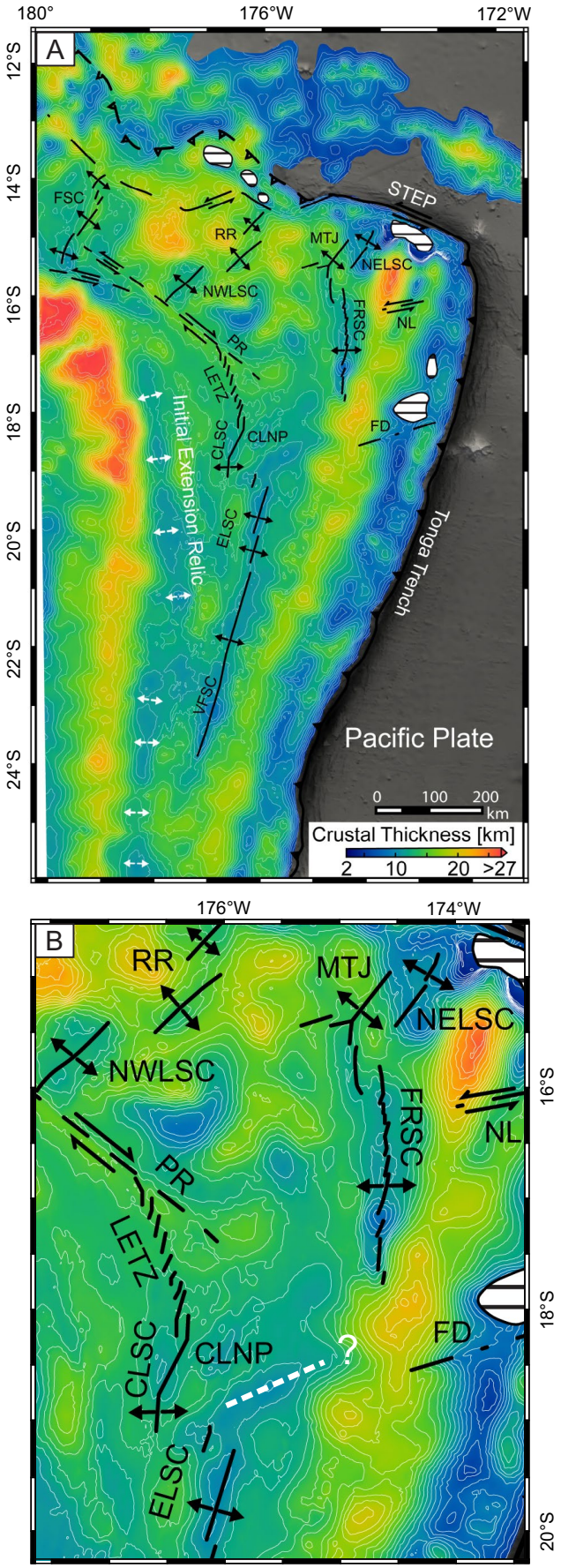

Fig. 14. (A) Crustal thickness map of the Lau basin from Galley et al. (2024) based on regional gravity. Crustal thickness was calculated from a constrained 3-D gravity inversion of the depth to the Moho (an iso-density surface at the base of the crust). The Moho depth varies significantly between the different centers of accretion, reflecting sea-floor spreading and subsurface melt accumulation. The white contour lines of crustal thickness are in 1-km intervals. The interpreted southern boundary of the Niuafo'ou microplate is indicated by a distinct gravity high in Figure 13B and by crustal thinning at the northern termination of the Eastern Lau spreading center (ELSC) in this figure. (B) Close-up of the crustal thickness map showing the Fonualei rift and spreading center (FRSC), the Fonualei discontinuity (FD), and the emerging southern boundary of the Niuafo'ou microplate (dashed line). Abbreviations: CLNP = Central Lau nanoplate, CLSC = Central Lau spreading center, ELSC = Eastern Lau spreading center, FD = Fonualei discontinuity, FSC = Futuna spreading center, LETZ = Lau extensional transform zone, MTJ = Mangatolu triple junction, NELSC = Northeast Lau spreading center, NL = Niuataputopu lineament, NWLSC = Northwest Lau spreading center, PR = Peggy Ridge, RR = Rochambeau rifts, STEP = subduction-transform edge propagator.

Table 1. Area-Age Relationships of Lau Basin Back-Arc Assemblages

Assemblage	Area (km²)	Approx. age (Ma)	Duration (m.y.)	Growth rate (km²/m.y.)
Mangatolu	1,871	0.5 to present	0.5	3,742
Rochambeau	8,155	0.5 to present	0.5	16,310
Niuafo'ou	3,509	1 to present	1	3,509
Northwest Lau	4,626	1 to present	1	4,626
Southeast Futuna	8,260	1 to present	1	8,260
Central Lau	11,030	1.5 to present	1.5	7,353
Northeast Lau	7,916	2.5 to present	2.5	3,166
Central Lau	11,030	1.5 to present	1.5	7,353
Tofua arc[1]	72,295	3 to present	3	-
North Fonualei	10,552	3.8–0.5	3.3	3,198
Fonualei	16,145	3.8 to present	3.8	4,249
Futuna	28,922	4.5 to present	4.5	6,427
East Lau	90,325	5.5 to present	5.5	16,423
North Futuna	17,529	5.5 to present	5.5	3,187
Peggy Ridge	6,341	5.5 to present	5.5	1,153
South Futuna	15,682	5.5 to present	5.5	2,851
Zephyr	31,580	5.5–1	4.5	7,018
South Vitiaz	40,967	12 to present	12	3,414
Cikobia	47,275	Uncertain	-	-
Qelelevu[1]	(7,417)	46–31, 28–15, 5.6–2.4	28	-
West Lau basin	143,775	46–31, 28–15, 5.6–2.4	28	5,135

Note: Areas and ages are from Stewart et al. (2022); the original Qelelevu assemblage is truncated by faults and therefore its original surface area is uncertain; a nominal spreading rate can be calculated by converting the area to a linear dimension ($x^{1/2}$) and dividing by the duration of growth; see text for discussion

[1]Not included in rate calculation

sive assemblages are at the outer margins of the basin, and the youngest are at the rapidly growing center (see internal versus external zones in Fig. 10B). The mapped assemblages correspond generally to the regional Bouguer gravity, confirming the differences in the composition of the crust (Fig. 15). Positive Bouguer anomalies can be interpreted as thinned crust, where dense mantle material is upwelling (e.g., at the center of the Fonualei assemblage) or where the crust is heavily intruded by mafic melts (e.g., as in the "ridges and knolls"). In contrast, the Lau Ridge and Tonga Ridge are dominated by relict arc crust, which is generally less dense, and fore-arc crust, which is thicker.

The major episodes of back-arc crust formation are represented by 13 of the 25 assemblages: the West Lau basin, East Lau basin, Central Lau basin, Fonualei, Mangatolu, Northeast Lau basin, Niuafo'ou, Rochambeau, Northwest Lau basin, Southeast Futuna, Futuna, Cikobia, and Peggy Ridge. Each assemblage encompasses an area with a distinct spreading fabric or map pattern that is demonstrably linked to a currently active or former spreading center. Many of the spreading centers have migrated in response to plate rotation and basin opening (Bevis et al., 1995; Hawkins, 1995; Sleeper and Martinez, 2016; Baxter et al., 2020), and so the origin of the assemblages must be traced back through several episodes of spreading. Some assemblages are structurally juxtaposed at transcurrent boundaries and triple junctions, but most are defined by regional unconformities (e.g., between the East Lau and Central Lau basin assemblages: see below). Widely distributed extension has produced many different assemblages of similar age that would be considered supergroups in ancient terranes. In the following, the assemblages are described generally from east to west, and the ages are indicated in Figure 10B.

Tofua arc assemblage: The active Tofua volcanic arc includes all volcanic rocks associated with the present-day subduction zone magmatism, including the volcanic front and extensive volcaniclastic apron. East of the arc is the Tonga Ridge (former Vitiaz fore arc), and to the west, the East Lau basin assemblage. The active arc is built on a basement of older crust that is at least 20 km thick (Crawford et al., 2003; Contreras-Reyes et al., 2011; Schmid et al., 2020). Volcanism at the arc

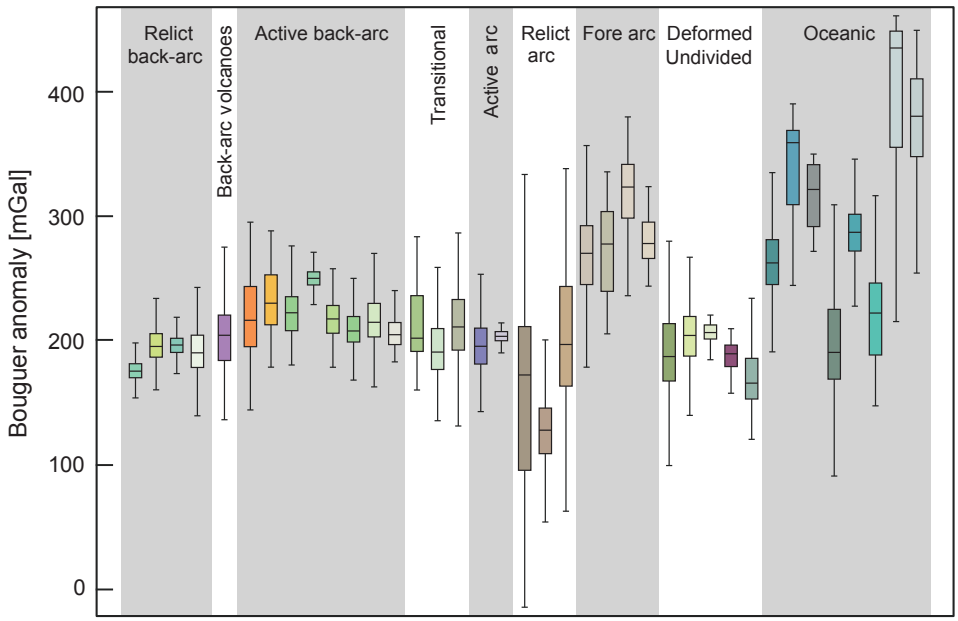

Fig. 15. Box-and-whisker plot of Bouguer anomalies associated with the mapped formations (see legend in Fig. 10C). The gravity anomalies vary with crustal type, reflecting differences in the composition and thickness of the formations and assemblages.

front began at ca. 3 Ma (Tappin et al., 1994), but most of the volcanoes are younger than 1 Ma (e.g., Stoffers et al., 2006; Arculus, 2008). Samples have been collected throughout, including from the subaerial Tafahi and Niuatoputapu volcanoes (e.g., Beier et al., 2017) and the adjacent fore arc (Meffre et al., 2012). The volcanic rocks vary in composition from basaltic andesite to andesite with lesser dacite and rhyolite. The most recent documented submarine eruptions occurred immediately south of the Fonualei rift in 2020 (Volcano F: Brandl et al., 2020) and at Tonga-Hunga Ha'apai, which produced the cataclysmic eruption of 2022.

West Lau basin assemblage: The West Lau basin assemblage is a corridor of thinned crust adjacent to the relict Lau Ridge (Fig. 10B). It was active until 2.5 Ma when spreading shifted to the Eastern Lau spreading center (Parson et al., 1992b; Parson and Hawkins, 1994; Hawkins, 1995; Taylor et al., 1996; Parson and Wright, 1996; Martinez and Taylor, 2006). Numerous sediment-filled basins characteristic for this early opening phase dominate the West Lau basin. The underlying crust is a combination of rifted arc crust and basalt from the earliest spreading. The eastern limit is marked by crust with a younger spreading fabric belonging to the East Lau basin assemblage.

East Lau basin assemblage: The East Lau basin assemblage contains the present-day Eastern Lau spreading center and occupies most of the south-central part of the basin. The eastern boundary corresponds generally to a gravity high and sharp discontinuities in the vertical gravity gradient, but it is mostly obscured by the volcaniclastic apron of the Tofua arc. The western boundary is a ~200-km-long pseudofault marked by dozens of en echelon subbasins (Martinez and Taylor, 2006). The pseudofault is currently aseismic (Baxter et al., 2020) but coincides with the Gauss magnetic polarity chron (3.58–2.58 Ma) identified by Zellmer and Taylor (2001) and Sleeper and Martinez (2016). Ship-based magnetic data reveal a strongly oblique magnetic fabric at the contact with the Tofua arc assemblage, consistent with plate rotation (Fig. 13: Barckhausen et al., 2019). ODP drilling and other sampling indicates that the crust is dominantly tholeiitic basalt and basaltic andesite, with an arc signature where the spreading axis approaches the Tofua arc, especially at the Valu Fa Ridge in the south. The influence of the arc decreases sharply in the north as the Valu Fa Ridge steps away from the volcanic front, and the northern segment of the Eastern Lau spreading center lacks any arc signature. Partially buried but prominent ridges adjacent to the Eastern Lau spreading center and between the Fonualei rift and Central Lau spreading center (Fig. 10A) have been identified as mafic intrusions (e.g., dike complexes) that are observed in seismic profiles (Hannington et al., 2019; Schmid et al., 2020).

Central Lau basin assemblage: The Central Lau basin assemblage contains the Central Lau spreading center and the Lau extensional transform zone. The Central Lau spreading center is currently rifting crust of the East Lau basin assemblage as the spreading center propagates south. It is considerably younger than the East Lau basin, having formed only in the last 1.5 to 1.2 m.y. (Parson and Hawkins, 1994; Hawkins, 1995). The northern part of the Central Lau spreading center is entirely basalt, but andesite has been sampled just south of the maximum inflation of the ridge. The western boundary is defined by the truncation of the spreading fabric against the East Lau basin assemblage. Several deep nodal basins with strongly rotated spreading fabric occur at the southern termination of the Central Lau spreading center where it overlaps with the northern end of the Eastern Lau spreading center.

Fonualei and Mangatolu triple junction assemblages: The Fonualei assemblage contains the Fonualei rift, which formed during a ridge jump simultaneously with southward propagation of the Eastern Lau spreading center. The two parallel spreading centers are now both propagating into the Tofua arc crust at the Valu Fa Ridge and at the southern tip of the Fonualei rift. At its widest, the Fonualei assemblage is nearly 110 km across, suggesting it began forming about 3.8 m.y. ago. However, there are few large earthquakes to characterize the most recent extension (Zellmer and Taylor, 2001; Conder and Wiens, 2011). Dredging of the high-standing flanks of the Fonualei rift indicates that they are mainly rifted arc crust, and reversed magnetization in the rift valley suggests relatively little new crust has been produced so far, except at a series of recent volcanic cones and dikes in the rift (Hannington et al., 2019). Dredged lavas include mainly basaltic andesite and show strong arc signatures consistent with the Fonualei rift capturing melt from the arc front (Keller et al., 2008; Escrig et al., 2012). The Fonualei assemblage is abruptly terminated in the north by the Mangatolu triple junction, which has produced a small amount of new back-arc crust constituting the Mangatolu assemblage. The dominant accretion at the Mangatolu triple junction is now occurring along the northern arm where the rift is occupied by an inflated axial high (Fig. 11C). Dredged material from the northern arm is mostly basaltic andesite, whereas samples from the southern arm are basalt (Mensing, 2019; Hannington et al., 2019).

Northeast Lau basin assemblage: The Northeast Lau basin assemblage contains the Northeast Lau spreading center as well as the Niuatahi silicic volcanic caldera and its surrounding volcanic field (Fig. 11C: Embley and Rubin, 2018; Anderson et al., 2021). This assemblage is bound by major faults (i.e., defining the Mata basin) that may have been inherited from the early stages of rifting of the Vitiaz arc. The western boundary is cut by the northern arm of the Mangatolu triple junction, which appears to be propagating into the Northeast Lau basin assemblage. The northern boundary is at the contact with fore-arc blocks belonging to the Tonga Ridge and is characterized by several dike-like volcanoes known as the Matas. The southern boundary is intruded by a series of "rear arc" volcanoes at the intersection of the Northeast Lau spreading center, Mangatolu triple junction, and northern Fonualei rift (Merle et al., 2013). Samples of the Northeast Lau spreading center are back-arc basin basalt and basaltic andesite, including the youngest lavas of the neovolcanic zone (Falloon et al., 2007; Michael et al., 2009), whereas the volcanic flow field surrounding the Niuatahi volcano is mainly dacite (Embley and Rubin, 2018). The Mata rift volcanoes are boninitic in composition (Resing et al., 2011) and have erupted as recently as 2018 (Chadwick et al., 2019).

Niuafo'ou and southeast Futuna assemblages: The Niuafo'ou volcanic complex, west of the Mangatolu triple junction, and the southeast Futuna volcanic zone are included as assemblages because they represent regions of significant back-arc

crustal growth. However, samples from the Niuafo'ou volcanic complex include a wide range of rock types from normal MORB to enriched MORB, ocean island basalt, and dacite (Hawkins, 1995; Regelous et al., 2008). The southeast Futuna volcanic zone and Rochambeau bank (Fig. 11C; Fouquet et al., 2015; Konn et al., 2016; Szitkar et al., 2020), which belong to the southeast Futuna assemblage, were possibly erupted along a buried spreading center connecting the Rochambeau rifts and Northwest Lau spreading center. The southeast Futuna assemblage is dominated by a number of large shield volcanoes (e.g., Kulo Lasi) and intraplate volcanic cones similar to the Niuafo'ou volcanic complex. Samples dredged from the perimeter of the field are all basaltic (Arculus, 2012). However, a distinctive feature of the volcanic rocks from southeast Futuna, Niuafo'ou, Northwest Lau basin, and Rochambeau is their plume-like signature indicated by exceptionally high $^{3}He/^{4}He$ (Lupton et al., 2015).

Rochambeau and Northwest Lau basin assemblages: The Rochambeau assemblage comprises the proximal back-arc crust and ridges of the Rochambeau spreading centers (Rochambeau rifts). The ridges are only ~40 km wide, suggesting that they are <500,000 years old, but they are characterized by distinctive ridge-centered volcanoes. The Northwest Lau basin assemblage is dominated by the axial volcanic ridge of the Northwest Lau spreading center with a 45-km-wide rift valley. To the north, the assemblage is truncated by the southeast Futuna volcanic field, and to the south, it is truncated by Peggy Ridge.

Futuna and West Cikobia assemblages: The Futuna assemblage in the west contains the large Futuna spreading center, with a very broad and poorly defined outer rift valley (155–190 km wide). The width is consistent with a presumed age of 4.5 Ma, assuming a spreading rate of 40 mm/yr (Pelletier et al., 2001). The spreading fabric is truncated by the Futuna transform fault and deformation zone in the north and by the western extension of the Peggy Ridge in the south, where it is in contact with the Qelelevu assemblage. The Cikobia assemblage, west of Futuna, is thought to be related to the north Cikobia spreading center and west Cikobia volcanic zone.

Relict back-arc basin assemblages: Five relict back-arc basin assemblages have been identified: Zephyr, North Fonualei, North Futuna, South Futuna, and Qelelevu (Fig. 10B). They are interpreted to have formed by rifting and sea-floor spreading but have less well-defined spreading fabric than the active assemblages, and the associated spreading centers are either no longer preserved or cannot be identified. The relict back-arc crust is commonly in fault contact with other assemblages, marked by discontinuities in the gravity gradient. The north Fonualei assemblage may have been isolated from the Fonualei assemblage by the formation of the Mangatolu triple junction. The North Futuna and South Futuna assemblages are characterized by an old spreading fabric of uncertain origin (Pelletier et al., 2001). The Qelelevu assemblage comprises mainly deformed back-arc crust trapped between the South Futuna assemblage, Peggy Ridge, the Qelelevu fault, and the North Fiji fracture zone. Some features in the relict back-arc crust, like Zephyr Deep, may represent failed rifts. The Zephyr shoal was sampled by Hawkins (1976) and found to include dacite as well as basalt, which may include relics of the former Vitiaz arc. Widespread intraplate volcanism continues within these older assemblages, indicating ongoing intrusion of the back arc in response to regional deformation (described below).

Peggy Ridge assemblage: A number of deformation zones have been designated assemblages where a significant amount of crust is involved. The Peggy Ridge assemblage, in particular, includes voluminous lava flows (covering 3,000 km²) associated with the leaky transform fault along much of its length (Parson and Tiffin, 1993; Taylor et al., 1996). A strong magnetic anomaly, clear volcanic morphology, high acoustic backscatter, and relatively fresh lava collected along the ridge are consistent with recent magmatism. Volcanic rock samples from thick flow units on Peggy Ridge are MORB-like (Volpe et al., 1988; Falloon et al., 2007), interpreted by Taylor et al. (1996) to be younger than magnetic chron 2n (1.77 Ma) but older than Brunhes-Matuyama (0.78 Ma). One sample of basalt from the northern end of the Peggy Ridge has elevated $^{3}He/^{4}He$, intermediate between MORB and the plume signature of the Northwest Lau spreading center and Rochambeau rifts (Lupton et al., 2015).

Area-age relationships for the different assemblages are detailed in Stewart et al. (2022) and illustrated in Figure 10B. They show a major pulse of crustal growth at ~5 Ma when multiple spreading centers became active at the same time in the northern Lau basin (Table 1). Despite slow individual spreading rates, cumulative growth rates for the entire basin jumped from 3,500 km²/m.y. to more than 7,000 km²/m.y. (Fig. 16), accommodated by the displacement along Peggy Ridge in the south and the Futuna deformation zone in the north. The growth curve shows a protracted period of slow growth that produced the West Lau, Cikobia, South Vitiaz, and Zephyr assemblages followed by a rapid transition from rifting to spreading with the sudden release of mantle melts that formed the East Lau and Futuna assemblages (Dunn and

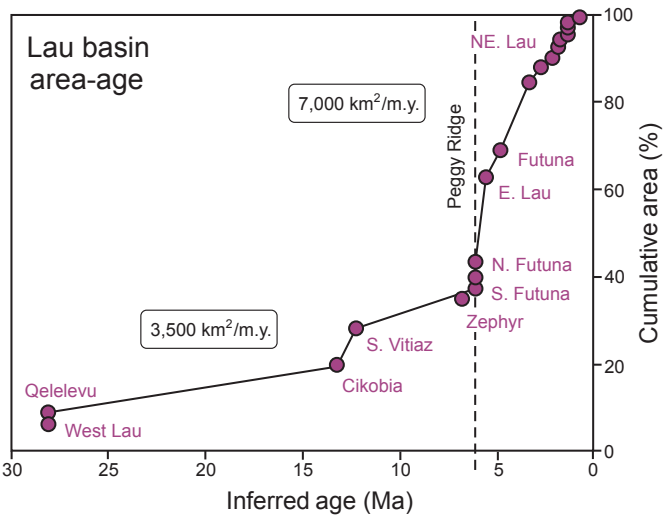

Fig. 16. Model of crustal growth of the Lau basin assemblages (back-arc crust only) based on area-age relationships in Stewart et al. (2022) and Table 1. The plot shows cumulative areas of the assemblages at the midpoints of their ages. A major pulse of crustal growth at ~5 Ma occurred when multiple spreading centers became active in the north of the basin. Growth rates jumped from an average of 3,500 km²/m.y. to more than 7,000 km²/m.y. after the appearance of Peggy Ridge.

Martinez, 2011; Sleeper et al., 2016). The significant expansion of the basin between 5 and 3 Ma coincided with the appearance of Peggy Ridge, and the accelerated growth during the last 3 m.y. produced the many small assemblages at the center of the basin.

The Lau Basin Microplate Mosaic

Chase (1971) first suggested several tectonic plates were needed to explain the opening of the Lau basin. The plates were defined in a number of different ways by Taylor et al. (1996), Zellmer and Taylor (2001), Martinez and Taylor (2002), Pelletier et al. (2001), Conder and Wiens (2011), and Sleeper and Martinez (2014, 2016). Other researchers also emphasized the highly variable geochemistry (Pearce et al., 1995; Eason and Dunn, 2015) and uneven seismic velocity of the plates (Dunn and Martinez, 2011; Arai and Dunn, 2014; Schmid et al., 2020). Zellmer and Taylor (2001) proposed a three-plate kinematic model involving the Australian Plate in the west, the Niuafo'ou microplate in the middle, and the Tonga platform in the east (Fig. 9). Baxter et al. (2020) reexamined this architecture by classifying the major faults in greater detail. They identified a cluster of seven microplates in the northern Lau basin that encompass most of the mapped assemblages (Fig. 11B; Table 2) with a total plate boundary length of more than 5,000 km and including 1,700 km of spreading centers. The four youngest microplates activated ~1,200 km of spreading centers in just the last 3 m.y.

The numerous microplates in the north of the Lau basin are products of the strong deformation associated with the subduction-transform edge propagator (STEP) fault occupying the former Vitiaz trench (now the Vitiaz fracture zone). Importantly, the identified microplates are not the same as the mapped assemblages, although they may share the same or similar names. The microplates are tectonic domains rather than lithostratigraphic packages and comprise crust of many different types (Table 2). Typically, they are bound by at least

Table 2. Lau Basin Microplate Mosaic and Assemblage Types (from Fig. 17)

Microplate	Included assemblages	Assemblage type	Area (km^2)	Area (%)	Total area (km^2)
Futuna	Futuna	Back-arc rifts and spreading centers	9,481	31.1	
	Northwest Lau basin	Back-arc rifts and spreading centers	2,263	7.4	
	Peggy Ridge	Leaky transform, deformation zone	1,283	4.2	
	Qelelevu	Relict back-arc crust	14	<0.1	
	South Futuna	Relict back-arc crust	15,152	49.7	
	Southeast Futuna	Relict back arc, back-arc shield volcano	2,321	7.6	30,513
Rochambeau	North Futuna	Relict back-arc crust	2,584	19.8	
	North Lau fore arc	Fore-arc crust	8	<0.1	
	Rochambeau	Back-arc rifts and spreading centers	4,328	33.1	
	South Vitiaz	Deformation zone	605	4.6	
	Southeast Futuna	Relict back arc, back-arc shield volcano	5,538	42.4	13,063
North Lau	Fonualei	Back-arc rifts and spreading centers	18	0.1	
	Mangatolu	Back-arc rifts and spreading centers	502	2.2	
	Niuafo'ou	Back-arc shield volcano	1,238	5.5	
	North Fonualei	Relict back arc	9,965	44.5	
	North Lau fore arc	Fore-arc crust	4,485	20.0	
	Northeast Lau basin	Back-arc rifts and spreading centers	3,966	17.7	
	Rochambeau	Back-arc rifts and spreading centers	2,222	9.9	22,396
Niuafo'ou	Central Lau basin	Back-arc rifts and spreading centers	5,011	6.0	
	East Lau basin	Back-arc rifts and spreading centers	28,759	34.6	
	Fonualei	Back-arc rifts and spreading centers	9,063	10.9	
	Mangatolu	Back-arc rifts and spreading centers	714	0.9	
	Niuafo'ou	Back-arc shield volcano	2,271	2.7	
	Northwest Lau basin	Back-arc rifts and spreading centers	2,361	2.8	
	Peggy Ridge	Leaky transform, deformation zone	1,711	2.1	
	Rochambeau	Back-arc rifts and spreading centers	1,583	1.9	
	Southeast Futuna	Relict back arc, back-arc shield volcano	84	0.1	
	Zephyr	Relict back-arc crust	31,580	38.0	83,137
North Tonga	Fonualei	Back-arc rifts and spreading centers	7,061	8.4	
	Mangatolu	Back-arc rifts and spreading centers	654	0.8	
	North Lau fore arc	Fore-arc crust	1,312	1.5	
	Northeast Lau basin	Back-arc rifts and spreading centers	3,950	4.7	
	Tofua arc	Arc crust	26,152	31.2	
	Tonga fore arc	Fore-arc crust	19,863	23.7	
	Tonga Ridge	Relict arc crust	24,957	29.7	83,950
South Tonga	East Lau basin	Back-arc rifts and spreading centers	22,694	14.1	
	Tofua arc	Arc crust	32,234	20.0	
	Tonga fore arc	Fore-arc crust	44,270	27.4	
	Tonga Ridge	Relict arc crust	62,292	38.6	161,490

Note: Cikobia-Balmoral microplate is not included

one active spreading center and therefore share assemblages with adjacent microplates. This relationship is best illustrated by overlaying the microplate framework on the assemblage map (Fig. 17). For example, it is clear that half of the Fonualei assemblage is accreted to the North Tonga plate and the other half to the Niuafo'ou microplate; the assemblage is bisected by the plate boundary along the Fonualei rift. Some of the larger microplates, like Niuafo'ou, may include both young and old crust from as many as 10 different assemblages. This relationship has implications for the interpretation of assemblages and assemblage boundaries in older volcanic terranes.

The microplates in the north are decoupled from the much simpler spreading regime in the south by Peggy Ridge (Wetzel et al., 1993; Baxter et al., 2020). The mappable features that mark the microplate boundaries include rift grabens, overlapping spreading centers, nodal basins at rift terminations, extensional transform zones, plume-related shield volcanoes, and central volcanic complexes, often located at triple junctions. Microplate boundaries that cross assemblages of different ages are a strong indication of propagating rifts. Figure 11 compares the interpreted microplate mosaic to the map of formations in the same area highlighting these features, and several examples of microplate boundaries mapped at 1:100,000 to 1:200,000 are shown in Figures 18 and 19. The individual microplates are described below.

Many of the plate boundaries are only partly continuous, and so their full geometry is not always certain. The boundaries can evolve rapidly in response to plate rotation, from strike-slip or transtensional to fully extensional (and back again) in less than a million years. As a result, the associated magmatic and hydrothermal activity may be highly episodic and abruptly terminated by overlapping spreading centers or ridge jumps. This style of growth has been difficult to model because of the lack of obvious magnetic chrons for dating the different events (e.g., Sleeper and Martinez, 2016). However, kinematic models that take into account far-field stresses and major plate motions can reproduce the progression of microplate formation (Baxter et al., 2020).

North Tonga microplate

The North Tonga microplate is bound by the Tonga trench in the east, the Vitiaz fracture zone in the north, and the Fonualei rift and Northeast Lau spreading center in the west (Figs. 11, 17). It comprises mostly relict arc crust of the Tonga Ridge, the Tonga fore arc, and the presently active Tofua arc. Several major structures in the arc basement cut across the

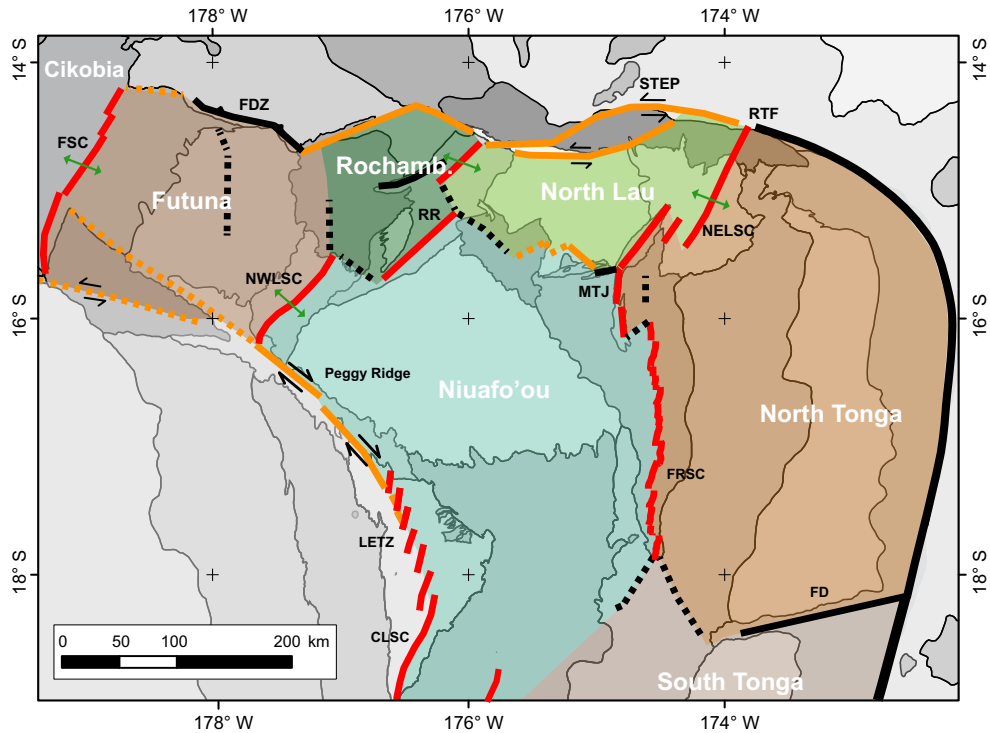

Fig. 17. Overlay showing the relationship between interpreted microplate boundaries and mapped assemblages of the northern Lau basin. Microplates from Figure 11B are highlighted as semitransparent polygons in contrasting colors and described in Table 2. The assemblages from Figure 10B are shown in grayscale in the background. Microplates are structures that may include crust from multiple assemblages. The assemblages are lithostratigraphic units that originate at plate boundaries where they may be accreted to several different microplates. As an example, the Fonualei assemblage, which originates at the Fonualei rift and spreading center (FRSC), is partly accreted to both the North Tonga plate and the Niuafo'ou plate, and the active spreading center is the boundary between the two plates. The Niuafo'ou microplate comprises crust from as many as 10 different assemblages, including active back-arc rift and spreading center crust (55% by area), relict spreading center crust (35%), rifted arc crust (5%), and crust from intraplate volcanic fields and central volcanoes (5%). Abbreviations: CLSC = Central Lau spreading center, FD = Fonualei discontinuity, FDZ = Futuna deformation zone, FSC = Futuna spreading center, LETZ = Lau extensional transform zone, MTJ = Mangatolu triple junction, NELSC = Northeast Lau spreading center, NL = Niuatapupu lineament, NWLSC = Northwest Lau spreading center, PR = Peggy Ridge, RR = Rochambeau rifts, RTF = ridge-trench-fault triple junction, STEP = subduction-transform edge propagator.

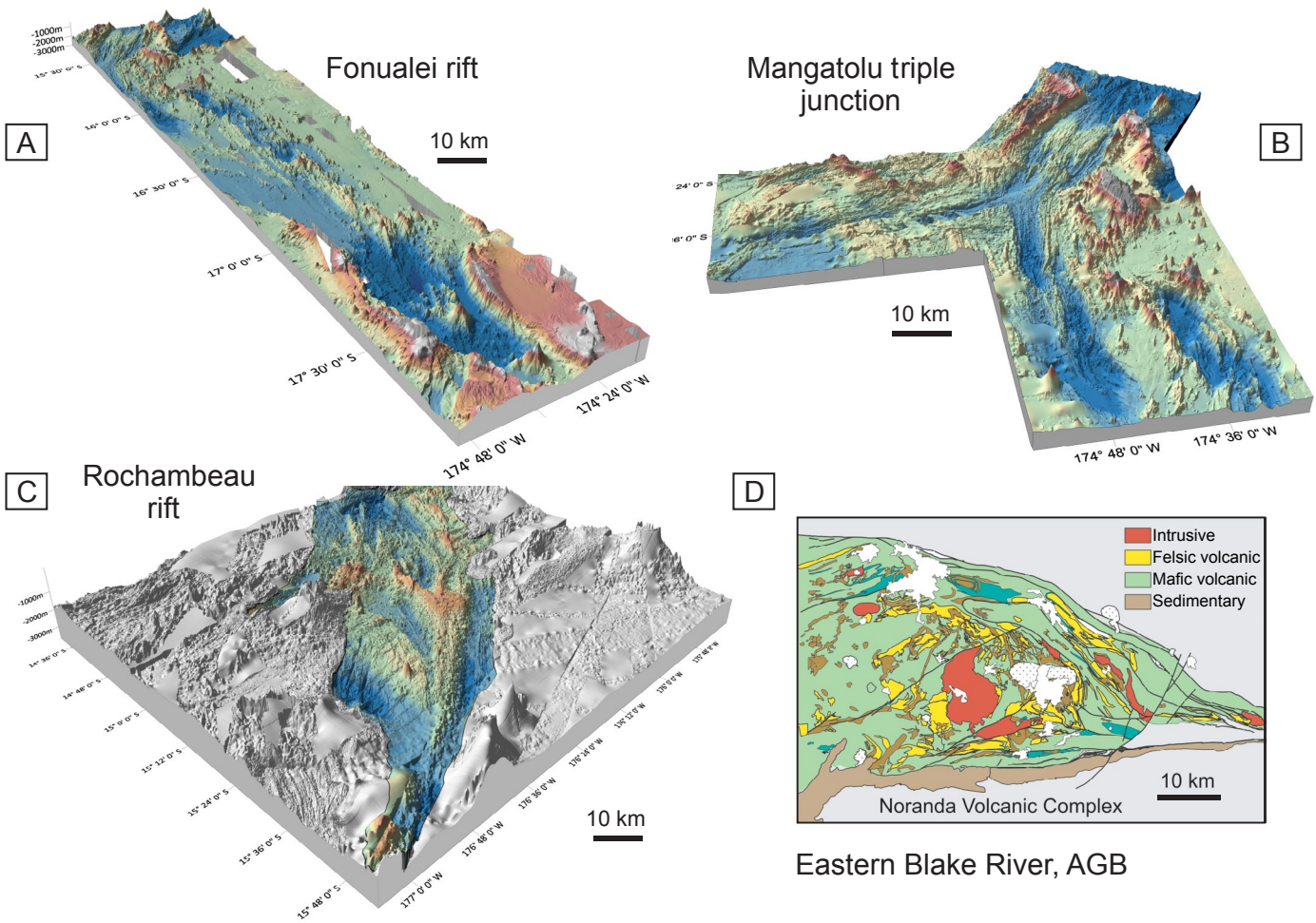

Fig. 18. 3-D bathymetric perspectives of different volcanic complexes of the Northeast Lau basin (all at the same scale). (A) Fonualei rift and spreading center (FRSC) from Hannington et al. (2019). The rift is propagating south into a deep depression at the rift tip a few tens of km in length and 3,000 m deep. Dike-centered volcanic complexes are distributed along the length of the rift as isolated ridges and cones. (B) Mangatolu triple junction (MTJ) from Mensing (2019). The three limbs of the triple junction include a failing southwest arm, en echelon rifts of the southeast arm, and a superinflated northeast arm. Each arm is 50 to 100 km in length. (C) Rochambeau rift (RR) from Ryan (2023) showing a volcanically robust ridge segment overgrown by a centrally located shield volcano. The axial volcano has a circular caldera several kilometers in diameter. (D) Simplified geologic map of the Eastern Blake River Group of the Abitibi greenstone belt (AGB), centered on the Noranda Volcanic Complex (from Monecke et al., 2017b). The image offers a same-scale comparison with the volcanic complexes at the FRSC, MTJ, and RR.

Tonga platform and appear to be controlling the breakup of the microplate at the Fonualei discontinuity in the south and the Niuatoputapu lineament in the north. They delimit uplifted portions of the Tonga Ridge and may play an important role in the location of future plate boundaries (e.g., connecting to the Fonualei rift in the south). However, there is currently a lack of seismicity on both structures, and we are still uncertain how they formed (Baxter et al., 2020).

Niuafo'ou microplate

The Niuafo'ou microplate is the largest of the seven microplates, at 90,000 km^2, occupying nearly half of the basin. It is bordered by the Fonualei rift in the east and by the Central Lau spreading center, Lau extensional transform zone, and Peggy Ridge in the west. The plate boundaries in the north and south are less certain but include the Mangatolu triple junction, Rochambeau rifts, and Northwest Lau spreading center in the north and highly deformed terrane in the south. The microplate comprises crust from 10 different assemblages (Fig. 17; Table 2), dominated by accretion from back-arc spreading centers that surround the plate (56% of the microplate by area) and by relict back-arc crust in the center of the plate (36% of the microplate). Some large, isolated blocks in the middle of the plate are thought to be pieces of the former Vitiaz arc that were transferred to the back-arc basin during rifting (a process referred to by Patriat et al., 2015, as "tectonic nibbling"). Lava flows from the Niuafo'ou Volcanic Complex and southeast Futuna volcanic field cover ~5% of the plate.

The active spreading centers and extensional transforms bordering the microplate have a total strike length of 1,400 km. Based on the aggregate spreading rates (Fig. 9), the microplate is expanding by as much as 50,000 km^2/m.y. (see also Baxter et al., 2020). However, the accretion has been highly asymmetric and episodic, and a mature back-arc spreading

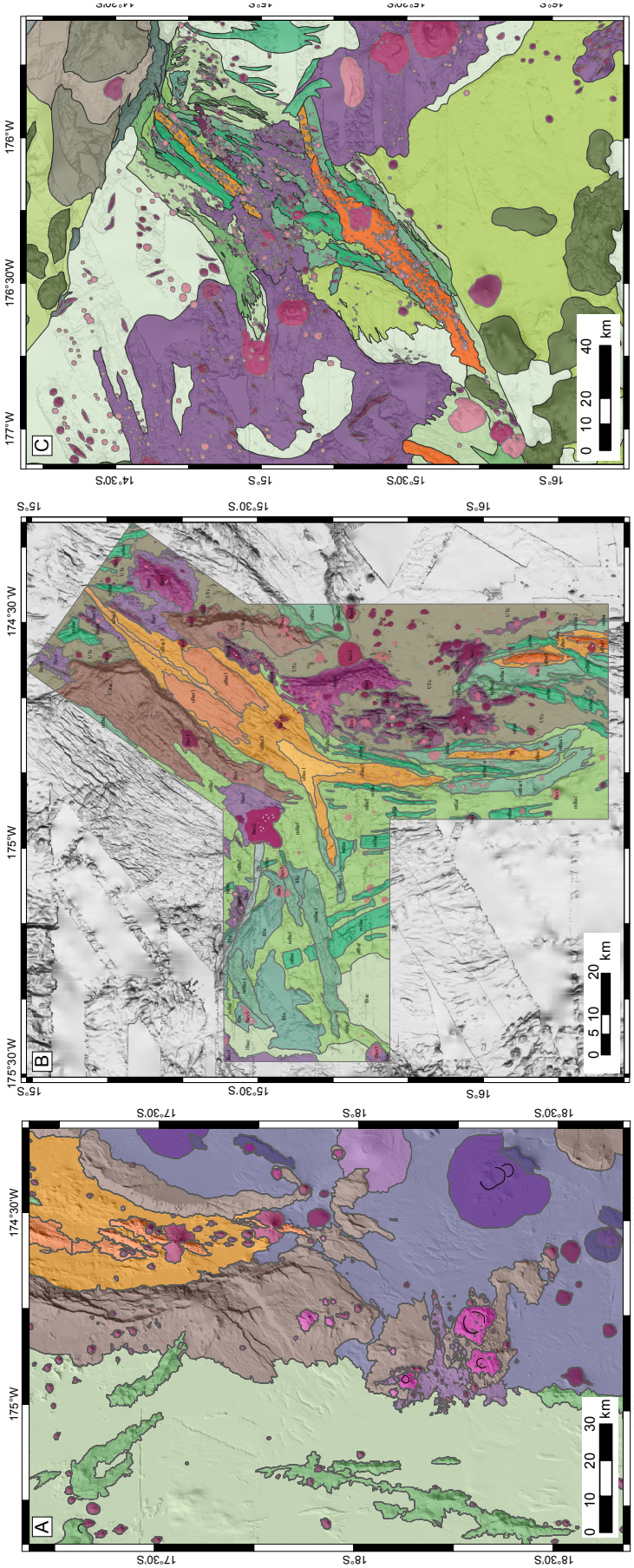

Fig. 19. 1:250,000 geologic maps of the major volcanic features of the Fonualei rift and spreading center (FRSC), Mangatolu triple junction (MTJ), and Rochambeau rift (RR). The legend corresponds to the units listed in Figure 10C; the sources are indicated in Figure 18. (A) Southernmost tip of the FRSC showing a dike-centered volcanic cone at nearly 3,000 m water depth and intense fracturing of arc crust on the walls of the rift. Voluminous pre-rift volcanics, including numerous young calderas, occur 30 to 40 km in advance of the propagating tip. (B) MTJ showing the super-inflated northeast arm, which is propagating northward into rifted arc crust of the Northeast Lau basin. (C) The large axial volcano on RR interpreted to be part of a plume-influenced ridge. The rift is surrounded by large volcanic flow fields of the Niuafo'ou shield volcano and the Southeast Futuna volcanic field. See Figure 18 for the same-scale comparison with the Eastern Blake River Group.

center like the Eastern Lau spreading center failed to develop because of repeated ridge jumps (Martinez and Taylor, 2006; Sleeper and Martinez, 2016). A paleo-spreading axis and plate boundary existed near the Tonga arc in the earliest stages of growth (proto-Eastern Lau spreading center), but the currently dominant spreading systems are now at the Central Lau spreading center and Lau extensional transform zone in the west and the Fonualei rift in the east (Zellmer and Taylor, 2001). Volcanic rocks sampled at the different spreading centers are products of distinctly different melt sources (Keller et al., 2008; Escrig et al., 2012; Fassbender et al., 2023, 2024; Jegen et al., 2023).

The microplate boundary along the Fonualei rift occupies a position behind the active volcanic front of the Tofua arc. This contrasts with the earlier Miocene rifting of the Vitiaz arc, which initiated in the old fore arc. From north to south, the plate boundary at the Fonualei rift steps progressively eastward towards the Tofua arc, with the distance to the volcanic front decreasing from about 75 km at 16°S to less than 20 km at 18°S (Zellmer and Taylor, 2001). The plate boundary is defined by a series of en echelon grabens, each ~50 km long and ~20 to 30 km wide, at 2,400-m water depth in the north and dropping to more than 3,000-m depth in the south. Early estimates of spreading at 28 mm/yr (Zellmer and Taylor, 2001; Ruellan and Lagabrielle, 2005) have been revised to 94 mm/yr at 16°S and 47 mm/yr at 18°S where the rift impinges on the arc. One model suggested a pole of rotation near 20° to 25°S (Zellmer and Taylor, 2001); another model suggested that the pole was closer to 18°30′S, which would reduce the opening rate further to as little as 18 mm/yr (Conder and Wiens, 2011). The most recent model by Sleeper et al. (2016) has settled on a spreading rate of only 8 mm/yr in the southernmost Fonualei rift. The slow spreading is in agreement with the overall lack of seismicity (Sleeper and Martinez, 2016; Baxter et al., 2020), with few shallow earthquakes in the southernmost rift zone confirming mainly normal faulting at the rift tip (Baxter et al., 2020).

The axial zones of the rift segments are intruded by elongate NNE-trending volcanic ridges, 10 to 20 km long and 8 to 15 km wide, that rise 200 to 600 m above the floors of the rifts (Fig. 18A). The largest of these volcanic features, in the southernmost Fonualei rift, is 1,000 m high and cut by a major, 18-km-long dike complex resembling a fissure volcano. The shift in axial morphology from semicontinuous volcanic ridges north of 17°S to isolated cones and fissure volcanoes south of 17°S is interpreted to reflect along-axis variation in the focusing of melt as the opening rates decrease from north to south (Sleeper et al., 2016).

The structure of the Fonualei rift fits well with different models of arc rifting (e.g., Stern et al., 1984; Cathles and Hallam, 1991). Narrow, deep grabens with short, trough-like subbasins, like the southern tip of the Fonualei rift, are characteristic when rates of extension and subsidence exceed the magmatic input (Martinez and Taylor, 2002). High rates of deposition of volcaniclastic material from the adjacent volcanic arc create the smooth floors of the grabens. At the southernmost Fonualei rift, faulting and local volcanism can be traced for almost 100 km in advance of the propagating tip before disappearing into less disturbed arc crust (Fig. 19A). However, the connection to the adjacent back arc is obscured. Conder and Wiens (2011) suggested that the area between the southern tip of the Fonualei rift and the Central Lau spreading center, referred to as the Central Lau nanoplate, should be accommodating ~45 mm/yr of strain. This area is characterized by complex intersecting fabric with a number of rotated back-arc crustal blocks stranded among sediment-filled "nodal" basins at the northern termination of the Eastern Lau spreading center. No clear structures forming a southern boundary of the Niuafo'ou microplate can be seen that link the Eastern Lau spreading center to the Fonualei rift, although notably thinned crust is suggested here by recent gravity inversions (Fig. 14). The young volcanic field south of the Fonualei rift is possibly a manifestation of an emerging microplate boundary and triple junction that would connect the Eastern Lau spreading center, Fonualei rift, and Fonualei discontinuity.

In the north, the boundary of the Niuafo'ou microplate is defined by the Mangatolu triple junction; however, it is unclear if the southeast arm of the triple junction is advancing south to meet the Fonualei rift, or if the Fonualei rift will join with the southward propagating Northeast Lau spreading center to complete the plate boundary (Jegen et al., 2023). The continuation of the west arm of the Mangatolu spreading center toward the Rochambeau rifts is obscured by the large volcanic flow field of the Niuafo'ou volcano (Fig. 11C). In the northwest, the plate boundary is more clearly defined by the Northwest Lau spreading center, Rochambeau rifts, and at least 200 km of the Peggy Ridge transform.

North Lau microplate

The interpreted northern boundary of Niuafo'ou is shared with a number of indistinct microplates bordering the Vitiaz lineament (Figs. 11, 17). The plates are partly obscured by a nearly 300-km-long alignment of large submarine volcanoes that include the Niuafo'ou volcanic complex. The North Lau microplate, in particular, is bound by major left-lateral shear zones related to the transition from subduction to basin opening (Conder and Wiens, 2011; Baxter et al., 2020). To the north, the Vitiaz lineament and eastward extension of the Futuna deformation zone separate the back arc from the dismembered fore-arc crust of the former Vitiaz arc.

In the northeast, wrench tectonics associated with the STEP fault are causing rifting of the relict fore-arc crust at the north end of the Northeast Lau spreading center (Embley et al., 2014; Anderson et al., 2021). Baxter et al. (2020) suggested a small microplate might be forming here between the Northeast Lau spreading center and the Mata volcanoes. Anomalous magmatism, including the Niuatahi dacite volcano and boninites of the Northeast Lau basin assemblage, is thought to be related to a ridge-trench-fault (RTF) triple junction forming at this location (Escrig et al., 2012; Regelous et al., 2014). The intense deformation across the entire region seems to indicate the northernmost part of the basin is actively breaking up.

Rochambeau microplate

The smaller Rochambeau microplate in the west is dominated by crust from the Rochambeau rift spreading centers and the southeast Futuna volcanic field, which are similar in age to the Niuafo'ou volcanic field and Northwest Lau spreading center (mostly younger than 1 Ma: Stewart et al., 2022). The south-

east Futuna volcanic field and Rochambeau bank are major volcanic outpourings that connect the two dominant spreading centers, Rochambeau rifts and the Northwest Lau spreading center, but obscure much of the plate boundary (Parson and Tiffin, 1993; Pelletier et al., 2001).

Futuna and Cikobia-Balmoral microplates

The Futuna microplate in the northwest of the basin is bordered by the Northwest Lau spreading center, the Peggy Ridge transform in the south, and the Futuna deformation zone in the north. It comprises 40,000 km^2 of mostly relict back-arc crust but also younger crust from the still-active Northwest Lau spreading center and Futuna spreading center (Pelletier et al., 2001). The Cikobia-Balmoral microplate, farther west, belongs to the North Fiji basin but is partly formed by westward accretion at the Futuna spreading center. It is one of three microplates that form the North Fiji basin orogenic zone (Bird, 2003; Baxter et al., 2020).

The Peggy Ridge transform cuts some of the oldest crust in the Lau basin belonging to the Futuna microplate and the Qelelevu block, but also some of the youngest crust of the Niuafo'ou microplate at the Lau extensional transform zone. It is one of the longest-lived structures in the region, initiated during early rotation of the Fiji platform at ~10 Ma (Taylor et al., 2000; Martin, 2013).

Imaging the plate boundaries

Crustal growth and microplate formation in the Lau basin have been occurring at time and length scales much smaller than those suggested by regional kinematic models. The strong influence of plate rotation and deformation is seen in patterns of crustal magnetization, which are broadly at right angles to the opening at the basin scale (Fig. 12C) but oblique to the east-west accretion at a finer scale (Fig. 13A). Regional Bouguer gravity anomalies reflect the broad compositional variation of the mapped assemblages (Fig. 12B), but higher-resolution ship-based data show much greater complexity (Figs. 13B, 14B). Seismic reflection shows the "edges" of the Niuafo'ou microplate are intricate deformation zones, 80 to 100 km wide, that include large blocks of relict arc crust, newly formed back-arc crust and sedimentary basins filled with volcaniclastic material from the nearby arc (Fig. 20). This complexity is a result of the plate boundary repeatedly jumping to the east (now in the Fonualei rift and spreading center). Some parts of the plate boundary are heavily intruded by magma, indicated by shallow reflectors that coincide with intraplate volcanism. Elsewhere, hundreds of meters to kilometers of buried structural relief are seen with isolated reflectors that are interpreted as possible focal points for hydrothermal upflow (Schnabel et al., 2022; Kehew, 2023: Fig. 20C). In the west, the plate boundary is more clearly defined by a discrete crustal-scale shear zone (PR shear) underlying Peggy Ridge (Fig. 20A).

The refraction data indicate a crustal thickness of about 10 to 15 km at the Fonualei rift with a strongly undulating mantle topography under the plate boundary (Fig. 21). A positive excursion in the Moho occurs immediately under the Fonualei rift, with a vertical displacement of nearly 5 km over a lateral distance of only 30 km. The mantle rise at the plate boundary is also shown by a strong positive Bouguer anomaly in the ship-based gravity (Fig. 13B). The elevated mantle spans nearly the entire 140-km distance between the Fonualei rift and Peggy Ridge at this location (Fig. 21). The seismic velocities confirm mostly lower density felsic crust under the arc and higher density mafic crust and intrusions in the back arc. However, strong lateral variation in the velocities in the lower crust are consistent with a microplate that is far from uniform in composition. Between the Fonualei rift and the volcanic front of the arc, coincident low-velocity anomalies and a gravity low (Fig. 13) have been interpreted as accumulation of felsic melt (Schmid et al., 2020). This might correspond to the magma being captured from the arc, as suggested by the local volcanic geochemistry (Keller et al., 2008; Escrig et al., 2012). A steeply dipping high conductivity zone in the southernmost Fonualei rift revealed by magnetotellurics (Franz et al., 2021; Jegen et al., 2024) coincides with a zone of intense microseismicity (Schmid et al., 2021) and may indicate hydrothermal fluid or intrusion of melt or both at the plate boundary.

Triple junction formation

Triple junctions are the hallmarks of microplate formation. Every new microplate produces at least two triple junctions (Rey and Mueller, 2010), and so major pulses of crustal growth governed by microplate breakouts are triple junction factories. The complex fabrics associated with triple junctions reflect changes in stresses that cause microplate formation and have a large structural and magmatic footprint (e.g., Matthews et al., 2016). Fault density is strongly correlated with the locations of triple junctions (Fig. 22), which are abundant at tightly arcuate boundaries (i.e., where contrasting surface velocities create differential stress and promote plate fragmentation: Schellart and Lister, 2004; Moresi et al., 2014; Mallard et al., 2016). Triple junctions are almost always centers of enhanced magmatic activity, owing to the crustal permeability created by intersecting faults and spreading centers. Because of the strong focusing of melt, they are sometimes obscured by large central volcanic complexes or shield volcanoes. Many are centers of mantle upwelling with distinctive melt compositions. In certain configurations, triple junctions can remain stable for millions of years, for example, if the regional stress field is perfectly isotropic, such as in ridge-ridge-ridge (RRR)-type triple junctions (McKenzie and Morgan, 1969; Cronin, 1992). However, these are rare. Most triple junctions are inherently unstable and abandoned by ridge jumps or simply terminated by free-slip boundaries, such as at ridge-transform intersections.

The Mangatolu triple junction is the largest triple junction in the Lau basin, measuring 50 to 100 km across (Fig. 18B) and overlapping the northernmost spreading segment of the Fonualei rift. The interpreted microplate mosaic (Fig. 17) suggests other triple junctions should be widespread. One may underlie the major volcanic fields of the southeast Futuna volcanic zone, possibly connecting the Rochambeau rifts and Northwest Lau spreading center (Fouquet et al., 2015; Konn et al., 2016); another connecting the Mangatolu triple junction and Rochambeau rifts may be obscured by the Niuafo'ou volcanic complex. Both volcanic fields are characterized by an unusual volume of melt and clear mantle signatures that may be related to the concealed triple junctions (Turner and Hawkesworth, 1998; Lupton et al., 2012, 2015). The north-

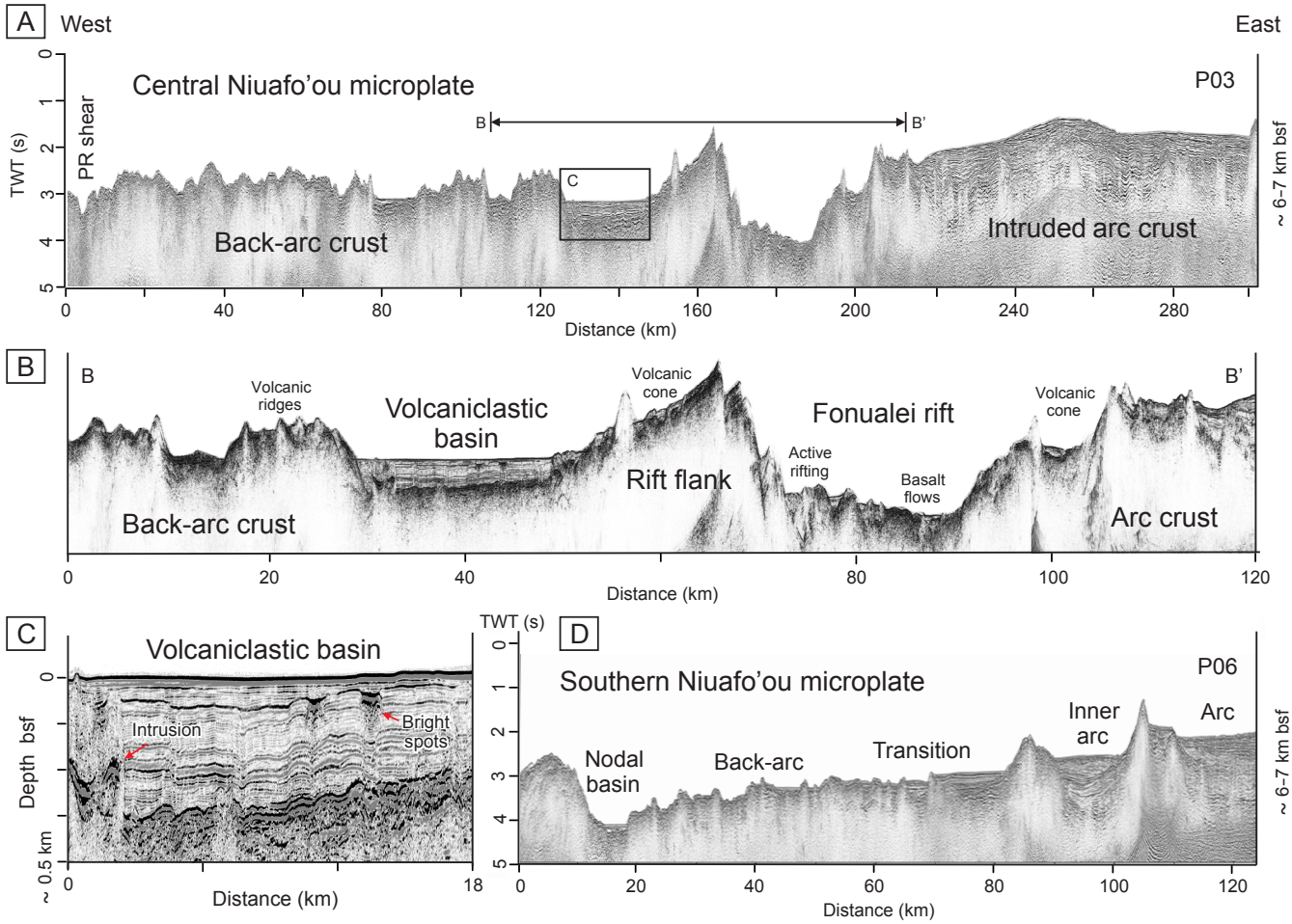

Fig. 20. Multichannel seismic (MCS) profiles across the Niuafo'ou microplate from Schnabel et al. (2019). MCS data and subbottom profiles were collected along several transects from the present-day arc front, across the back arc, to the Peggy Ridge shear zone (profile locations in Fig. 9C). Six G-Gun clusters with a total volume of 84 l were fired at –190 bar every 50 m for the MCS and 170 m for the refraction lines (see Hannington et al., 2019; Fig. 21). MCS data were recorded with a 3.9-km-long streamer towed behind the vessel. The crust was imaged to a depth of 7 km in the reflection profiles and then 20 km in the refraction lines. (A) MCS data of the central Niuafo'ou microplate from line P03 (300 km). In the west, the plate margin is defined by a near-vertical crustal-scale shear zone (part of Peggy Ridge, PR). (B) Annotated close-up (B-B′) of the arc-to-back-arc transition from A. Normal faults dip eastward in the western part of the Fonualei rift and spreading center (FRSC) and westward within the volcanic arc. (C) Low-frequency Parasound subbottom profiler image of buried features in the back-arc volcaniclastic basin (box in A). Some parts are heavily intruded by magma, and some have shallow reflectors and "chimneys" interpreted to be magmatic sills and hydrothermal upflow zones (bright spots in C: Schnabel et al., 2022; Kehew, 2023; see text for discussion). (D) MCS data of the southern Niuafo'ou microplate from line P06 (120 km). The transition between the arc crust of the Tonga plate and the back-arc crust of the Niuafo'ou microplate is a broad, 80- to 100-km-wide deformation zone that includes large blocks of rifted arc crust as well as sedimentary basins filled with volcaniclastic material shed from the retreating arc. The complexity of the plate boundary is a result of repeated jumps in spreading to the east (now in the FRSC in the north), and the seismic data show hundreds of meters to kilometers of subseafloor structural relief.

ern termination of the Northeast Lau spreading center is a ridge-trench-fault triple junction, where back-arc spreading intersects the old Vitiaz fore arc and lineament. Second-stage melting at this location is thought to be the source of boninitic magma at the Mata volcanoes (Falloon et al., 2007; Resing et al., 2011; Regelous et al., 2014), although a heterogeneous upper mantle in this area adds significant complications (Haase et al., 2022).

At the southern propagating tip of the Fonualei rift, we mapped crustal thinning in several different directions suggesting the early stages of triple junction formation (Hannington et al., 2019: Fig. 19A). The southwest arm projects toward the thinned crust at the southern boundary of the Niuafo'ou microplate (Fig. 14B) and could eventually connect to form a new triple junction with the Fonualei discontinuity, solving the problem of the missing strain in the area of the Central Lau nanoplate.

Crustal permeability, melting, and hydrothermal activity

Triple junction formation and distributed extension among a large number of small plates result in highly variable magmatic activity, ranging from high rates of extrusion at axial volcanoes to little or no volcanism between rift segments (Eason and Dunn, 2015; Anderson et al., 2016; Sleeper et al., 2016).

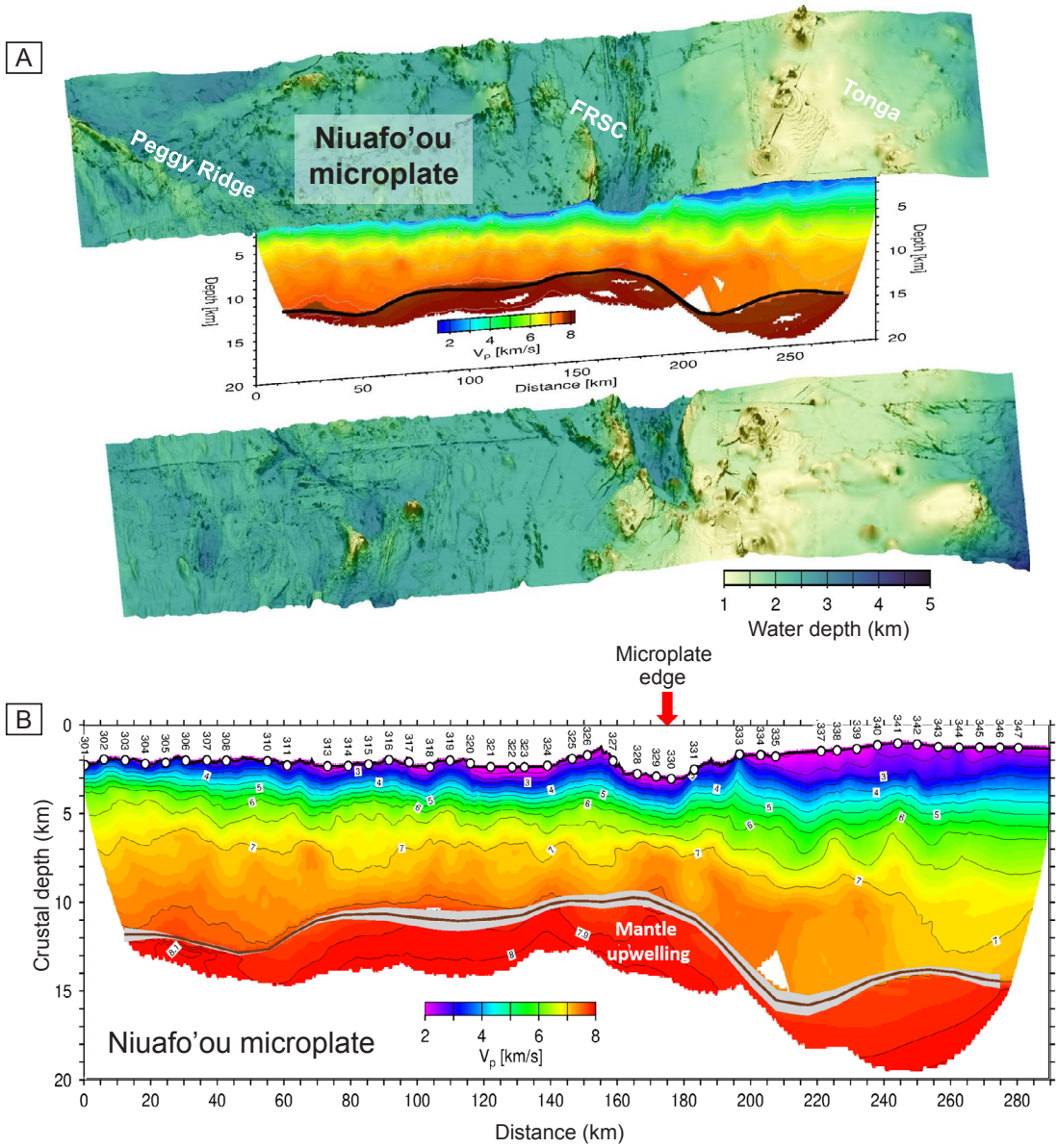

Fig. 21. (A) P-wave tomography (velocity) model of Schmid et al. (2020) corresponding to the multichannel seismic (MCS) line P03 in Figure 20, with bathymetry shown adjacent to the profile. The upper crust and lower crust are at 2.5 < Vp < 6.5 km s^{-1}. The modeled Moho is at 8 km s^{-1}. (B) Details of the velocity model showing the strong compositional heterogeneity (i.e., velocity differences) in the lower crust. The contour interval is 0.5 km s^{-1}. The band along the Moho reflector is the calculated uncertainty from Schmid et al. (2020). The crust is 10 to 15 km thick beneath the arc, with a clear excursion in the mantle of at least 5 km at exactly the location of the plate boundary. Notable is the correlation between the mantle topography and the observable geology at the sea floor. The sea-floor structures mark a distinct mantle domain underlying the microplate with the zone of upwelling spanning ~140 km in width. Abbreviation: FRSC = Fonualei rift and spreading center.

Continuously deforming microplates, including some parts of Niuafo'ou, are notably sieve-like, evidenced by the significant numbers of small intraplate volcanoes. Although intense magmatism is focused at triple junctions and propagating rifts, there is still uncertainty about the manner in which melt rises through the crust and at what stage of plate fragmentation the melts may be focused (Zellmer et al., 2005; Stern et al., 2013). Highly variable melting can occur (Fig. 23), especially at ridge-arc intersections (e.g., Deschamps and Lallemand, 2003; Resing et al., 2011; Regelous et al., 2014) and slab tears (e.g., Turner and Hawkesworth, 1998; Nebel and Arculus, 2015). These findings have important implications for interpreting volcanic rock compositions at the same scale in greenstone belts (Fassbender et al., 2023, 2024).

Continuously evolving crustal permeability in a microplate framework is also a major constraint on fluid flow. During deformation, some pathways remain open to fluids and others may be blocked (e.g., Ruellan et al., 2003). The permanence of the pathways and the episodic nature of the magmatic and hydrothermal activity, such as the release of crustal fluids by tectonic switching (e.g., Huston et al., 2016), is strongly influenced by the geometry of the microplates. Although there are many near-

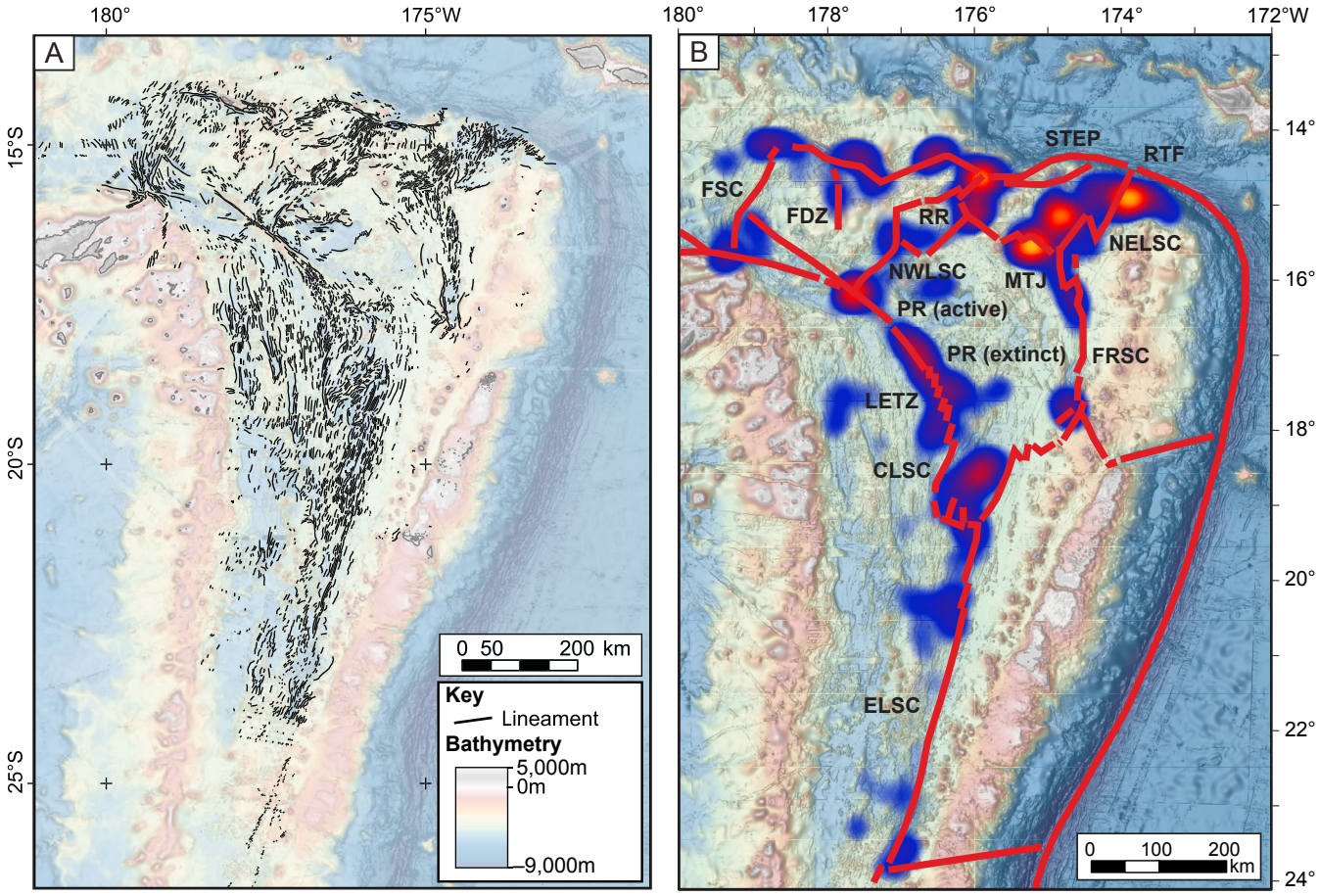

Fig. 22. (A) Mapped lineaments in the Lau basin after Baxter et al. (2020). A total of 4,075 lineaments were mapped from bathymetric data and vertical gravity gradient. (B) Heat map corresponding to the number of intersections between the mapped lineaments. Structures that would intersect within 5 km of their mapped terminations are included. The heat map was calculated using a kernel density function with a search radius of 10 km. The areas of maximum intersections correspond closely to the locations of known triple junctions. Abbreviations: CLSC = Central Lau spreading center, ELSC = Eastern Lau spreading center, FDZ = Futuna deformation zone, FSC = Futuna spreading center, LETZ = Lau extensional transform zone, MTJ = Mangatolu triple junction, NELSC = Northeast Lau spreading center, NWLSC = Northwest Lau spreading center, PR = Peggy Ridge, RR = Rochambeau rifts, RTF = ridge-trench-fault triple junction, STEP = subduction-transform edge propagator.

surface faults (e.g., Fig. 22A), shallow permeability is unlikely to be a primary control on hydrothermal upflow, which is most probably rooted in deeper crustal-scale structures at the plate boundaries (e.g., Ingebritsen and Manning, 2010; Rowland et al., 2012). The slow-spreading regimes of microplate mosaics could also promote enhanced hydrothermal activity owing to deeper circulation of fluids. The largest sea-floor hydrothermal systems tend to occur at slow- rather than fast-spreading ridges (Hannington et al., 2011; German et al., 2016), which contrasts with the long-standing view of increased hydrothermal venting at high spreading rates (Baker, 2007, 2017).

Comparison with Greenstone Belts

Comparisons with modern microplate tectonics are shedding light on some of the important considerations in the metal endowment of greenstone belts. The intense magmatic and hydrothermal activity of the northern Lau basin is thought to be related to its high heat flow (Wiens et al., 2006). Likewise, predicted mantle temperatures in the Archean were at least 150 to 200 degrees hotter than today (e.g., Herzberg et al., 2010: Fig. 8B), and heat loss two to three times greater (Bickle, 1986). In the modern oceans, heat flow is directly related to the amount of new crust being produced at the ridges (proportional to the cube root of the ridge length, $L^{1/3}$: Hargraves, 1986). In order to remove 2 to 3 times more crustal heat in the Archean than today, the ridges must have been 8 to 27 times longer (i.e., 2^3 to 3^3) for the same global spreading rates. Simple numerical modeling shows that an early Earth with 35 plates (e.g., Bleeker, 2003) would have had a minimum of 500,000 km of plate boundaries compared to the 60,000 km of ridges today (Abbott and Menke, 1990; Bird, 2003). Global hydrothermal convection would have been at least an order of magnitude greater (Lowell and Keller, 2003). By the simple rule that equates crustal accretion to ridge length × spreading rate, fast spreading would not have been required if the ridge system was longer. Instead, we suggest average spreading rates were slow, much as they are today, but distributed across many more plate boundaries.

Most authors agree the pulse of crustal growth at 2700 Ma represented a peak in extraction of melt from the mantle (Stein and Hofmann, 1994; Condie, 1998; Albarède, 1998; Hawkesworth et al., 2013; Condie et al., 2017). Other papers suggest

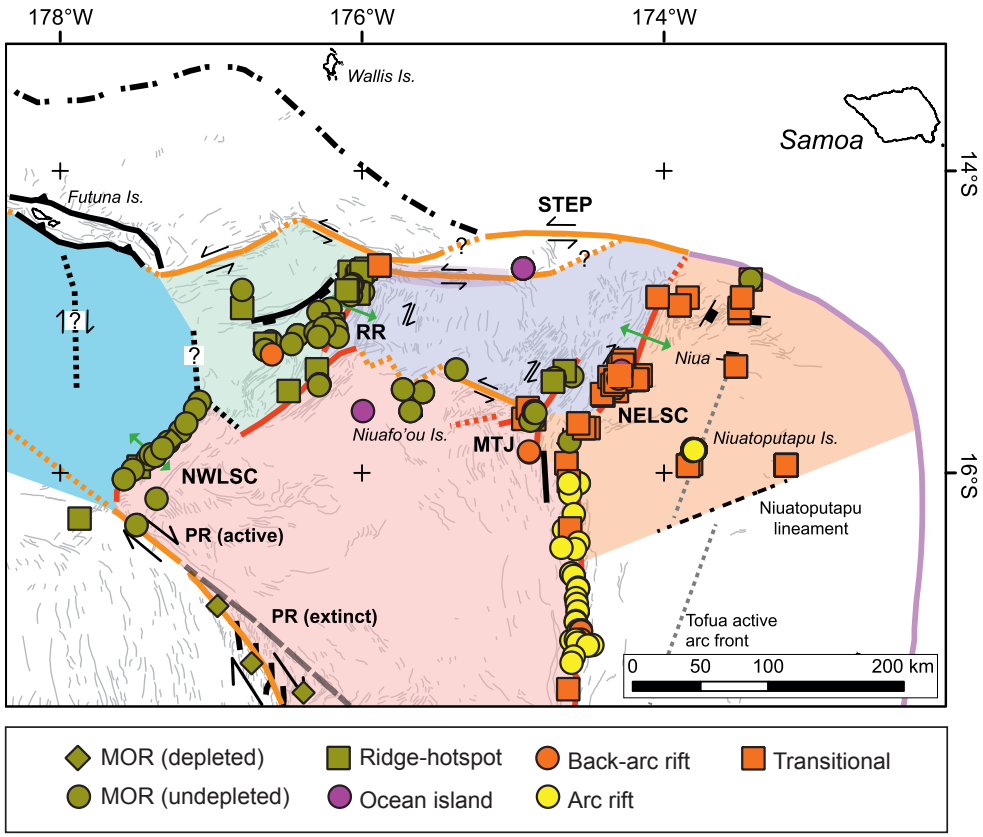

Fig. 23. Summary of mafic volcanic rock geochemistry from the northern Lau basin modified from Fassbender et al. (2024). The microplate outlines are from Figure 11B. Approximately 500 samples are represented. The data indicate a strong heterogeneity at the microplate scale, including melts with depleted mid-ocean ridge basalt (MORB)-like signatures (green diamonds) typical of Peggy Ridge (PR); MORB and enriched (E)-MORB (green squares and circles, respectively) at the Northwest Lau spreading center (NWLSC) and the Rochambeau rifts (RR); nascent back-arc rift signatures (orange squares and circles) such as the Mangatolu triple junction (MTJ) and Northeast Lau spreading center (NELSC); rifted arc and arc-related basalt (yellow circles) in the Fonualei rift and spreading center (FRSC); ocean island basalt (purple circles) typical of the Niuafo'ou volcanic complex. Abbreviation: STEP = subduction-transform edge propagator.

the pattern reflects enhanced preservation of crust during the assembly of the first large continents (Condie and Aster, 2009, 2010; Hawkesworth et al., 2009; Voice et al., 2011; Condie et al., 2017). However, evidence of anomalous melting correlated with the 2700 Ma peak supports a major pulse of crustal growth and not just greater preservation (Pearson et al., 2007; Condie et al., 2015; Wyman, 2018). We suggest the pulses of growth coincided with episodes of peak microplate formation, similar to that observed in the Lau basin today.

The Superior province of Canada is the largest exposed Archean craton, with an area of more than 1.5 million km² (Fig. 24). It comprises a number of distinct subprovinces assembled into E-W–trending granite-greenstone terranes and metasedimentary belts described by many authors (Langford and Morin, 1976; Ludden and Hubert, 1986; Ludden et al., 1986; Card, 1990; Jackson and Sutcliffe, 1990; Corfu, 1993; Jackson and Cruden, 1995; Card and Poulsen, 1998; Percival., 2007; Percival et al., 2012 and references therein). The Superior province is similar in scale to the entire Indo-Australian province and is thought to include many of the same or similar tectonic elements.

The greenstone belts have been described variously as successive lateral accretions of volcano-plutonic arcs, oceanic plateaus, and rift sequences. They are, in general, no larger than modern back-arc basins (e.g., Fig. 7B), and many are much smaller. Some of the greenstone belts were settings for prolific VMS formation (Franklin and Thorpe, 1982; Poulsen et al., 1992). Of the 170 known Archean VMS deposits worldwide, more than 130 are located in the Superior and Slave provinces; the remainder are widely distributed between Western Australia, north China, the Kaapvaal craton, Baltica, and Brazil (Fig. 24). The pulses of crustal growth that formed the best-endowed greenstone belts were the first to produce abundant juvenile oceanic crust together with island arc and back-arc-like crust (e.g., O'Neill et al., 2007; Cawood and Hawkesworth, 2015). Lead, Nd, and Hf isotopes, among other indicators, suggest a primitive crust distinct from other Archean cratons played a role in the spectacular mineral endowment of some belts (Huston et al., 2014; Mole et al., 2022). Nearly all of the VMS deposits in the Superior province are in the Abitibi greenstone belt (Mercier et al., 2014), which formed during a period of accelerating crustal growth (see below). The total tonnage of VMS deposits per km² of volcanic rock is nearly 10 times greater than anywhere else in the Superior province, implying a unique set of conditions responsible for the mineral endowment.

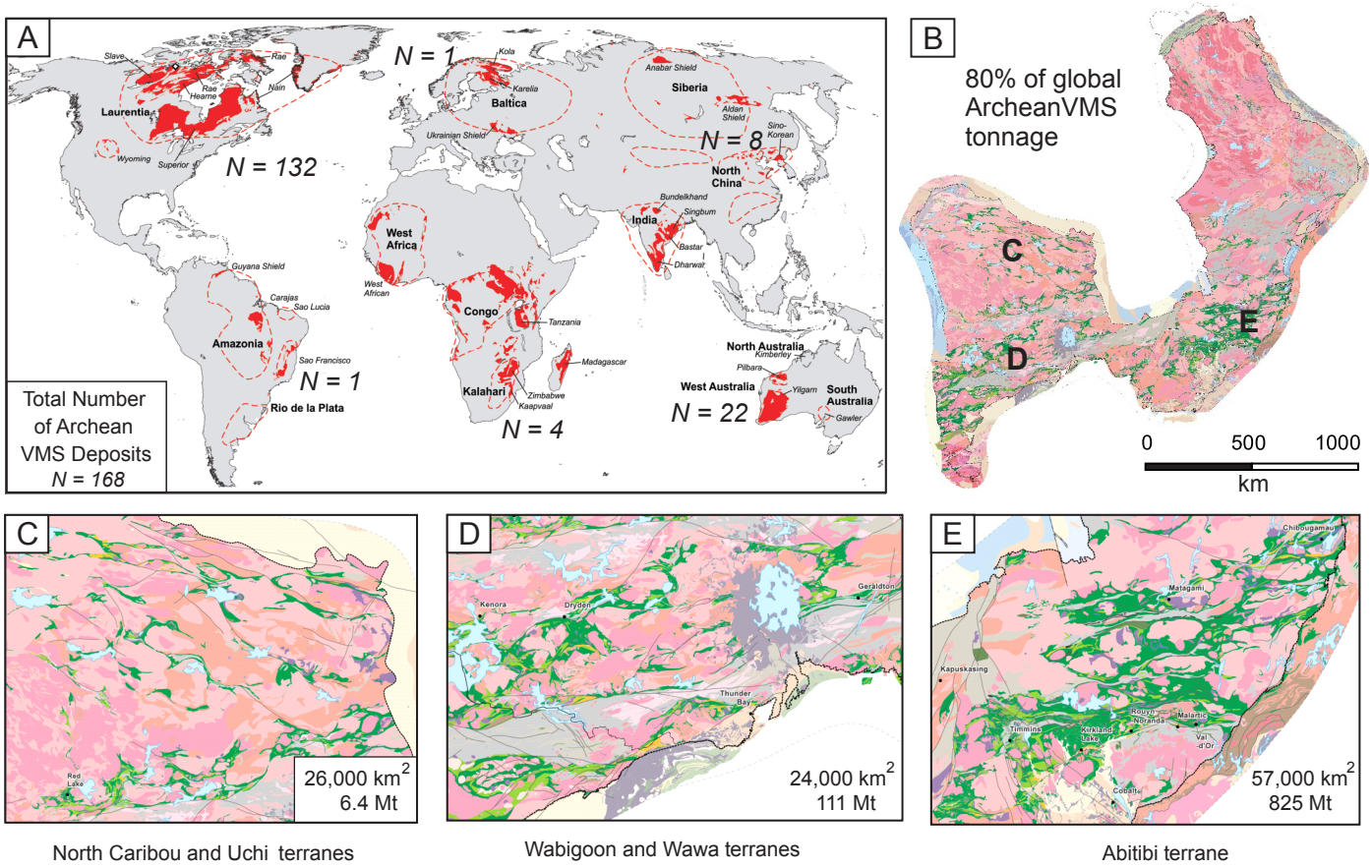

Fig. 24. (A) Global distribution of Archean cratons with numbers of contained volcanogenic massive sulfide (VMS) deposits (modified from Mercier-Langevin et al., 2014). Two thirds of all Archean VMS deposits are located in the Abitibi greenstone belt. (B) Inset geologic map of the Superior province of Canada showing the locations of the major greenstone belts from Montsion et al. (2018). (C-E) Comparison of the distribution of volcanic rocks in the Uchi (3000–2735 Ma), Wabigoon (2735–2726 Ma), and Abitibi (2735–2695 Ma) subprovinces and the corresponding tonnage of massive sulfide deposits: see Appendix Table A2 and data in Franklin et al. (2005). Areas in km² correspond to the total area of exposed volcanic rocks in each map.

Several authors have highlighted craton margins as the most favorable locations for large-scale mineral systems (Begg et al., 2010; Huston et al., 2014, 2023; Mole et al., 2015; Koursch and Doublier, 2016). However, the proposed terrane boundaries are thousands of km in strike length and therefore difficult to relate to specific ore districts. Lithoprobe transects confirmed the broad structure of the Superior craton but showed few details of the greenstone belts at the scale of even the largest hydrothermal systems (Thurston, 2015). The structures that define modern microplate mosaics, in contrast, are only a few hundreds of kilometers in size and therefore at the right scale to explain the focusing of melt and fluid flow. Recent surveys in the Abitibi, including the Discover Abitibi and Metal Earth transects (Snyder et al., 2008, 2021; Smith et al., 2023), provide much better images of the greenstone belt architecture that more closely match the scale of known magmatic and hydrothermal systems.

Greenstone belt architecture and endowment

A range of models have been advanced to explain the architecture of Archean greenstone belts, from vertical tectonics producing dome-and-keel structures to plume-driven and subduction-related processes (Thurston, 2015; Wyman, 2018). The interpretations are complicated by deformation and metamorphism, but many relationships have been preserved. Throughout most of the Superior province, metamorphic grades did not exceed greenschist facies, with subgreenschist assemblages common in parts of the Abitibi (Jolly, 1978; Powell et al., 1995). Although intense deformation, including folding, shearing, and dragging of units up against rising plutons, has strongly affected the crust (e.g., Hubert et al., 1984; Ludden and Hubert, 1986), the relative volumes, densities, and compositions of the rocks are largely preserved, and the Archean Moho is thought to be mostly intact (Benn, 2006; Galley et al., 2025).

Area-age relationships of the greenstone belts in the Superior province give a picture of the crustal growth (Fig. 25A; App. Table A2), which seems to indicate an increase in volcanism in the last 30 to 40 m.y. of craton assembly and a corresponding increase in endowment of VMS in the youngest rocks (Fig. 25B). Deeper erosion of the older assemblages likely accounts for the limited exposures of greenstone belts in the North Caribou and Uchi terranes (Fig. 24C-E), but the only way to account for differences in VMS endowment of similarly prospective rocks would be to selectively erode the most productive units in the older terranes. Some evidence

from the older parts of the craton in the Uchi subprovince argues for shallow submarine to subaerial conditions (e.g., Thurston et al., 1992a, b) that could have limited VMS formation. However, differential erosion and different conditions of ore formation cannot account for the contrasting VMS endowment of the younger belts. Metamorphic grades in the Abitibi, Wawa, and Wabigoon terranes suggest that they experienced the same or similar depths of erosion, and there appear to be few differences in the conditions of mineralization—VMS deposits are present in all of the belts. Instead, the much better endowed Abitibi (in terms of tonnes of VMS per km^2 of volcanic rocks) appears to be related to the dramatic increase in growth of juvenile oceanic-type crust. This could have been a result of faster spreading or a larger number of slow spreading centers characteristic of a microplate mosaic.

The Abitibi greenstone belt

The Abitibi subprovince is the largest Archean granite-greenstone terrane, measuring 300 × 700 km (Fig. 26), and contains the major gold and base metal mining districts of Canada, with production and reserves totaling more than 800 Mt of massive sulfide and nearly 5,000 t of Au (Mercier-Langevin et al., 2014, 2023; Monecke et al., 2017a; Dubé and Mercier-Langevin, 2020). Although commonly referred to as a single belt, it comprises a number of different volcanic assemblages that are individually larger than many of the other greenstone belts in the Superior craton (e.g., see Thurston et al., 1992a, b; Table 3). Seven distinct assemblages are identified, based mainly on U-Pb zircon ages (Ayer et al., 2002; Thurston et al., 2008). They are separated by major E-W–trending structures that are now transcurrent faults, shear zones, and thrusts (Fig. 26A). Although their early history is uncertain and complicated by the north-south shortening and east-west shearing, the arrangement of the faults bears a close resemblance to the microplate architecture of the Lau basin (Fig. 11B).

The oldest volcanic rocks in the Abitibi belong to the Pacaud assemblage (2750–2735 Ma), which is present only locally in the central and southwestern parts of the subprovince. It comprises mafic, ultramafic, and felsic volcanic rocks of tholeiitic to calc-alkaline affinity. The Deloro assemblage (2734–2724 Ma), mostly in the north of the belt, accounts for about 15% of the volcanic rock by area and is dominantly calc-alkaline with lesser tholeiitic mafic and felsic rocks. The Stoughton-Roquemaure assemblage (2723–2720 Ma), which accounts for 40% of the volcanic rock in the Abitibi, is dominated by tholeiitic basalts and lesser komatiite with minor felsic volcanics. The Kidd-Munro assemblage (2719–2711 Ma), in the central part of the belt, accounts for 15% of the volcanic rock and includes abundant komatiite as well as felsic volcanic rocks of boninitic and tholeiitic affinity. The Tisdale assemblage (2710–2704 Ma) in the southwest accounts for another 15% of the volcanic assemblages and comprises tholeiitic mafic rocks in the lower part and intermediate to calc-alkaline felsic rocks in the upper part. The Blake River assemblage (2704–2695 Ma), in the south of the belt, accounts for about 10% of the volcanic rocks and ranges from tholeiitic basalt to calc-alkaline rhyolite. Sedimentary rocks, including mainly carbonaceous mudstone, graywacke, and conglomerate (Porcupine and Timiskaming assemblages) occupy discontinuous subbasins covering about 10% of the map area. The

Table 3. Area-Age Relationships of Abitibi Greenstone Belt Assemblages

Assemblage	Area (km^2)	Approx. age (Ma)	Duration (m.y.)	Growth rate (km^2/m.y.)
Upper Blake River	3,022	2701–2695	6	504
Lower Blake River	2,463	2704–2701	3	821
Upper Tisdale	1,187	2706–2704	2	594
Lower Tisdale	4,989	2711–2706	5	999
Upper Kidd-Munro	4,579	2717–2711	6	793
Lower Kidd-Munro	2,600	2720–2717	3	867
Stoughton-Roquemaure	16,502	2724–2720	4	4,125
Deloro	11,256	2734–2724	10	1,126
Pacaud	734	>2735	15	-

Note: See Appendix Table A2 for areas and ages; a nominal spreading rate can be calculated by converting the area to a linear dimension ($x^{1/2}$) and dividing by the duration of growth; see text for discussion; an updated compilation of Abitibi assemblages and ages can be found in Jørgensen and Gibson (2024)

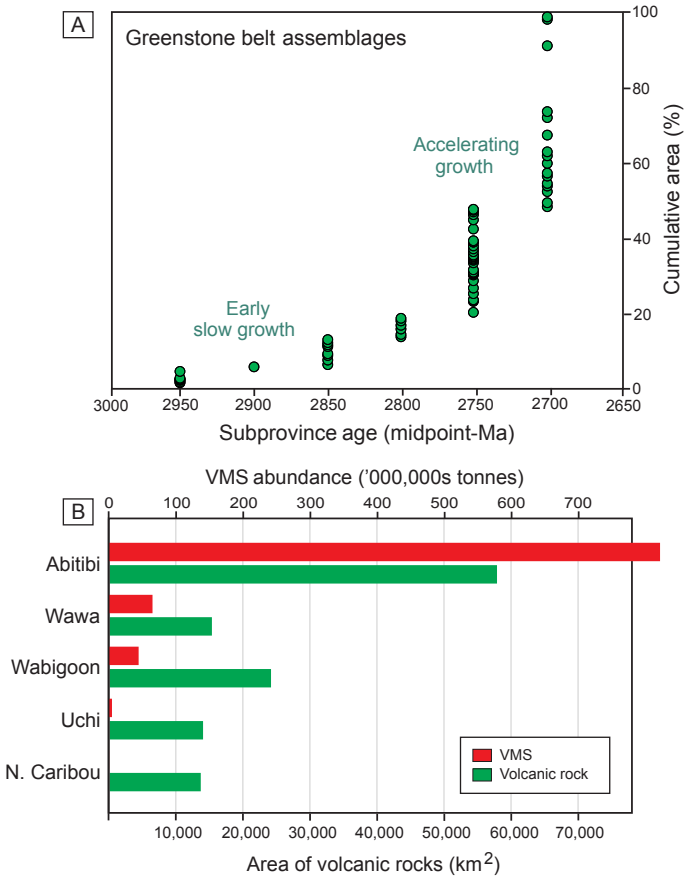

Fig. 25. (A) Model growth curve of greenstone belts of the Southern and Western Superior. Cumulative areas of individual greenstone belt assemblages (volcanic rocks only) are plotted at the midpoints of their reported age range (App. Table A2). The growth rates are quantifiable in terms of area-age relationships, assuming rates of preservation are approximately uniform. In this case, there appears to have been accelerating crustal growth, especially in the Southern Superior, beginning at ~2750 Ma (e.g., Percival et al., 2012). Deeper erosion of older terranes could account for the change of slope but would mean significantly different rates of removal of the older crust. (B) Area of volcanic rocks and endowment of volcanogenic massive sulfide (VMS) in different terranes of the Superior province (data from App. Table A2 and Franklin et al., 2005). The Abitibi belt contains more than three times as much volcanic rock as the N. Caribou, Uchi, and Wabigoon terranes (see also Fig. 24), but nearly 10 times as much massive sulfide.

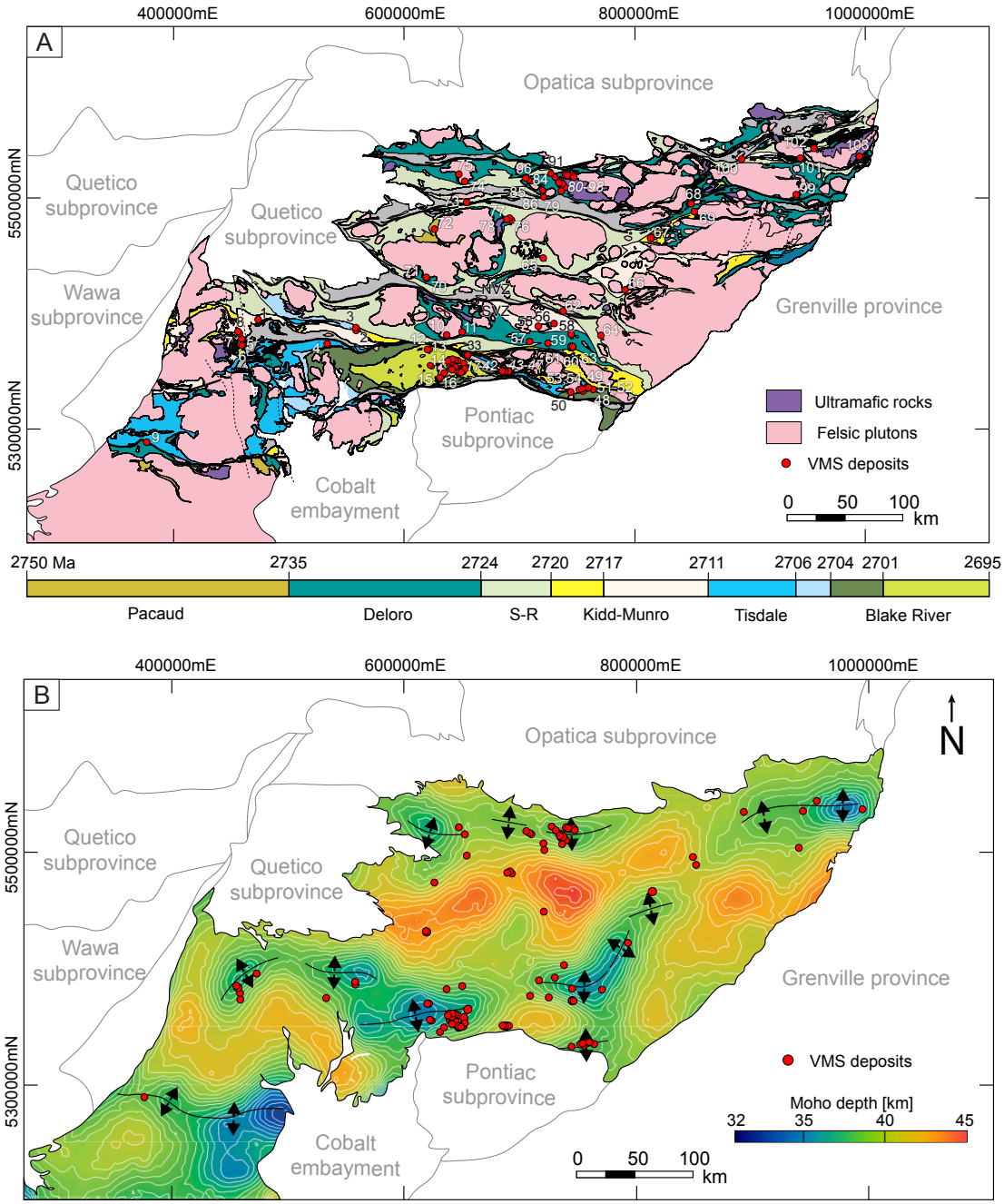

Fig. 26. (A) Assemblage map of the Abitibi greenstone belt from Ayer et al. (2002) and Thurston et al. (2008), modified by Dubé and Mercier-Langevin (2020). Seven distinct assemblages are identified, based mainly on U-Pb zircon ages and bound by major unconformities or structural breaks. The spatial distribution of volcanic rocks of different ages indicates distributed extension occurred across the belt. Mafic volcanic rocks comprise about 90 percent of the eruptive sequences. Felsic volcanic rocks and minor ultramafic rocks account for the remainder. In the southern volcanic zone (SVZ), the volcanic rocks are tholeiitic and calc-alkaline; in the northern volcanic zone (NVZ), they are dominantly tholeiitic. Volcanic rocks are older in the NVZ, and more plutonic rocks and higher-grade metamorphism imply deeper erosion. The major structural "breaks" form a sinuous network of interconnected transcurrent faults and shear zones. See reviews in Monecke et al. (2017a) and Mercier-Langevin et al. (2023). Numbers refer to the index of volcanogenic massive sulfide (VMS) deposits listed in Appendix Table A3. The major fault zones are CBfz = Casa Berardi fault zone, Chfz = Chicobi fault zone, LLCfz = Larder Lake-Cadillac fault zone, PDfz = Porcupine-Dester fault zone, SLfz = Sunday Lake fault zone. (B) Moho topography of the Abitibi region from Galley et al. (2025). The map shows the depth to the Moho, contoured at 500-m intervals. The iso-density surface was calculated from a 3-D gravity inversion model constrained by Lithoprobe seismic data. The strong variability in Moho topography is interpreted to reflect the Archean crustal architecture and corresponds to a map of the base of the Archean crust. The shallow Moho, e.g., below Noranda, Matagami, and the other VMS districts, is interpreted in terms of paleorifts (cf. Mole et al., 2022). One-third of the volcanic rocks by area are underlain by the shallowest Moho (<37.5-km depth), and they contain virtually all of the known VMS deposits.

appearance of voluminous graywacke sequences after 2700 Ma in the Porcupine assemblage suggests rapid emergence of the volcanic terranes, most likely in response to the late-stage accretion of the volcanic plateaus and arcs.

Although the different assemblages are well established on the basis of age, lithology, geochemistry, and structural style, many contact relationships are still unclear and thus complicate a reconstruction at the subprovince scale (Ayer et al., 2002; Thurston et al., 2008). Generally, the older volcanic rocks are in the north (north volcanic zone) and younger rocks are in the south (south volcanic zone; Fig. 26A). An abundance of komatiite distinguishes the Kidd-Munro and Stoughton-Roquemaure assemblages. They are interpreted as part of oceanic rift-like sequences, some with a distinct plume signature. The bimodal tholeiitic to calc-alkaline assemblages, such as Blake River and Deloro, are interpreted as arc-like and back-arc sequences. The repetition of these sequences from north to south throughout the belt may be best thought of in terms of multiple subparallel rift zones, opening sequentially or at the same time (e.g., Thurston, 2015).

Order-of-magnitude estimates of the rate of growth of the Abitibi assemblages range from very fast for Stoughton-Roquemaure (4,125 km²/m.y.) to much slower for the Upper Blake River assemblage (500 km²/m.y.) (Fig. 27; Table 3). These differences may reflect dominantly magmatic extension during fast growth of the Stoughton-Roquemaure assemblage and dominantly tectonic extension during slower growth of the Blake River, similar to modern ridges (Buck et al., 2005). Although Stoughton-Roquemaure is the largest assemblage by area, representing a significant amount of accretion in a relatively short period of time, it contains few significant VMS deposits (Fig. 26A; App. Table A3). An analogy may be the fast-spreading East Pacific Rise, where oceanic crust is accreting at 17 cm/y, but few large sea-floor massive sulfide deposits have formed compared to slower, plume-influenced ridges (Hannington et al., 2005, 2011). In contrast, the well-endowed Blake River assemblage (Mercier-Langevin et al., 2014) took nearly 10 m.y. to form; at 5,485 km² (Table 3), this would have equated to a nominal spreading rate of only ~1 cm/y, similar to the slow- and ultraslow-spreading ridges in the modern oceans. High-precision geochronology and area-age relationships confirm the slow growth of the Blake River in the Noranda area, where more than 30 VMS deposits were formed (McNicoll et al., 2014; Jörgensen et al., 2022). In general, rapid changes in the rates of crustal growth appear to be broadly correlated with metal endowment (Fig. 27B). The apparent contradiction of slow spreading rates but increased crustal growth may be best explained by the longer total ridge length caused by microplate formation.

Abitibi Microplates?

Modern back-arc basins have long been recognized as possible analogs of Archean greenstone belts, where mafic tholeiites occur together with calc-alkaline volcanic rocks having subduction-like geochemical signatures (Kerrich et al., 1998; Polat et al., 1998; Ayer et al., 2002; Thurston, 2002, 2015; Wyman et al., 2002; Wyman, 2013; Vite-Sánchez et al., 2024). The juxtaposition of different magmatic suites and coexistence of arc-like and plume-like sequences compares with the diverse assemblages of the Lau basin (e.g., Fig. 23). A role for microplates has been suggested for the growth of some Archean cratons and greenstone belts (Goodwin, 1977, 1981; Jackson and Fyon, 1992; Jackson et al., 1994; de Wit, 1998; Van Kranendonk et al., 2002; Ernst, 2009; Mole et al., 2015; Gerya et al., 2015), and a mosaic of small plate-like domains, distant from an active subduction zone, is a possible model for autochthonous growth inferred for the Abitibi (Ayer et al., 2002; Thurston, 2002). Small-scale heterogeneity in mantle sources is easier to envision in a microplate framework, as opposed to the large plume heads suggested in other models (e.g., Ernst and Buchan, 2002). Shield volcanoes that occur at triple junctions between the microplates are also a good fit for some of the central volcanic complexes of the NVZ and SVZ (e.g., Dimroth et al., 1982; Goodwin, 1982; Chown et al., 1992; Lafrance et al., 2000; Daigneault et al., 2002).

The melt volumes, structural styles, and sedimentation patterns of volcanic complexes in the Abitibi are also similar to modern examples (e.g., Jörgensen et al., 2022). The Eastern Blake River, in particular, was a paleotopographic depression thinned by rift propagation, similar in size and shape to the southernmost rift basins of the Fonualei rift and the Mangatolu triple junction (Fig. 18A, B). Other centers, including parts of the Kidd-Munro assemblage, formed at plume-influenced boundaries similar to the Rochambeau rifts and Northwest Lau spreading center (Fig. 18C). Assemblages that are distributed more broadly, such as Deloro and Stoughton-Roquemaure (Fig. 26A), may have formed in more complex, distributed rift networks. Some of the narrow synvolcanic sedimentary basins between the volcanic assemblages resemble nodal basins that are catchments for volcaniclastic material in the Lau basin. High-angle fault intersections that are now flattened by north-south shortening (e.g., Harris et al., 2023; Bethell et al., unpub. data) could also have originated as part of a network of intersecting spreading centers and transform faults like that of the Lau basin, including crustal-scale transcurrent structures like Peggy Ridge.

The present-day Moho topography of the Abitibi region, which is revealed in 3-D gravity inversions (Fig. 26B; Galley et al., 2025), appears to reflect the Archean crustal structure. In particular, anomalies in the depth to the Moho closely match the locations of paleorifts previously suggested by Mole et al. (2022). In many depictions of the Abitibi crustal architecture, the Moho is either not present, or it is as a relatively flat iso-density surface under the greenstone belt (Benn, 2006; Smith et al., 2023). The better-constrained 3-D inversion of the regional gravity gives a more precise map of the base of the crust. One interpretation is that the gravity anomalies simply follow the distribution of volcanic rocks between the major plutons (e.g., in a dome-and-keel fashion). However, the density differences between the volcanic rocks and plutons are not large enough to account for the anomalies (Galley et al., 2025). Instead, major excursions in the modeled Moho depth (e.g., depths of less than ~37.5 km; Fig. 26B) are most reasonably interpreted in terms of dense mantle rising into paleo-rift structures. Moreover, a high magma budget associated with a positive excursion in the mantle may have been necessary to rift the thick Archean crust, as in modern-day Iceland (Karson, 2017). The Moho topography also shows a close spatial correspondence to steeply dipping, ~10- to 30-km-wide and 20-km-deep, low-resistivity features in

the Metal Earth transects (e.g., Jørgensen et al., 2022; Smith et al., 2023).

Previous evidence of rifting has included a wide range of geochemical and isotopic data indicating strong rift-zone signatures (Lesher et al., 1986; Barrie et al., 1993; Hart et al., 2004; Huston et al., 2014; Mole et al., 2021, 2022), but until now it has not been possible to say much about the actual structure and geometry of the rifts. We interpret the variations in Moho depth as part of an original microplate architecture, as observed in the Lau basin. Several of the interpreted structures cross assemblage boundaries, which is consistent with rift propagation—an essential part of microplate formation. The conductivity anomalies observed in the Metal Earth transects are also similar to the magnetotelluric (MT) anomalies in the Fonualei rift (Schmid et al., 2021; Franz et al., 2021), which we interpret as occupying the microplate boundary. The deepest structures in the Abitibi are not quite transcrustal; they are listric at depth, becoming ductile shear zones before reaching the base of the crust. However, microplate structures still might have formed if flow occurred in the lower crust.

Most of the interpreted paleo-rifts have an east-west trend, but at least one anomaly in the gravity model is oblique to this trend (Fig. 26B). This conspicuous northeast-southwest anomaly could be analogous to an extensional transform between major spreading centers, similar to the Lau extensional transform zone or Peggy Ridge in the Lau basin (compare Fig. 7B). The major syn- to postcollisional structures of the greenstone belt, such as the Destor Porcupine (DPfz) and Larder Lake-Cadillac (LLCfz) faults, could be reactivated structures related to the ancestral rift zones (Figs. 26A, 28A). They are located at the margins of the Moho anomalies and therefore are positioned to have been rift-bounding faults. Ayer et al. (2002) suggested these faults were active from at least 2724 to 2697 Ma and pointed to changes in stratigraphic thicknesses and truncation of units across the faults as evidence of their synrift origin. They would have accommodated significant horst-and-graben extension during the early development of the rifts, with spreading eventually becoming established at the centers of the rifts.

Although the VMS deposits are highly clustered in mining districts—namely Chibougamau, Matagami, Joutel, Val d'Or, Bousquet, Noranda, Kidd Creek, and Kamiskotia (see App. Table A3 for a complete list)—they are closely aligned along corridors of an elevated Moho. By analogy with modern sea-floor hydrothermal systems, these deposits mark the plate boundaries and may be the most reliable indicators of a microplate architecture. Figure 26B shows 90% of the deposits are located within a few kilometers of an inferred paleo-rift center. Clusters of deposits, such as in Noranda, Matagami, or Val d'Or, could represent intersecting rift zones (i.e., triple junctions) where anomalous magmatic and hydrothermal activity would be expected. Some well-endowed parts of the Abitibi appear to have ended as failed rifts, thus preserving the deposits (e.g., Blake River), whereas others opened into wider basins with far less VMS (e.g., Stoughton-Roquemaure). Orogenic gold deposits that occur in the same districts appear to be related to later reactivation of the rift-bounding faults (Fig. 28).

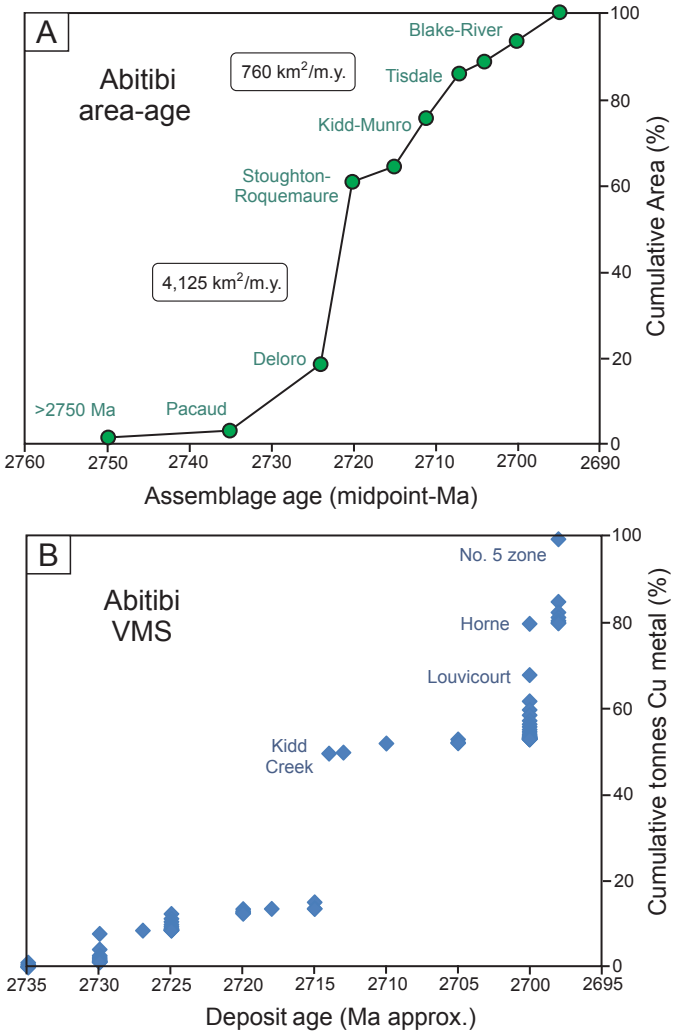

Fig. 27. (A) Model growth curve of the Abitibi greenstone belt (volcanic assemblages only). The cumulative areas of different assemblages shown in Figure 26 are plotted at the midpoints of their inferred ages (Table 3). Upper and Lower units of the Blake River, Tisdale, and Kidd-Munro assemblages are plotted separately. The rate of crustal growth based on area-age relationships ranges from very fast in the Stoughton-Roquemaure assemblage (4,125 km²/m.y.) to much slower in the Upper Blake River assemblage (500 km²/m.y.). 760 km²/m.y. is the average for the Blake River, Tisdale, and Kidd-Munro assemblages. See text for discussion. (B) Cumulative metal addition in tonnes of Cu metal according to the ages of the host assemblages (based on data in Franklin et al., 2005). Changes in rates of crustal growth shown in A are broadly correlated with significant addition of Cu metal to the belt.

Discussion and Conclusions

Anomalous crustal growth in the Lau back-arc basin is a result of fast subduction, slab rollback, and mantle inflow (Bevis et al., 1995; Turner and Hawkesworth, 1998; Smith et al., 2001; Wiens et al., 2006). Early models focused on a simple two-stage progression from arc rifting to sea-floor spreading. However, it is clear that more complex growth began soon after initial opening of the basin, with highly distributed extension resulting in multiple spreading centers and mainly slow rates of accretion at microplate boundaries. The dominant structures controlling crustal growth (and hydrothermal venting) have been active at different places at the same time and, in some cases, at different times in the same location. Propagating rifts are common, and failed spreading centers, abandoned ridges, and deformation zones are widespread.

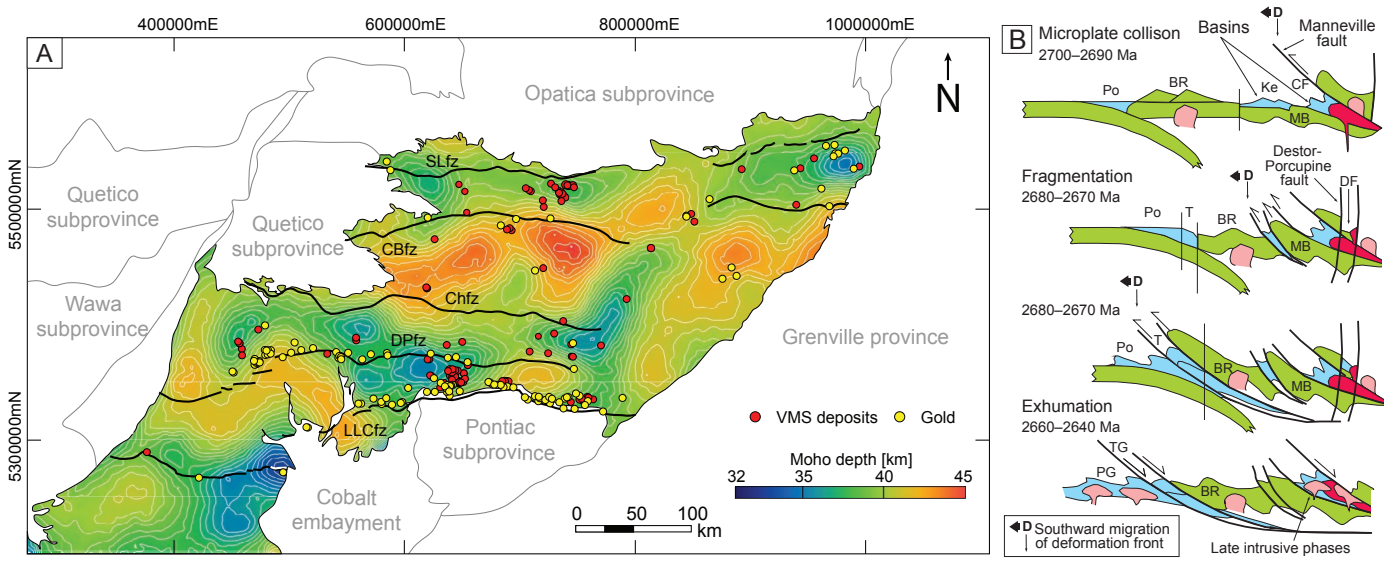

Fig. 28. (A) Locations of orogenic gold deposits and volcanogenic massive sulfide (VMS) in the Abitibi greenstone belt. Data are from Mercier-Langevin et al. (2023) and Dubé and Mercier-Langevin (2020) and references therein. VMS deposits, which form exclusively at plate boundaries, occur at the centers of the inferred paleorifts (shallow Moho: Galley et al., 2025). Later orogenic gold deposits occur in reactivated extensional faults at the rift boundaries (e.g., Ayer et al., 2002). The major fault zones are CBfz = Casa Berardi fault zone, Chfz = Chicobi fault zone, LLCfz = Larder Lake-Cadillac fault zone, PDfz = Porcupine-Dester fault zone, SLfz = Sunday Lake fault zone. (B) Schematic illustration of the late stages of tectonic evolution of the upper crust of the southern Abitibi (modified from Daigneault et al., 1992, 2002). VMS deposits formed during early rift stages (e.g., Blake River stage), followed by extension and then reactivation of rift-bounding faults that contain the orogenic gold deposits. Most structures do not reach the Moho, becoming listric as they pass through the brittle-ductile transition, as observed in Lithoprobe and Metal Earth transects (Smith et al., 2023; Jørgensen et al., 2022). Abbreviations: BR = Blake River volcanics, CF = Cadillac fault, D = Deformation front, Ke = Kewagama sediments, MB = Monstabrais volcanic rocks, Po = Porcupine sediments, T = Timiskaming sediments.

The result is a mix of arc and back-arc crust throughout the basin, with extensive overprinting and inheritance.

We identified seven distinct microplates formed during basin opening with cumulative plate boundaries exceeding 5,000 km in length in a space only 600 km wide. Enhanced magmatic productivity correlates with the number of microplates, plus the spatial density of the spreading ridges and their intersections at triple junctions. Today, at least 12 different spreading centers are simultaneously accreting crust at the plate boundaries. Despite the slow rate of accretion at individual spreading centers, the overall rate of crustal growth is many times greater than for an equivalent span of the global mid-ocean ridge system dominated by a single ridge. Although the architecture can be mapped mostly at the sea floor, some plate boundaries are still hidden, such as the emerging southern boundary of the Niuafo'ou microplate and a proposed triple junction at the southern end of the Fonualei rift. Modeled crustal thickness highlights the microplate architecture (Galley et al., 2024), which is far more granular than previously supposed. This is supported by geochemical data showing the variable composition of the different microplate domains (Fassbender et al., 2023, 2024).

The range of magma compositions includes normal MORB, fractionated andesite and dacite suites, boninitic melts where back-arc spreading centers interact with older arc crust (Northeast Lau spreading center and Fonualei rift), and enriched melts at plume-influenced spreading centers (Rochambeau rifts and Northwest Lau spreading center). Although the back-arc crust is only 6 to 8 km thick, unexpected high-velocity zones at the base of the crust may indicate underplating due to the elevated upper-mantle temperatures (e.g., Dunn and Martinez, 2011; Arai and Dunn, 2014), as observed in other arc-back-arc systems (in the Izu Bonin-Mariana arc: Takahashi et al., 2008; the Yamato basin: Sato et al., 2014). Wei and Wiens (2018) also interpreted anomalous P-wave attenuation at 20 to 60 km as evidence of hydrous partial melting and inflow of hot material from the mantle. Elsewhere, these processes have been linked to the formation of continental crust (e.g., Kodaira et al., 2007; Tamura et al., 2009; Gazel et al., 2015; Jicha and Jagoutz, 2015). Although magmatic arcs are widely viewed as the birthplace of continents, volume calculations show most of the crustal growth in the Lau-Tonga arc-back-arc system is instead happening in the back-arc basin (Galley et al., 2024; see also Jicha and Jagoutz, 2015).

In greenstone belts such as the Abitibi, a rift network responsible for large outpourings of melt at different locations and at different times is suggested for the complex distribution of assemblages, but the major structures have been difficult to unravel (e.g., Mole et al., 2022). Regions of fast growth and slow growth can be distinguished based on area-age relationships (e.g., Jörgensen et al., 2022; this study), but the plate boundaries and spreading centers have not been worked out. New 3-D inversions of the regional gravity are revealing the Archean mantle topography (Galley et al., 2025) and strongly suggest a microplate architecture. This is supported by a growing database of whole-rock geochemistry that indicates much greater heterogeneity in the crust and mantle than can be explained by large-scale plate dynamics (e.g.,

Fassbender et al., 2023, 2024; Vite-Sánchez et al., 2024). We suggest the filter of microplates may account for the petrogenetic diversity, preventing the rise of some melts and promoting others (e.g., Arndt, 2003; Albarède, 1998). The resulting back-arc crust is neither entirely oceanic nor entirely arc-like, as observed in many greenstone belts. Other geochemical signatures have been linked to slab tears (Thorkelson, 1996; Thurston, 2015; Wyman, 2018), which are also increasingly recognized in modern microplate mosaics (e.g., Turner and Hawkesworth, 1998; Bonnardot et al., 2007).

To explain its spectacular mineral endowment, many authors have suggested the Abitibi was uniquely hot, uniquely timed to the beginning of subduction, and uniquely preserved. Ayer et al. (2002) noted the long history of crustal growth in the Abitibi (e.g., from 2750 to 2700 Ma) is difficult to reconcile with a hot Archean mantle that should have promoted faster rather than slower growth. Microplates offer a solution where crustal growth and heat loss are instead accommodated by many more closely spaced plate boundaries dominated by relatively slow spreading. Huston et al. (2014) concluded that the different endowment of VMS between the Abitibi and the Yilgarn was most likely due to the abundant juvenile crust in the Abitibi versus more evolved crust in the Yilgarn—the juvenile crust related to rifting in a high-heat flow regime and the more evolved crust related to a more stable cratonic setting and therefore containing far fewer VMS deposits. Lower grades of metamorphism in the Abitibi support the suggestion of better preservation of VMS, but similarly low metamorphic grades are found in other belts and cratons with far fewer deposits (e.g., Pilbara, Barberton; Kitajima et al., 2001; Terabayashi et al., 2003; Shibuya et al., 2007). We suggest a microplate breakout was responsible for the abundance of juvenile crust and the corresponding endowment of mineral deposits in the Abitibi, like that in the present-day Lau basin.

Acknowledgments

Large-scale geophysical surveys of the type described in this paper require access to major research infrastructure. This has been possible through a long-standing partnership with the Helmholtz Centre for Ocean Research Kiel – GEOMAR and many other research groups internationally. These partnerships have resulted in unprecedented opportunities for scientists and students to participate in major seagoing research and conduct work that is directly relevant to the goals of Metal Earth. Comparisons with land-based studies have been possible through close collaboration with the research team at Laurentian University and the Mineral Exploration Research Centre (MERC). The work has been funded by the Canada First Research Excellence Fund, by the German Federal Ministry of Education and Research (BMBF) which supported numerous research cruises to the study area, and by Discovery Grants from the Natural Sciences and Engineering Research Council of Canada to MDH. Special thanks to S. Piercey and an anonymous reviewer who commented on the manuscript. This is Metal Earth contribution MERC-ME-2025-31.

REFERENCES

Abbott, D., and Menke, W., 1990, Length of the global plate boundary at 2.4 Ga: Geology, v. 18, p. 58–61.

Albarède, F., 1998, The growth of continental crust: Tectonophysics, v. 296, p. 1–14.

Anderson, M.O., Hannington, M.D., Haase, K., et al., 2016, Tectonic focusing of voluminous basaltic eruptions in magma-deficient backarc rifts: Earth and Planetary Science Letters, v. 440, p. 43–55.

Anderson, M.O., Norris-Julseth, C., Rubin, K.H., et al., 2021, Geologic and structural evolution of the NE Lau Basin, Tonga: Morphotectonic analysis and classification of structures using shallow seismicity: Frontiers in Earth Science, v. 9, https://doi.org/10.3389/feart.2021.665185

Arai, R., and Dunn, R.A., 2014, Seismological study of Lau back arc crust: Mantle water, magmatic differentiation, and a compositionally zoned basin: Earth and Planetary Science Letters, v. 390, p. 304–317, https://doi.org/10.1016/j.epsl.2014.01.014.

Arculus, R.J., 2008, Voyage summary SS07/2008: Northern Lau Vents Expedition (NoLauVE): Hobart, Tasmania, Australia, Marine National Facility, 23 p.

Arculus, R.J., 2009, Voyage summary SS02/2009: Hydrothermal plume and structural geology mapping in the Tonga/Fiji region: Hobart, Tasmania, Australia, Marine National Facility, 39 p.

Arculus, R.J., 2012, Voyage summary SS2012/V02: Northern Lau Transit Expedition (NoLauTE): Hobart, Tasmania, Australia, Marine National Facility, 26 p.

Argus, D.F., Gordon, R.G., and DeMets, C., 2011, Geologically current motion of 56 plates relative to the no-net-rotation reference frame: G-Cubed, v. 12, article Q11001, https://doi.org/10.1029/2011GC003751.

Arndt, N., 2003, Komatiites, kimberlites, and boninites: Journal of Geophysical Research, Solid Earth, v. 108, B6, article 2293, https://doi.org/10.1029/2002JB002157.

Ayer, J., Amelin, Y., Corfu, F., et al., 2002, Evolution of the southern Abitibi greenstone belt based on U-Pb geochronology: Autochthonous volcanic construction followed by plutonism, regional deformation and sedimentation: Precambrian Research, v. 115, p. 63–95.

Badham, J.P.N., and Halls, C., 1975, Microplate tectonics, oblique collisions, and evolution of the Hercynian orogenic systems: Geology, v. 3, no. 7, p. 373–376.

Baker, E.T., 2007, Hydrothermal cooling of midocean ridge axes: Do measured and modeled heat fluxes agree?: Earth and Planetary Science Letters, v. 263, p. 140–150.

Baker, E.T., 2017, Exploring the ocean for hydrothermal venting: New techniques, new discoveries, new insights: Ore Geology Reviews, v. 86, p. 55–69, https://doi.org/10.1016/j.oregeorev.2017.02.006

Baker, E.T., Resing, J.A., Walker, S.L., et al., 2006, Abundant hydrothermal venting along melt-rich and melt-free ridge segments in the Lau back-arc basin: Geophysical Research Letters, v. 33, article L07308, https://doi.org/10.1029/2005GL025283.

Baker, E.T., Lupton, J.E., Resing, J.A., et al., 2011, Unique event plumes from a 2008 eruption on the Northeast Lau spreading center: G-Cubed, v. 12, article Q0AF02, https://doi.org/10.1029/2011GC003725.

Baker, E.T., Walker, S.L., Massoth, G.J., and Resing, J.A., 2019, The NE Lau basin: Widespread and abundant hydrothermal venting in the back-arc region behind a superfast subduction zone: Frontiers in Marine Science, v. 6, https://doi.org/10.3389/fmars.2019.00382.

Baldwin, S.L., Fitzgerald, P.G., and Webb, L.E., 2012, Tectonics of the New Guinea Region: Annual Reviews of Earth and Planetary Science, v. 40, p. 495–520, https://doi.org/10.1146/annurev-earth-040809-152540.

Barckhausen, U., Heyde, I., Kopp, H., and Hannington, M.D., 2019, Seafloor spreading and crustal extension of the Central and Northern Lau basin: Some insights from new magnetic data: American Geophysical Union, Fall Meeting, San Francisco, December 2019, Proceedings, Abstract T33F-0424.

Barley, M.E., and Groves, D.I., 1992, Supercontinent cycles and the distribution of metal deposits through time: Geology, v. 20, p. 291–294.

Barrie, C.T., and Hannington, M.D., 1999, Classification of volcanic-associated massive sulfide deposits based on host-rock composition: Reviews in Economic Geology, v. 8, p. 1–11.

Barrie, C.T., Ludden, J.N., and Green, T.H., 1993, Geochemistry of volcanic rocks associated with Cu-Zn and Ni-Cu deposits in the Abitibi subprovince: Economic Geology, v. 88, p. 1341–1358.

Barthelmes, F., and Koehler, W., 2012, International Centre for Global Earth Models (ICGEM): Journal of Geodesy, v. 86, p. 932–934, https://doi.org/10.1007/s00190-012-0584-1.

Baxter, A.T., Hannington, M.D., Stewart, M.S., et al., 2020, Shallow seismicity and the classification of structures in the Lau back-arc basin: G-Cubed, v. 21, https://doi.org/10.1029/2020GC008924.

Beaulieu, S.E., and Szafrański, K.M., 2020, InterRidge global database of active submarine hydrothermal vent fields version 3.4: PANGAEA Data Repository, https://doi.org/10.1594/PANGAEA.917894.

Beaulieu, S.E., Baker, E.T., German, C.R., and Maffei, A., 2013, An authoritative global database for active submarine hydrothermal vent fields: G-Cubed, v. 14, p. 4892–4905.

Bednarz, U., and Schmincke, H-U., 1994, Composition and origin of volcaniclastic sediments in the Lau basin, *in* Hawkins, J.W., Parson, L.M., Allan, J.F., et al., 1994, Proceedings of the Ocean Drilling Program, Scientific Results, v. 135: College Station, Texas, Ocean Drilling Program, p. 51–74, https://doi.org/ 10.2973/odp.proc.sr.135.101.1994.

Begg, G.C., Hronsky, J.A.M., Arndt, N.T., et al., 2010, Lithospheric, cratonic, and geodynamic setting of Ni-Cu-PGE sulfide deposits: Economic Geology, v. 105, p. 1057–1070.

Beier, C., Turner, S.P., Haase, K.M., et al., 2017, Trace element and isotope geochemistry of the northern and central Tongan Islands with an emphasis on the genesis of high Nb/Ta signatures at the northern volcanoes of Tafahi and Niuatoputapu: Journal of Petrology, v. 58, p. 1073–1106.

Benn, K., 2006, Tectonic delamination of the lower crust during late Archean collision of the Abitibi-Opatica and Pontiac terranes, Superior province, Canada: American Geophysical Union, Geophysical Monograph Series 164, p. 267–282.

Bertine, K.K., and Keene, J.B., 1975, Submarine barite-opal rocks of hydrothermal origin: Science, v. 188, p. 150–152.

Bevis, M., Taylor, F.W., Schutz, B.E., et al., 1995, Geodetic observations of very rapid convergence and back-arc extension at the Tonga arc: Nature, v. 374, p. 249–251, https://doi.org/10.1038/374249a0.

Bickle, M.J., 1986, Implications of melting for stabilization of the lithosphere and heat loss in the Archean: Earth and Planetary Science Letters, v. 80, p. 314–324.

Bird, P., 2003, An updated digital model of plate boundaries: G-Cubed, v. 4, no. 3, p. 1–52, https://doi.org/10.1029/2001GC000252.

Bleeker, W., 2003, The late Archean record: A puzzle in ca. 35 pieces: Lithos, v. 71, p. 99–134, https://doi.org/10.1016/j.lithos.2003.07.003.

Blundell, D.J., 2002, The timing and location of major ore deposits in an evolving orogeny: Geological Society of London, Special Publication 204, p. 1–12.

Bonnardot, M.-A., Régnier, M., Ruellan, E., Christova, C., and Tric, E., 2007, Seismicity and state of stress within the overriding plate of the Tonga-Kermadec subduction zone: Tectonics, v. 26, TC5017, p. 1–15, https://doi.org/10.1029/2006TC002044.

Bortnikov, N.S., Fedorov, D.T., and Murav'ev, K.G., 1993, Mineral composition and conditions of the formation of sulfide edifices in the Lau basin (southwestern sector of the Pacific Ocean): Geology of Ore Deposits, v. 35, p. 476–488.

Brandl, P., Hannington, M., Geersen, J., Gennerich, H-H., and Petersen, S., 2020, The submarine tectono-magmatic framework of Cu-Au endowment in the Tabar-to-Feni island chain, PNG: Ore Geology Reviews, v. 121, https://doi.org/10.1016/j.oregeorev.2020.103491.

Buck, W.R., Lavier, L.L., and Poliakov, A.N.B., 2005, Modes of faulting at mid-ocean ridges: Nature, v. 434, no. 7034, p. 719–723, https://doi.org/10.1038/nature03358.

Card, K.D., 1990, A review of Superior province of the Canadian shield, a product of Archean accretion: Precambrian Research, v. 48, p. 99–156.

Card, K.D., and Poulsen, K.H., 1998, Geology and mineral deposits of the Superior province of the Canadian Shield, *in* Lucas, S.B., and St-Onge, M.R., eds., Geology of the Precambrian Superior and Grenville provinces and Precambrian fossils in North America: Geological Society of America, DNAG, Geology of North America, https://doi.org/10.1130/DNAG-GNA-C1.13.

Cathles, A., and Hallam, A., 1991, Stress-induced changes in plate density, vail sequences, epiorogeny and short-lived global sea level fluctuations: Tectonics, v. 10, no. 4, p. 659–671.

Cawood, P.A., and Hawkesworth, C.J., 2015, Temporal relations between mineral deposits and global tectonic cycles: Geological Society of London, Special Publication 393, p. 9–21, https://doi.org/10.1144/SP393.1.

Chadwick, W.W., Jr., Rubin, K.H., Merle, S.G., et al., 2019, Recent eruptions between 2012 and 2018 discovered at West Mata submarine volcano (NE Lau Basin, SW Pacific) and characterized by new ship, AUV, and ROV data: Frontiers in Marine Science, v. 6, no. 495, https://doi.org/10.3389/fmars.2019.00495.

Chase, C.G., 1971, Tectonic history of the Fiji Plateau: Geological Society of America Bulletin, v. 82, p. 3087–3110.

Chown, E.H., Daigneault, R.B., Mueller, D., and Mortensen, J.K., 1992, Tectonic evolution of the Northern volcanic zone, Abitibi belt, Quebec: Canadian Journal of Earth Sciences, v. 29, p. 2211–2225.

Clift, P.D., and Dixon, J.E., 1994, Variations in arc volcanism and sedimentation related to rifting of the Lau basin (southwest Pacific), *in* Hawkins, J.W., Parson, L.M., Allan, J.F., et al., 1994, Proceedings of the Ocean Drilling Program, Scientific Results, v. 135: College Station, Texas, Ocean Drilling Program, p. 23–49, https://doi.org/10.2973/odp.proc.sr.135.102.1994.

Clift, P.D., MacLeod, C.J., Tappin, D.R., Wright, D.J., and Bloomer, S.H., 1998, Tectonic controls on sedimentation and diagenesis in the Tonga trench and forearc, southwest Pacific: Geological Society of America Bulletin, v. 110, p. 483–496.

Collins, W.J., 2002, Hot orogens, tectonic switching, and creation of continental crust: Geology, v. 30, no. 6, p. 535–538.

Collot, J., Vendé-Leclerc, M., Rouillard, P., Lafoy, Y., and Géli, L., compilers, 2011, Structural provinces of the southwest Pacific (first edition), Noumea, New Caledonia: Geological Survey of New Caledonia, Direction de l'Industrie, des Mines et de l'Energie de Nouvelle Calédonie (DIMENC), L'Institut Français de Recherche pour l'Exploitation de la Mer (IFREMER).

Coltice, N., Rolf, T., Tackley, P.J., and Labrosse, S., 2012, Dynamic causes of the relation between area and age of the ocean floor: Science, v. 336, p. 335–338, https://doi.org/10.1126/science.1219120.

Conder, J.A., and Wiens, D.A., 2011, Shallow seismicity and tectonics of the central and northern Lau basin: Earth and Planetary Science Letters, v. 304, p. 538–546, https://doi.org/10.1016/j.epsl.2011.02.032.

Condie, K.C., 1998, Episodic continental growth and supercontinents: A mantle avalanche connection?: Earth and Planetary Science Letters, v. 163, p. 97–108.

Condie, K.C., and Aster, R.C., 2009, Zircon age episodicity and growth of continental crust: Eos, Transactions of the American Geophysical Union, v. 90, no. 41, p. 364–365.

Condie, K.C., and Aster, R.C., 2010, Episodic zircon age spectra of orogenic granitoids: The supercontinent connection and continental growth: Precambrian Research, v. 180, p. 227–236.

Condie, K.C., Pisarevsky, S.A., Korenaga, J., and Gardoll, S., 2015, Is the rate of supercontinent assembly changing with time?: Precambrian Research, v. 259, p. 278–289, https://doi.org/10.1016/j.precamres.2014.07 .015.

Condie, K.C., Arndt, N., Davaille, A., and Puetz, S.J., 2017, Zircon age peaks: Production or preservation of continental crust?: Geosphere, v. 13, no. 2, p. 227–234, https://doi.org/10.1130/GES01361.1.

Contreras-Reyes, E., Grevemeyer, I., Watts, A.B., et al., 2011, Deep seismic structure of the Tonga subduction zone: Implications for mantle hydration, tectonic erosion, and arc magmatism: Journal of Geophysical Research, v. 116, B10103, https://doi.org/10.1029/2011JB008434.

Corfu, F., 1993, The evolution of the southern Abitibi belt in the light of precise U-Pb geochronology: Economic Geology, v. 88, p. 1323–1340.

Craw, D., Koons, P.O., Horton, T., and Chamberlain, C.P., 2002, Tectonically driven fluid flow and gold mineralization in active collisional orogenic belts: comparison between New Zealand and western Himalaya: Tectonophysics, v. 348, p. 135–153.

Crawford, W.C., Hildebrand, J.A., Dorman, L.M., Webb, S.C., and Wiens, D.A., 2003, Tonga Ridge and Lau basin crustal structure from seismic refraction data: Journal of Geophysical Research, v. 108, B4, https://doi.org/10.1029/2001JB001435.

Cronin, V.S., 1992, Types and kinematic stability of triple junctions: Tectonophysics, v. 207, p. 287–301, dio:10.1016/0040-1951(92)90391-I.

Daigneault, R., Chown, E.H., and Mueller, W., 1992, Tectonic boundary between the Northern and the Southern volcanic zones, Abitibi subprovince, Quebec: LITHOPROBE, Abitibi-Grenville Project, Workshop IV, Report 33, p. 7–10.

Daigneault, R., Mueller, W.U., and Chown, E.H., 2002, Oblique Archean subduction: Accretion and exhumation of an oceanic arc during dextral transpression, Southern volcanic zone, Abitibi subprovince Canada: Precambrian Research, v. 115, p. 261–290.

Deschamps, A., and Lallemand, S., 2003, Geodynamic setting of Izu-Bonin-Mariana boninites: Geological Society of London, Special Publication 219, p. 163–185.

de Wit, M.J., 1998, On Archean granites, greenstones, cratons and tectonics: Does the evidence demand a verdict?: Precambrian Research, v. 91, p. 181–226.

Dimroth, E., Imreh, L., Rocheleau, M., and Goulet, N., 1982, Evolution of the south-central part of the Archean Abitibi belt, Quebec. Part 1:

Stratigraphy and paleogeographic model: Canadian Journal of Earth Sciences, v. 19, p. 1729–1758, https://doi.org/10.1139/e82-154.
Dubé, B., and Mercier-Langevin, P., 2020, Gold deposits of the Archean Abitibi greenstone belt, Canada: Society of Economic Geologists, Special Publication 23, p. 669–708.
Dunn, R.A., and Martinez, F., 2011, Contrasting crustal production and rapid mantle transitions beneath back-arc ridges: Nature, v. 469, p. 198–202, https://doi.org/10.1038/nature09690
Dunn, R.A., Martinez, F., and Conder, J., 2013, Crustal construction and magma chamber properties along the Eastern Lau spreading center: Earth and Planetary Science Letters, v. 371–372, p. 112–124, https://doi.org/10.1016/j.epsl.2013.04.008.
Eason, D.E., and Dunn, R.A., 2015, Petrogenesis and structure of oceanic crust in the Lau backarc basin: Earth and Planetary Science Letters, v. 429, p. 128–138, https://doi.org/10.1016/j.epsl.2015.07.065.
Embley, R.W., and Rubin, K.H., 2018, Extensive young silicic volcanism produces large deep submarine lava flows in the NE Lau basin: Bulletin of Volcanology, v. 80, no. 36, https://doi.org/10.1007/s00445-018-1211-7.
Embley, R.W., Merle, S.G., Lupton, J.E., et al., 2009, Extensive and diverse submarine volcanism and hydrothermal activity in the NE Lau basin: Eos, Transactions of the American Geophysical Union, v. 90, no. 52, p. 1719.
Embley, R.W., Merle, S.G., Baker, E.T., et al., 2014, Eruptive modes and hiatus of volcanism at West Mata seamount, NE Lau basin: 1996-2012: G-Cubed, v. 15, p. 4093–4115, https://doi.org/10.1002/2014GC005387.
Ernst, R.E., and Buchan, K.L., 2002, Recognizing mantle plumes in the geological record: Annual Reviews in Earth and Planetary Science, v. 31, p. 469–523.
Ernst, W.G., 2009, Archean plate tectonics, rise of Proterozoic supercontinentality and onset of regional, episodic stagnant-lid behavior: Gondwana Research, v. 15, no. 3–4, p. 243–253, https://doi.org/10.1016/j.gr.2008.06.010.
Escrig, S., Bézos, A., Langmuir, C.H., Michael, P.J., and Arculus, R., 2012, Characterizing the effect of mantle source, subduction input and melting in the Fonualei spreading center, Lau basin: Constraints on the origin of the boninitic signature of the back-arc lavas: G-Cubed, v. 13, no. 10, article Q10008, https://doi.org/10.1029/2012GC004130.
Evans, G.N., Tivey, M.K., Seewald, J.S., and Wheat, G., 2017, Influences of the Tonga subduction zone on seafloor massive sulfide deposits along the Eastern Lau spreading center and Valu Fa Ridge: Geochimica et Cosmochimica Acta, v. 215, p. 214–246, https://doi.org/10.1016/j.gca.2017.08.010.
Faccenna, C., Becker, T.W., Lallemand, S., et al., 2010, Subduction-triggered magmatic pulses: A new class of plumes?: Earth and Planetary Science Letters, v. 299, p. 54–68.
Falloon, T.J., Danyushevsky, L.V., Crawford, T.J., et al., 2007, Multiple mantle plume components involved in the petrogenesis of subduction-related lavas from the northern termination of the Tonga arc and northern Lau basin: Evidence from the geochemistry of arc and backarc submarine volcanics: G-Cubed, v. 8, no. 9, article Q09003, https://doi.org/10.1029/2007GC001619.
Fassbender, M.L., Hannington, M.D., Stewart, M., et al., 2023, Geochemical signatures of felsic volcanic rocks in modern oceanic settings and implications for Archean greenstone belts: Economic Geology, v. 118, p. 319–345.
Fassbender, M.L., Hannington, M.D., Baxter, A.T., et al., 2024, Geochemical signatures of mafic volcanic rocks in modern oceanic settings and implications for Archean mafic magmatism: Economic Geology, v. 119, p. 445–470.
Fouquet, Y., von Stackelberg, U., Charlou, J.-L., et al., 1993, Metallogenesis in back-arc environments: The Lau basin example: Economic Geology, v. 88, p. 2154–2181.
Fouquet, Y., Alix, A.-S., Birot, D., et al., 2015, Discovery of extensive hydrothermal fields in the Wallis and Futuna back-arc environment (SW Pacific): Society for Geology Applied to Mineral Deposits, Biennial SGA Meeting, 13th, 24-27 August 2015, Nancy, Proceedings, v. 3, p. 1223–1226.
Fouquet, Y., Pelleter, E., Konn, C., et al., 2018, Volcanic and hydrothermal processes in submarine calderas: The Kulo Lasi example (SW Pacific): Ore Geology Reviews, v. 99, p. 314–343, https://doi.org/10.1016/j.oregeorev.2018.06.006.
Franklin, J.M., and Thorpe, R.I., 1982, Comparative metallogeny of the Superior, Slave and Churchill provinces: Geological Association of Canada, Special Paper 25, p. 3–90.
Franklin, J.M., Gibson, H.L., Jonasson, I.R., and Galley, A.G., 2005, Volcanogenic massive sulfide deposits: Economic Geology, 100th Anniversary Volume, p. 523–560.
Franz, G., Jegen, M., Neska, A., et al., 2021, Crustal structure of the nascent Fonualei rift and spreading center, Lau basin, derived from magnetotelluric measurements: International Association of Seismology and Physics of the Earth's Interior, IAGA-IASPEI 2021, August 27, 2021, Proceedings, https://oceanrep.geomar.de/id/eprint/54639.
Fujiwara, T., Yamazaki, T., and Joshima, M., 2001, Bathymetry and magnetic anomalies in the Havre Trough and southern Lau basin: From rifting to spreading in back-arc basins: Earth and Planetary Science Letters, v. 185, p. 253–264, https://doi.org/10.1016/S0012-821X(00)00378-2.
Galley, C., Baxter, A., Hannington, M., et al., 2024, Quantifying crustal growth in arc-backarc systems: Gravity inversion modelling of the Lau basin: Journal of Geophysical Research, v. 129, https://doi.org/10.1029/2024JB029013.
Galley, C., Hannington, M., Bethell, E., Baxter, A., and Lelièvre, P., 2025, Archean rifts and triple-junctions revealed from gravity modelling of the Superior craton: Nature Communications, v. 16, article 8872, https://doi.org/10.1038/s41467-025-63931-z.
Garwin, S., Hall, R., and Watanabe, Y., 2005, Tectonic setting, geology, and gold and copper mineralization in Cenozoic magmatic arcs of southeast Asia and the west Pacific: Economic Geology, 100th Anniversary Volume, p. 891–930.
Gazel, E., Hayes, J.L., Hoernle, K., et al., 2015, Continental crust generated in oceanic arcs: Nature Geoscience, v. 8, p. 321–327, https://doi.org/10.1038/NGEO2392.
German, C.R., Baker, E.T., Connelly, D.P., et al., 2006, Hydrothermal exploration of the Fonualei rift and spreading center and the Northeast Lau spreading center: G-Cubed, v. 7, no. 11, Q11022, https://doi.org/10.1029/2006GC001324.
German, C.R., Petersen, S., and Hannington, M.D., 2016, Hydrothermal exploration of mid-ocean ridges: Where might the largest sulfide deposits occur?: Chemical Geology, v. 420, no. 1, p. 114–126.
Gerya, T.V., Stern, R.J, Baes, M., Sobolev, S.V., and Whattam, S.A., 2015, Plate tectonics on the Earth triggered by plume-induced subduction initiation: Nature, v. 527, p. 221–225, https://doi.org/10.1038/nature15752.
Goodwin, A.M., 1977, Archean basin craton complexes and the growth of Precambrian shields: Canadian Journal of Earth Sciences, v. 14, p. 2737–2759.
Goodwin, A.M., 1981, Precambrian perspectives: Science, v. 213, no. 4503, p. 55–61.
Goodwin, A.M., 1982, Archaean volcanoes in the southwestern Abitibi belt, Ontario and Quebec: Canadian Journal of Earth Science, v. 19, p. 1140–1155.
Govers, R., and Wortel, M.J.R., 2005, Lithosphere tearing at STEP faults: Response to edges of subduction zones: Earth and Planetary Science Letters, v. 236, p. 505–523, https://doi.org/10.1016/j.epsl.2005.03.022.
Grevemeyer, I., and Flüh, E.R., 2008, FS Sonne cruise report SO195, Tonga thrust earthquake asperity at Louisville ridge, Suva/Fiji-Suva/Fiji, 07.01.-16.02.2008: Kiel, Germany, Leibniz-Institut für Meereswissenschaften, IFM-GEOMAR, https://doi.org/10.3289/ifm-geomar_rep_14_2008, 106 p.
Groves, D.I., and Bierlein, F.P., 2007, Geodynamic settings of mineral deposit systems: Journal of the Geological Society, v. 164, p. 19–30, https://doi.org/10.1144/0016-76492006-065.
Haase, K.M., Schönhofen, M.V., Storch, B., et al., 2022, Effects of the hydrous domain in the mantle wedge on magma formation and mixing at the Northeast Lau spreading center, SW Pacific: G-Cubed, v. 23, no. 2, p. 1–22, article e2021GC010066, https://doi.org/10.1029/2021GC010066.
Hannington, M.D., de Ronde, C.E.J., and Petersen, S., 2005, Modern seafloor tectonics and submarine hydrothermal systems: Economic Geology, 100th Anniversary Volume, p. 111–142.
Hannington, M.D., Jamieson, J., Monecke, T., Petersen, S., and Beaulieu, S., 2011, The abundance of seafloor massive sulfide deposits: Geology, v. 39, no. 12, 1155–1158.
Hannington, M.D., Kopp, H., and Schnabel, M., 2019, FS Sonne cruise report SO267: ARCHIMEDES I: Arc rifting, metallogeny and microplate evolution—an integrated geodynamic, magmatic and hydrothermal study of the Fonualei rift system, NE Lau basin, Suva (Fiji)-Suva (Fiji), 11.12.2018-26.01.2019: GEOMAR Helmholtz-Zentrum für Ozeanforschung, GEOMAR Report N. Ser. 049, 275 p., https://doi.org/10.3289/GEOMAR_REP_NS_49_2019.
Hargraves, R.B., 1986, Faster spreading or greater ridge length in the Archean?: Geology, v. 14, p. 750–752.
Harmon, N., and Blackman, D.K., 2010, Effects of plate boundary geometry and kinematics on mantle melting beneath the back-arc spreading centers along the Lau basin: Earth and Planetary Science Letters, v. 298, no. 3–4, p. 334–346, https://doi.org/10.1016/j.epsl.2010.08.004.
Harris, J.R., Ayer, J., Naghizadeh, M., et al., 2023, A study of faults in the Superior province of Ontario and Quebec using the random forest machine

learning algorithm: Ore Geology Reviews, v. 157, p. 1–17, https://doi.org/10.1016/j.oregeorev.2023.105403.
Harris, P.T., Macmillan-Lawler, M., Rupp, J., and Baker, E.K., 2014, Geomorphology of the oceans: Marine Geology, v. 352, p. 4–24, https://doi.org/10.1016/j.margeo.2014.01.011.
Harrison, C.G.A., 2016, The present-day number of tectonics plates: Earth, Planets and Space, v. 68, p. 37–51.
Hart, T.R., Gibson, H.L., and Lesher, C.M., 2004, Trace element geochemistry and petrogenesis of felsic volcanic rocks associated with volcanogenic massive Cu-Zn-Pb sulfide deposits: Economic Geology, v. 99, p. 1003–1013.
Hasterok, D., Halpin, J.A., Collins, A.S., et al., 2022, New maps of global geological provinces and tectonic plates: Earth-Science Reviews, v. 231, https://doi.org/10.1016/j.earscirev.2022.104069.
Hawkesworth, C.J., Cawood, P.A., Kemp, A.I.S., Storey, C.D., and Dhuime, B., 2009, A matter of preservation: Science, v. 323, p. 49–50.
Hawkesworth, C.J., Cawood, P.A., and Dhuime, B., 2013, Continental growth and the crustal record: Tectonophysics, v. 609, p. 651–660, https://doi.org/10.1016/j.tecto.2013.08.013.
Hawkins, J.W., 1976, Petrology and geochemistry of basaltic rocks of the Lau basin: Earth and Planetary Science Letters, v. 28, p. 283–297, https://doi.org/10.1016/0012-821X(76)90190-4.
Hawkins, J.W., 1995, Evolution of the Lau basin—Insights from ODP Leg 135: American Geophysical Union, Geophysical Monograph 88, p. 125–173, https://doi.org/10.1029/GM088p0125.
Hawkins, J.W., and Allan, J.F., 1994, Petrologic evolution of Lau basin Sites 834 through 839, *in* Hawkins, J.W., Parson, L.M., Allan, J.F., et al., Proceedings of the Ocean Drilling Program, Scientific Results, v. 135: College Station, Texas, Ocean Drilling Program, p. 427–470, https://doi.org/10.2973/odp.proc.sr.135.136.1994.
Hawkins, J., and Helu, S., 1986, Polymetallic sulfide deposits from a "black smoker" chimney: Lau basin: EOS, Transactions of the American Geophysical Union, v. 67, no. 16, abstract T32B-11.
Herzberg, C., Condie, K., and Korenaga, J., 2010, Thermal history of the Earth and its petrological expression: Earth and Planetary Science Letters, v. 292, p. 79–88, https://doi.org/10.1016/j.epsl.2010.01.022.
Herzig, P.M., Hannington, M.D., Fouquet, Y., von Stackelberg, U., and Petersen, S., 1993, Gold-rich polymetallic sulfides from the Lau back arc and implications for the geochemistry of gold in sea-floor hydrothermal systems of the southwest Pacific: Economic Geology, v. 88, p. 2182–2209.
Hey, R.N., 1977, A new class of pseudofaults and their bearing on plate tectonics: A propagating rift model: Earth and Planetary Science Letters, v. 37, p. 321–325, https://doi.org/10.1016/0012-821X(77)90177-7.
Heyde, I., Barckhausen, U., and Hagedorn, D., 2019, Gravity measurements and data report, *in* Hannington, M.D., Kopp, H., and Schnabel, M., eds., FS Sonne cruise report SO267: ARCHIMEDES I: GEOMAR Helmholtz-Zentrum für Ozeanforschung, GEOMAR Report N. Ser. 049, 275 p., https://doi.org/10.3289/GEOMAR_REP_NS_49_2019.
Holm, R.J., Rosenbaum, G., and Richards, S.W., 2016, Post 8Ma reconstruction of Papua New Guinea and Solomon Islands: Microplate tectonics in a convergent plate boundary setting: Earth-Science Reviews, v. 156, p. 66–81, https://doi.org/10.1016/j.earscirev.2016.03.
Hubert, C., Gelinas, C., and Trudel, P., 1984, Archaean wrench fault tectonics and volcanism related to a central ring complex in the Blake River Group, Abitibi belt, Quebec: Canadian Journal of Earth Science, v. 22, p. 240–255.
Huston, D.L., Pehrsson, S., Eglinton, B.M., and Zaw, K., 2010, The geology and metallogeny of volcanic-hosted massive sulfide deposits: Variations through geologic time and with tectonic setting: Economic Geology, v. 105, p. 571–591.
Huston, D.L., Champion, D.C., and Cassidy, K.F., 2014, Tectonic controls on the endowment of Neoarchean cratons in volcanic-hosted massive sulfide deposits: Evidence from lead and neodymium isotopes: Economic Geology, v. 109, p. 11–26.
Huston, D.L., Mernagh, T.P., Hagemann, S.G., et al., 2016, Tectono-metallogenic systems–The place of mineral systems within tectonic evolution, with an emphasis on Australian examples: Ore Geology Reviews, v. 76, p. 168–210, https://doi.org/10.1016/j.oregeorev.2015.09.005.
Huston, D.L., Champion, D.C., Czarnota, K., et al., 2023, Zinc on the edge—isotopic and geophysical evidence that cratonic edges control world-class shale-hosted zinc-lead deposits: Mineralium Deposita, v. 58, p. 707–729, https://doi.org/10.1007/s00126-022-01153-9.
Ince, E.S., Barthelmes, F., Reißland, S., et al., 2019, ICGEM - 15 years of successful collection and distribution of global gravitational models, associated services and future plans: Earth System Science Data, v. 11, p. 647–674, https://doi.org/10.5194/essd-11-647-2019.
Ingebritsen, S.E., and Manning, C.E., 2010, Permeability of the continental crust: dynamic variations inferred from seismicity and metamorphism: Geofluids, v. 10, p. 193–205, https://doi.org/10.1111/j.1468-8123.2010.00278.
Ishizuka, O., Yuasa, M., Tamura, Y., et al., 2010, Migrating shoshonitic magmatism tracks Izu-Bonin-Mariana intra-oceanic arc rift propagation: Earth and Planetary Science Letters, v. 294, p. 111–122, https://doi.org/10.1016/j.epsl.2010.03.016.
Jackson, S.L., and Cruden, A.R., 1995, Formation of the Abitibi greenstone belt by arc-trench migration: Geology, v. 23, no. 5, p. 471–474.
Jackson, S.L., and Fyon, J.A., 1992, The western Abitibi subprovince in Ontario, *in* Thurston et al., eds., Geology of Ontario, Special Volume 4, Part 2: Ontario Geological Survey, Ministry of Northern Development and Mines, p. 405–484.
Jackson, S.L., and Sutcliffe, R.H., 1990, Central Superior province geology: Evidence for an allochthonous, ensimatic, southern Abitibi greenstone belt: Canadian Journal of Earth Sciences, v. 27, p. 582–589.
Jackson, S.L., Fyon, J.A., and Corfu, F., 1994, Review of Archean supracrustal assemblages of the southern Abitibi greenstone belt in Ontario, Canada: Products of microplate interaction within a large-scale plate-tectonic setting: Precambrian Research, v. 65, p. 183–205.
Jegen, A., Dannowski, A., Schnabel, M., et al., 2023, Extension dynamics of the Northern Fonualei rift and spreading center and the southern Mangatolu triple junction in the Lau basin at 16°S: G-Cubed, v. 24, no. 4, https://doi.org/10.1029/2022GC010550.
Jegen, M., Franz, G., Avdeeva, A., et al., 2024, Back-arc rifting in the eastern Lau basin - a magnetotelluric study of the nascent Fonualei rift system: American Geophysical Union, Annual Fall Meeting, Washington D.C., December 9–13, 2024, Proceedings.
Jicha, B.R., and Jagoutz, O., 2015, Magma production rates for intra-oceanic arcs: Elements, v. 11, p. 105–112, https://doi.org/10.2113/gselements.11.2.105.
Jolly, W.T., 1978, Metamorphic history of the Archean Abitibi belt: Geological Survey of Canada, Paper 78-10, p. 63–78.
Jørgensen, T.R.C., and Gibson, H.L., 2024, Assemblage compilation of the Abitibi subprovince, Superior province, Canada: Metal Earth Project, Mineral Exploration Research Centre, https://metalearth.files.com/f/81ca7963c83475a6.
Jørgensen, T.R.C., Gibson, H.L., Roots, E.A., et al., 2022, The implications of crustal architecture and transcrustal upflow zones on the metal endowment of a world-class mineral district: Scientific Reports, v. 12, article 14710, https://doi.org/10.1038/s41598-022-18836-y.
Karig, D.E., 1970, Ridges and basins of the Tonga-Kermadec island arc system: Journal of Geophysical Research, v. 75, p. 239–254, https://doi.org/10.1029/JB075i002p00239.
Karson, J.A., 2017, The Iceland plate boundary zone: Propagating rifts, migrating transforms, and rift-parallel strike-slip faults: G-Cubed, v. 18, p. 4043–4054, https://doi.org/10.1002/2017GC007045.
Kehew, J., 2023, Intrabasinal sediments and tectonostratigraphy of the N.E. Lau basin: Contributions to extensional models of back-arc basins: Unpub. MSc thesis, University of Ottawa, Canada, 202 p.
Keller, N.S., Arculus, R.J., Hermann, J., and Richards, S., 2008, Submarine back-arc lava with arc signature: Fonualei spreading center, northeast Lau basin, Tonga: Journal of Geophysical Research, Solid Earth, v. 113, B08S07, https://doi.org/10.1029/2007JB005451.
Kerrich, R., Wyman, D., Fan, J., and Bleeker, W., 1998, Boninite series: Low Ti-tholeiite associations from the 2.7 Ga Abitibi greenstone belt: Earth and Planetary Science Letters, v. 164, p. 303–316.
Kim, J., Son, S.-K., Son, J.-W., et al., 2009, Venting sites along the Fonualei and northeast Lau spreading centers and evidence of hydrothermal activity at an off-axis caldera in the northeastern Lau basin: Geochemical Journal, v. 43, p. 1–13, https://doi.org/10.2343/geochemj.0.0164.
Kitajima, K., Maruyama, S., Tsunomiya, S., and Liou, J.G., 2001, Seafloor hydrothermal alteration at an Archaean mid-ocean ridge: Journal of Metamorphic Geology, v. 19, p. 583–599.
Kodaira, S., Sato, T., Takahashi, N., et al., 2007, New seismological constraints on growth of continental crust in the Izu-Bonin intra-oceanic arc: Geology, v. 35, p. 1031–1034, https://doi.org/10.1130/G23901A.1.
Konn, C., Fourré, E., Jean-Baptiste, P., et al., 2016, Extensive hydrothermal activity revealed by multi-tracer survey in the Wallis and Futuna region (SW Pacific): Deep-Sea Research, Part I, Oceanographic Research Papers, v. 116, p. 127–144, https://doi.org/10.1016/j.dsr.2016.07.012.

Konn, C., Donval, J.P., Guyader, V., et al., 2018, Organic, gas, and element geochemistry of hydrothermal fluids of the newly discovered extensive hydrothermal area in the Wallis and Futuna Region (SW Pacific): Geofluids, article 7692839, https://doi.org/10.1155/2018/7692839.

Korenaga, J., 2008a, Plate tectonics, flood basalts, and the evolution of Earth's oceans: Terra Nova, v. 20, p. 419–439.

Korenaga, J., 2008b, Urey ratio and the structure and evolution of Earth's mantle: Reviews in Geophysics, v. 46, no. 2, article RG2007, https://doi.org/10.1029/2007RG000241.

Koursch, R.J., and Doublier, M.P., 2016, Major crustal boundaries of Australia, and their significance in mineral systems targeting: Ore Geology Reviews, v. 76, p. 211–228, https://doi.org/10.1016/j.oregeorev.2015.05.010.

Kreemer, C., Blewitt, G., and Klein, E.C., 2014, A geodetic plate motion and global strain rate model: G-Cubed, v. 15, p. 3849–3889, https://doi.org/10.1002/2014GC005407.

Lafrance, B., Mueller, W.U., Daigneault, R., and Dupras, N., 2000, Evolution of a submerged composite arc volcano: Volcanology and geochemistry of the Normétal volcanic complex, Abitibi greenstone belt, Québec, Canada: Precambrian Research, v. 101, p. 277–311, https://doi.org/10.1016/S0301-9268(99)00092-3.

Lagabrielle, Y., Goslin, J., Martin, H., Thirot, J.-L., and Auzende, J.-M., 1997, Multiple active spreading centres in the hot North Fiji basin (Southwest Pacific): A possible model for Archaean seafloor dynamics?: Earth and Planetary Science Letters, v. 149, p. 1–13.

Langford, F.F., and Morin, J.A., 1976, The development of the Superior province of northwestern Ontario by merging island arcs: American Journal of Science, v. 276, p. 1023–1034.

Lesher, C.M., Goodwin, A.M., Campbell, I.H., and Gorton, M.P., 1986, Trace-element geochemistry of ore-associated and barren, felsic metavolcanic rocks in the Superior province, Canada: Canadian Journal of Earth Sciences, v. 23, p. 222–237.

Li, S., Suoa, Y., Li, X., et al., 2018, Microplate tectonics: New insights from micro-blocks in the global oceans, continental margins and deep mantle: Earth Science Reviews, v. 185, p. 1029–1064.

Lisitsyn, A.P., Malahoff, A.R., Bogdanov, Y.A., et al., 1992, Hydrothermal formations in the northern part of the Lau basin, Pacific Ocean: International Geology Review, v. 34, p. 828–847.

Lister, C.R.B., 1972, On the thermal balance of a mid-ocean ridge: Geophysical Journal of the Royal Astronomical Society, v. 26, p. 515–535.

Lister, C.R.B., 1980, Heat flow and hydrothermal circulation: Annual Reviews in Earth and Planetary Science, v. 8, p. 95–117.

Liu, Y., Li, S., Jiang, S., et al., 2023, Origin of microplates under oblique subduction system in New Guinea: Inferences from gravity and magnetic data: Gondwana Research, v. 120, p. 175–189, https://doi.org/10.1016/j.gr.2022.09.001.

Lowell, R.P., and Keller, S.M., 2003, High-temperature seafloor hydrothermal circulation over geologic time and Archean banded iron formations: Geophysical Research letters, v. 30, no. 7, article 1391, https://doi.org/10.1029/2002GL016536.

Ludden, J., and Hubert, C., 1986, The tectonic evolution of the Abitibi greenstone belt of Canada: Geology, v. 14, p. 707–711.

Ludden, J., Hubert, C., and Clement, G., 1986, Geological evolution of the Late Archean Abitibi greenstone belt of Canada: Geological Magazine, v. 123, no. 2, p. 153–166.

Lupton, J.E., Arculus, R.J., Resing, J., et al., 2012, Hydrothermal activity in the northwest Lau backarc basin: Evidence from water column measurements: Geochemistry Geophysics Geosystems, v. 13, no. 5, article Q0AF04, https://doi.org/10.1029/2011GC003891.

Lupton, J., Rubin, K.H., Arculus, R., et al., 2015, Helium isotope, C/3He, and Ba-Nb-Ti signatures in the northern Lau basin: Distinguishing arc, back-arc, and hotspot affinities: G-Cubed, v. 16, p. 1133–1155, https://doi.org/10.1002/2014GC005625.

MacLeod, S.J., Williams, S.E., Matthews, K.J., Müller, R.D., and Qin, X., 2017, A global review and digital database of large-scale extinct spreading centers: Geosphere, v. 13, p. 911–949, https://doi.org/10.1130/GES01379.1.

Mallard, C., Coltice, N., Seton, M., Müller, R.D., and Tackley, P.J., 2016, Subduction controls the distribution and fragmentation of Earth's tectonic plates: Nature, v. 535, p. 140–143, https://doi.org/10.1038/nature17992.

Mammerickx, J., and Klitgord, K.D., 1982, Northern East Pacific Rise: Evolution from 25 m.y. B.P. to the present: Journal of Geophysical Research, Solid Earth, v. 87, p. 6751–6759.

Martin, A.K., 2013, Double-saloon-door tectonics in the north Fiji basin: Earth and Planetary Science Letters, v. 374, p. 191–203.

Martin, H., and Pinti, D., 2011, Archean eon, *in* Encyclopedia of astrobiology: Berlin, Springer-Verlag, p. 61–69, https://doi.org/10.1007/978-3-642-11274-4.

Martinez, F., and Taylor, B., 2002, Mantle wedge control on back-arc crustal accretion: Nature, v. 416, p. 417–420, https://doi.org/10.1038/416417a.

Martinez, F., and Taylor, B., 2006, Modes of crustal accretion in back-arc basins: Inferences from the Lau basin: American Geophysical Union, Geophysical Monograph 166, p. 5–30, https://doi.org/10.1029/166GM03.

Martinez, F., Taylor, B., Baker, E.T., Resing, J.A., and Walker, S.L., 2006, Opposing trends in crustal thickness and spreading rate along the back-arc eastern Lau spreading center: Implications for controls on ridge morphology, faulting, and hydrothermal activity: Earth and Planetary Science Letters, v. 245, p. 655–672, https://doi.org/10.1016/j.epsl.2006.03.049.

Martinez, F., Stern, R.J., Kelley, K.A., et al., 2018, Diffuse extension of the southern Mariana margin: Journal of Geophysical Research, Solid Earth, v. 123, p. 892–916, https://doi.org/10.1002/2017JB014684.

Matthews, K.J., Müller, R.D., and Sandwell, D.T., 2016, Oceanic microplate formation records the onset of India-Eurasia collision: Earth and Planetary Science Letters, v. 433, p. 204–214.

Maus, S., Barckhausen, U., Berkenbosch, H., et al., 2009, EMAG2: A 2-arc min resolution Earth Magnetic Anomaly Grid compiled from satellite, airborne, and marine magnetic measurements: G-Cubed, v. 10, no. 8, article Q08005, https://doi.org/10.1029/2009GC002471.

McKenzie, D.P., and Morgan, W.J., 1969, Evolution of triple junctions: Nature, v. 224, no. 5215, p. 125–133, https://doi.org/10.1038/224125a0

McNicoll, V., Goutier, J., Dubé, B., et al., 2014, U-Pb Geochronology of the Blake River Group, Abitibi greenstone belt, Quebec, and implications for base metal exploration: Economic Geology, v. 109, p. 27–59.

Meffre, S., Falloon, T.J., Crawford, T.J., et al., 2012, Basalts erupted along the Tonga fore arc during subduction initiation: Evidence from geochronology of dredged rocks from the Tonga fore arc and trench: G-Cubed, v. 13, article Q12003, https://doi.org/10.1029/2012GC004335.

Mensing, R., 2019, The tectonic and volcanic evolution of the Mangatolu triple junction: Unpub. MSc thesis, Halle-Wittenberg, Germany, Martin Luther University, 78 p.

Mercier-Langevin, P., Gibson, H.L., Hannington, M., et al., 2014, Preface for a special issue on Archean magmatism, volcanism, and ore deposits - Part 2. Volcanogenic massive sulfide deposits: Economic Geology, v. 109. no. 1, p. 1–9.

Mercier-Langevin, P., Dubé, B., Houlé, M.G., et al., 2023, Chapter 2. Metallogeny of the Abitibi greenstone belt, Canada, *in* Decrée, S., ed., Metallic resources 2: Geodynamic framework and remarkable examples in the world: ISTE Ltd., Wiley, p. 63–41.

Merle, S., Resing, J., and Embley, R., 2013, Submarine Ring of Fire 2012 (SRoF-12) northeast Lau basin: R/V Roger Revelle Expedition RR1211, Sept 9–25, 2012, Suva Fiji to Apia Samoa: Washington, D.C., National Oceanic and Atmospheric Administration, 260 p., https://doi.org/10.7284/903953.

Michael, P.J., Escrig, S., Rubin, K.H., et al., 2009, Major and trace elements and volatiles in glasses from the 2009 rapid response expedition to West Mata volcano and northeast Lau spreading center (NELSC): American Geophysical Union, Fall Meeting, San Francisco, December 14–18, 2009, abstract V51D-1720.

Millen, D.W., and Hamburger, M.W., 1998, Seismological evidence for tearing of the Pacific plate at the northern termination of the Tonga subduction zone: Geology, v. 26, p. 659–662.

Mole, D.R., Fiorentini, M.L., Cassidy, K.F., et al., 2015, Crustal evolution, intra-cratonic architecture and the metallogeny of an Archaean craton: Geological Society of London, Special Publication 393, p. 23–80, https://doi.org/10.1144/SP393.8.

Mole, D., Thurston, P., Marsh, J., et al., 2021, The formation of Neoarchean continental crust in the south-east Superior craton by two distinct geodynamic processes: Precambrian Research, v. 356, https://doi.org/10.1016/j.precamres.2021.106104.

Mole, D.R., Frieman, B.M., Thurston, P.C., et al., 2022, Crustal architecture of the south-east Superior craton and controls on mineral systems: Ore Geology Reviews, v. 148, https://doi.org/10.1016/j.oregeorev.2022.105017.

Monecke, T., Mercier-Langevin, P., Dubé, B., Frieman, B., and Goutier, J., 2017a, Geology of the Abitibi greenstone belt: Reviews in Economic Geology, v. 19, p. 7–49.

Monecke, T., Gibson, H., and Goutier, J., 2017b, Volcanogenic massive sulfide deposits of the Noranda Camp: Reviews in Economic Geology, v. 19, p. 169–224.

Montsion, R., Thurston, R., and Ayer, J., 2018, 1:2,000,000 scale geological compilation of the Superior craton - version 1: Laurentian University,

Mineral Exploration Research Centre, Harquail School of Earth Sciences, document no. MERC-ME-2018-017, merc.laurentian.ca/research/metal-earth/superior-compilation.

Moresi, L., Betts, P.G., Miller, M.S., and Cayley, R.A., 2014, Dynamics of continental accretion: Nature, v. 508, p. 245–249, https://doi.org/10.1038/nature13033.

Morra, G., Seton, M., Quevedo, L., and Müller, R.D., 2013, Organization of the tectonic plates in the last 200 Myr: Earth and Planetary Science Letters, v. 373, p. 93–101, https://doi.org/10.1016/j.epsl.2013.04.020.

Mortimer, N., Campbell, H.J., Tulloch, A.J., et al., 2017, Zealandia: Earth's hidden continent: GSA Today, v. 27, no. 3, p. 27–35, https://doi.org/10.1130/GSATG321A.1.

Mosier, D.L., Berger, V.I., and Singer, D.A., 2009, Volcanogenic massive sulfide deposits of the world; Database and grade and tonnage models: U.S. Geological Survey, Open-File Report 2009-1034, 50 p., http://pubs.usgs.gov/of/2009/1034/.

Mueller, R.D., Gaina, C., Roest, W., and Lundbeck, D., 2001, A recipe for microcontinent formation: Geology, v. 29, no. 3, p. 203–206.

Mueller, R.D., Qin, X., Sandwell, D.T., et al., 2016, The GPlates Portal: Cloud-based interactive 3D visualization of global geophysical and geological data in a web browser: PLOS ONE, v. 11, no. 3, e0150883, https://doi.org/10.1371/journal.pone.0150883.

Nebel, O., and Arculus, R.J., 2015, Selective ingress of a Samoan plume component into the northern Lau backarc basin: Nature Communications v. 6, article 6554.

O'Neill, C., Lenardic, A., Moresi, L., Torsvik, T.H., and Lee, C.T.A, 2007, Episodic Precambrian subduction: Earth and Planetary Science Letters, v. 262, p. 552–562.

Parson, L.M., and Hawkins, J.W., 1994, Two-stage propagation and the geological history of the Lau backarc basin, *in* Hawkins, J.W., Parson, L.M., Allan, J.F., et al., 1994, Proceedings of the Ocean Drilling Program, Scientific Results, v. 135: College Station, Texas, Ocean Drilling Program, p. 819–828, https://doi.org/10.2973/odp.proc.sr.135.153.1994.

Parson, L.M., and Tiffin, D.L., 1993, Northern Lau basin: Backarc extension at the leading edge of the Indo-Australian Plate: Geo-Marine Letters, v. 13, p. 107–115, https://doi.org/10.1007/BF01204552.

Parson, L.M., and Wright, I.C., 1996, The Lau-Havre-Taupo back-arc basin: A southward-propagating, multi-stage evolution from rifting to spreading: Tectonophysics, v. 263, p. 1–22, https://doi.org/10.1016/S0040-1951(96)00029-7.

Parson, L.M., Pearce, J.A., Murton, B.J., et al., 1990, Role of ridge jumps and ridge propagation in the tectonic evolution of the Lau back-arc basin, southwest Pacific: Geology, v. 18, p. 470–473.

Parson, L., Hawkins, J., and Allan, J., and Shipboard Scientific Party, 1992a, Introduction, background, and principal results of Leg 135, Lau basin, *in* Parson, L., Hawkins, J., Allan, J., et al., 1992, Proceedings of the Oceanic Drilling Program, initial reports, v. 135: College Station, Texas, Ocean Drilling Program, p. 5–47, https://doi.org/10.2973/odp.proc.ir.135.101.1992.

Parson, L.M., Hawkins, J.W., and Hunter, P.M., 1992b, Morphotectonics of the Lau basin seafloor— implications for the opening history of back-arc basins, *in* Parson, L., Hawkins, J., Allan, J., et al., 1992, Proceedings of the Oceanic Drilling Program, initial reports, v. 135: College Station, Texas, Ocean Drilling Program, p. 81–82, https://doi.org/10.2973/odp.proc.ir.135.103.1992.

Parson, L.M., Rothwell, R.G., and MacLeod, C.J., 1994, Tectonics and sedimentation in the Lau basin (southwest Pacific), *in* Hawkins, J.W., Parson, L.M., Allan, J.F., et al., 1994, Proceedings of the Ocean Drilling Program, Scientific Results, v. 135: College Station, Texas, Ocean Drilling Program, p. 9–21, https://doi.org/10.2973/odp.proc.sr.135.111.1994.

Patriat, M., Collot, J., Danyushevsky, L., et al., 2015, Propagation of back-arc extension into the arc lithosphere in the southern New Hebrides volcanic arc: G-Cubed, no. 16, p. 3142–3159, https://doi.org/10.1002/2015GC005717.

Pearce, J.A., Ernewein, M., Bloomer, S.H., et al., 1995, Geochemistry of Lau basin volcanic rocks: Influence of ridge segmentation and arc proximity: Geological Society of London, Special Publication 81, p. 53–75, https://doi.org/10.1144/GSL.SP.1994.081.01.04.

Pearson, D.G., Parman, S.W., and Nowell, G.M., 2007, A link between large mantle melting events and continent growth seen in osmium isotopes: Nature, v. 449, p. 202–205, https://doi.org/10.1038 /nature06122.

Pelletier, B., Calmant, S., and Pillet, R., 1998, Current tectonics of the Tonga-New Hebrides region: Earth and Planetary Science Letters, v. 164, p. 263–276, https://doi.org/10.1016/S0012-821X(98)00212-X.

Pelletier, B., Lagabrielle, Y., Benoit, M., et al., 2001, Newly identified segments of the Pacific-Australia plate boundary along the north Fiji transform zone: Earth and Planetary Science Letters, v. 193, p. 347–358, https://doi.org/10.1016/S0012-821X(01)00522-2.

Percival, J.A., 2007, Geology and metallogeny of the Superior province, Canada: Geological Association of Canada, Mineral Deposits Division, Special Publication 5, p. 903–928.

Percival, J.A., Skulski, T., Sanborn-Barrie, M., et al., 2012, Geology and tectonic evolution of the Superior province, Canada: Geological Association of Canada, Special Paper 49, p. 321–378.

Polat, A., Kerrich, R., and Wyman, D.A., 1998, The late Archean Schreiber-Hemlo and White River-Dayohessarah greenstone belts, Superior province: Collages of oceanic plateaus, oceanic arcs, and subduction-accretion complexes: Tectonophysics, v. 289, 295–326.

Poulsen, K.H., Card, K.D., and Franklin, J.M., 1992, Archean tectonic and metallogenic evolution of the Superior province of the Canadian Shield: Precambrian Research, v. 58, p. 25–54.

Powell, W.G., Carmichael, D.M., and Hodgson, C.J., 1995, Conditions and timing of metamorphism in the southern Abitibi greenstone belt, Quebec: Canadian Journal of Earth Sciences, v. 32, p. 787–805.

Ratcliff, J.T., Bercovici, D., Schubert, G., and Kroenke, L.W., 1998, Mantle plume heads and the initiation of plate tectonic reorganizations: Earth and Planetary Science Letters, v. 156, p. 195–207.

Regelous, M., Turner, S., Falloon, T.J., et al., 2008, Mantle dynamics and mantle melting beneath Niuafo'ou Island and the northern Lau back-arc basin: Contributions to Mineralogy and Petrology, v. 156, p. 103–118, https://doi.org/10.1007/s00410-007-0276-7.

Regelous, M., Haase, K.M., Freund, S., et al., 2014, Formation of the Troodos Ophiolite at a triple junction: Evidence from trace elements in volcanic glass: Chemical Geology, v. 386, p. 66–79, https://doi.org/10.1016/j.chemgeo.2014.08.006.

Resing, J.A., Rubin, K.H., Embley, R.W., et al., 2011, Active submarine eruption of boninite in the northeastern Lau basin: Nature Geoscience, v. 4, p. 799–806, https://doi.org/10.1038/NGEO1275.

Rey, P.F., and Mueller, R.D., 2010, Fragmentation of active continental plate margins owing to the buoyancy of the mantle wedge: Nature Geoscience, v. 3, p. 257–261.

Rowland, J.V., and Simmons, S.F., 2012, Hydrologic, magmatic, and tectonic controls on hydrothermal flow, Taupo volcanic zone, New Zealand: Implications for the formation of epithermal vein deposits: Economic Geology, v. 107, no. 3, p. 427–457, https://doi.org/10.2113/econgeo.107.3.427.

Rowland, J.V., Bardsley, C., Downs, D., et al., 2012, Tectonic controls on hydrothermal fluid flow in a rifting and migrating arc, Taupo volcanic zone, New Zealand: New Zealand Geothermal Workshop, November 19–21, 2012, Auckland, New Zealand, Proceedings, 17 p.

Ruellan, E., and Lagabrielle, Y., 2005, Subductions et ouvertures océaniques dans le Sud-Ouest Pacifique: Géomorphologie, Relief, Processus, Environnement, v. 11, p. 121–142, https://doi.org/10.4000/geomorphologie.307.

Ruellan, E., Delteil, J., Wright, I., and Matsumoto, T., 2003, From rifting to active spreading in the Lau basin-Havre Trough backarc system (SW Pacific): Locking/unlocking induced by seamount chain subduction: G-Cubed, v. 4, article 8909, https://doi.org/10.1029/2001GC000261.

Ryan, M., 2023, The origin and evolution of active spreading segments in the northwest Lau basin: Unpub, MSc thesis, University of Ottawa, Canada, 105 p.

Ryan, W.B.F., Carbotte, S.M., Coplan, J.O., et al., 2009, Global multi-resolution topography synthesis (GMRT version 3.6): G-Cubed, v. 10, no. 3, article Q03014, https://doi.org/10.1029/2008GC002332.

Sandwell, D.T., Müller, R.D., Smith, W.H.F., Garcia, E., and Francis, R., 2014, New global marine gravity model from CryoSat-2 and Jason-1 reveals buried tectonic structure: Science, v. 346, p. 65–67, https://doi.org/10.1126/science.1258213.

Sato, T., No, T., Kodaira, S., Takahashi, N., and Kaneda, Y., 2014, Seismic constraints of the formation process on the back-arc basin in the southeastern Japan Sea: Journal of Geophysical Research: Solid Earth, v. 119, p. 1563–1579, https://doi.org/10.1002/2013JB010643.

Sawkins, F.J., 1984, Metal deposits in relation to plate tectonics: Minerals and rocks, v. 17: Berlin, Springer, 328 p.

Sawkins, F.J., 1990, Integrated tectonic-genetic model for volcanic-hosted massive sulfide deposits: Geology, v. 18, no. 11, p. 1061–1064.

Scheibner, E., Moore, G.W., Drummond, K.J., et al., 2013, Tectonic map of the circum-Pacific region, Pacific basin sheet: U.S. Geological Survey Circum-Pacific Map CP-52, pamphlet 134 p., 2 sheets, scale 1:17,000,000, and GIS data, pubs.usgs.gov/cp/52/.

Schellart, W.P., and Lister, G.S., 2004, Tectonic models for the formation of arc-shaped convergent zones and backarc basins: Geological Society of America, Special Paper 383, p. 237–258.

Schellart, W.P., Lister, G.S., and Toy, V.G., 2006, A Late Cretaceous and Cenozoic reconstruction of the southwest Pacific region: Tectonics controlled by subduction and slab rollback processes: Earth-Science Reviews, v. 76, p. 191–233, https://doi.org/10.1016/j.earscirev.2006.01.002.

Schmid, F., Kopp, H., Schnabel, M., et al., 2020, Crustal structure and evolution of the Niuafo'ou Microplate in the northeastern Lau basin, southwestern Pacific: Journal of Geophysical Research, Solid Earth, v. 125, article e2019JB019184, https://doi.org/10.1029/2019JB019184.

Schmid, F., Cremanns, M., Augustin, N., et al., 2021, Microseismicity and lava flows hint at magmato-tectonic processes near the southern tip of the Fonualei Rift and spreading center in the Lau basin: Journal of Geophysical Research, Solid Earth, v. 126, article e2020JB021340, https://doi.org/10.1029/2020JB021340.

Schnabel, M., Kopp, H., and Shipboard Scientific Party, 2019, Multichannel seismics operations and equipment, *in* Hannington, M.D., Kopp, H., and Schnabel, M., eds., FS Sonne cruise report SO267: ARCHIMEDES I: GEOMAR Helmholtz-Zentrum für Ozeanforschung, GEOMAR Report N. Ser. 049, 275 p., https://doi.org/10.3289/GEOMAR_REP_NS_49_2019.

Schnabel, M., Engels, M., Schramm, B., et al., 2022, Relationship between saucer-shaped igneous sills and sedimentary layers: An example from the Tofua volcanic arc: Status Conference of German Research Vessels, ICBM/University of Oldenburg, February 22–23, 2022, Proceedings, Status_Conference_Research_Vessels_2022_Conference_Transcript.pdf

Searle, R.C., and Escartin, J., 2013, The rheology and morphology of oceanic lithosphere and mid-ocean ridges: American Geophysical Union, Geophysical Monograph 148, p. 63–93, https://doi.org/10.1029/148GM03.

Seton, M., Müller, R.D., Zahirovic, S., et al., 2012, Global continental and ocean basin reconstructions since 200 Ma: Earth-Science Reviews, v. 113, no. 3–4, p. 212–270, https://doi.org/10.1016/j.earscirev.2012.03.002.

Seton, M., Müller, R.D., Zahirovic, S., et al., 2020, A global data set of present-day oceanic crustal age and seafloor spreading parameters: G-Cubed, v. 21, article e2020GC00921, https://doi.org/10.1029/2020GC009214.

Shibuya, T., Kitajima, K., Komiya, T., Terabayashi, M., and Maruyama, S., 2007, Middle Archean ocean ridge hydrothermal metamorphism and alteration recorded in the Cleaverville area, Pilbara craton, Western Australia: Journal of Metamorphic Geology, v. 25, p. 751–767.

Siddoway, C., 2010, Mircoplate motion: Nature Geoscience, v. 3, p. 225–226.

Sillitoe, R.H., 2010, Porphyry copper systems: Economic Geology, v. 105, p. 3–41.

Sleeper, J.D., and Martinez, F., 2014, Controls on segmentation and morphology along the backarc eastern Lau spreading center and Valu Fa ridge: Journal of Geophysical Research, Solid Earth, v. 119, p. 1678–1700, https://doi.org/10.1002/2013JB010545.

Sleeper, J.D., and Martinez, F., 2016, Geology and kinematics of the Niuafo'ou microplate in the northern Lau basin: Journal of Geophysical Research, Solid Earth, v. 121, p. 4852–4875, https://doi.org/10.1002/2016JB013051.

Sleeper, J.D., Martinez, F., and Arculus, R., 2016, The Fonualei rift and spreading center: Effects of ultraslow spreading and arc proximity on backarc crustal accretion: Journal of Geophysical Research, Solid Earth, v. 121, p. 4814–4835, https://doi.org/10.1002/2016JB013050.

Smith, G.P., Wiens, D.A., Fischer, K.M., et al., 2001, A complex pattern of mantle flow in the Lau backarc: Science, v. 292, p. 713–716.

Smith, R.S., Naghizadeh, M., Cheraghi, S., et al., 2023, Geophysical transects in the Abitibi greenstone belt of Canada from the mineral-exploration-oriented Metal Earth project: Society of Exploration Geophysicists, The Leading Edge, April 2023, p. 245–55, https://doi.org/10.1190/tle42040245.1.

Smith, W.H.F., and Sandwell, D.T., 1997, Global sea floor topography from satellite altimetry and ship depth soundings: Science, v. 277, p. 1956–1962, https://doi.org/10.1126/science.277.5334.1956.

Snyder, D.B., Bleeker, W., Reed, L.E., et al., 2008, Tectonic and metallogenic implications of regional seismic profiles in the Timmins Mining Camp: Economic Geology, v. 103, p. 1135–1150, https://doi.org/10.2113/gsecongeo.103.6.1135.

Snyder, D.B., Savard, G., Kjarsgaard, B.A., et al., 2021, Multidisciplinary modelling of mantle lithosphere structure within the Superior craton, North America: G-Cubed, v. 22, no. 4, article e2020GC009566, https://doi.org/10.1029/2020GC009566.

Stein, M., and Hofmann, A.W., 1994, Mantle plumes and episodic crustal growth: Nature, v. 372, p. 63–68, https://doi.org/10 .1038 /372063a0.

Stern, R.J., Smoot, N.C., and Rubin, M., 1984, Unzipping of the volcano arc, Japan: Tectonophysics, v. 102, p. 153–174, https://doi.org/10.1016/0040-1951(84)90012-X.

Stern, R.J., Tamura, Y., Masuda, H., et al., 2013, How the Mariana volcanic arc ends in the south: Island Arc, v. 22, p. 133–148.

Stewart, M.S., Hannington, M.D., Emberley, J., et al., 2022, A new geological map of the Lau basin reveals crustal growth processes in arc-backarc systems: Geological Society of America, Geosphere, v. 17, https://doi.org/10.1130/GES02340.1.

Stoffers, P., Worthington, T., Schwarz, U., et al., 2006, Submarine volcanoes and high-temperature hydrothermal venting on the Tonga Island arc, S.W. Pacific: Geology, v. 34, no. 6, p. 453–456.

Szitkar, F., Dyment, J., and Fouquet, Y., 2020, Widespread volcanism southeast of Futuna Island (SW Pacific Ocean): Near-seafloor magnetic dating and regional consequences: Journal of Volcanology and Geothermal Research, v. 406, article 107064, https://doi.org/10.1016/j.jvolgeores.2020.1070640377-0273.

Takahashi, N., Kodaira, S., Tatsumi, Y., Kaneda, Y., and Suyehiro, K., 2008, Structure and growth of the Izu-Bonin-Mariana arc crust: 1. Seismic constraint on crust and mantle structure of the Mariana arc-back-arc system: Journal of Geophysical Research, Solid Earth, v. 113, B01104, https://doi.org/10.1029/2007JB005120.

Tamura, Y., Gill, J.B., Tollstrup, D., et al., 2009, Silicic magmas in the Izu-Bonin oceanic arc and implications for crustal evolution: Journal of Petrology, v. 50, no. 4, p. 685–723, https://doi.org/10.1093/petrology/egp017.

Tappin, D.R., Bruns, T.R., and Geist, E.L., 1994, Rifting of the Tonga/Lau Ridge and formation of the Lau backarc basin: Evidence from Site 840 on the Tonga Ridge, *in* Hawkins, J.W., Parson, L.M., Allan, J.F., et al., 1994, Proceedings of the Ocean Drilling Program, Scientific Results, v. 135: College Station, Texas, Ocean Drilling Program, p. 367–371, https://doi.org/10.2973/odp.proc.sr.135.163.1994.

Taylor, B., Zellmer, K., Martinez, F., and Goodliffe, A., 1996, Sea-floor spreading in the Lau backarc basin: Earth and Planetary Science Letters, v. 144, p. 35–40, https://doi.org/10.1016/0012-821X(96)00148-3.

Taylor, G.K., Gascoyne, J., and Colley, H., 2000, Rapid rotation of Fiji: Paleomagnetic evidence and tectonic implications: Journal of Geophysical Research, Solid Earth, v. 105, p. 5771–5781, https://doi.org/10.1029/1999JB900305.

Terabayashi, M., Masada, Y., and Ozawa, H., 2003, Archean ocean-floor metamorphism in the North Pole area, Pilbara craton, Western Australia: Precambrian Research, v. 127, nos. 1–3, p. 167–180.

Thorkelson, D.J., 1996, Subduction of diverging plates and the principles of slab window formation: Tectonophysics, v. 255, p. 47–63, https://doi.org/10.1016/0040-1951(95)00106-9.

Thurston, P.C., 2002, Autochthonous development of Superior province greenstone belts?: Precambrian Research, v. 115, p. 11–36.

Thurston, P.C., 2015, Igneous rock associations 19. Greenstone belts and granite-greenstone terranes: Constraints on the nature of the Archean world: Geoscience Canada, v. 42, p. 437–484, https://doi.org/10.12789/geocanj.2015.42.081.

Thurston, P.C., Williams, H.R., Sutcliffe, R.H., and Stott, G.M., eds., 1992a, Geology of Ontario, special volume 4, part 2: Ontario Geological Survey, Ministry of Northern Development and Mines, 683 p.

Thurston, P.C., Osmani, I.A., and Stone, D., 1992b, Northwestern Superior province: Review and terrane analysis, *in* Thurston et al., eds., Geology of Ontario, special volume 4, part 2: Ontario Geological Survey, Ministry of Northern Development and Mines, p. 81–144.

Thurston, P.C., Ayer, J.A., Goutier, J., and Hamilton, M.A., 2008, Depositional gaps in Abitibi greenstone belt stratigraphy: A key to exploration for syngenetic mineralization: Economic Geology, v. 103, p. 1097–1134, https://doi.org/10.2113/gsecongeo.103.6.1097.

Turner, I.M., Peirce, C., and Sinha, M.C., 1999, Seismic imaging of the axial region of the Valu Fa ridge, Lau basin—The accretionary processes of an intermediate back-arc spreading ridge: Geophysical Journal International, v. 138, p. 495–519, https://doi.org/10.1046/j.1365-246X.1999.00883.x.

Turner, S., and Hawkesworth, C., 1998, Using geochemistry to map mantle flow beneath the Lau basin: Geology, v. 26, p. 1019–1022.

Van Kranendonk, M.J., Hickman, H., Smithies, R.H., Nelson, D.R., and Pike G., 2002, Geology and tectonic evolution of the Archean North Pilbara terrain, Pilbara craton, Western Australia: Economic Geology, v. 97, p. 695–732, https://doi.org/10.2113/gsecongeo.97.4.695.

Vite-Sánchez, O., Ross, P.-S., and Mercier-Langevin, P., 2024, Mafic to intermediate volcanic rocks of the Blake River Group, Abitibi greenstone

belt, Canada: Geochemistry, petrogenesis and relation with VMS deposits: Precambrian Research, v. 404, article 107331, https://doi.org/10.1016/j.precamres.2024.107331.
Voice, P.J., Kowalewski, M., and Eriksson, K.A., 2011, Quantifying the timing and rate of crustal evolution: Global compilation of radiometrically dated detrital zircon grains: The Journal of Geology, v. 119, p. 109–126, https://doi.org/10.1086 /658295.
Volpe, A.M., MacDougall, J.D., and Hawkins, J.W., 1988, Lau basin basalts (LBB): Trace element and Sr-Nd isotopic evidence for heterogeneity in backarc basin mantle: Earth and Planetary Science Letters, v. 90, p. 174–186, https://doi.org/10.1016/0012-821X(88)90099-4.
Von Stackelberg, U., and Shipboard Scientific Party, 1985, FS Sonne cruise report SO35, Back-arc hydrothermalism SW-PAC: Hannover, Bundesanstalt für Geowissenschaften und Rohstoffe, 109 p.
Von Stackelberg, U., and Shipboard Scientific Party, 1987, FS Sonne cruise report SO48, Lau basin hydrothermalism: Hannover, Bundesanstalt für Geowissenschaften und Rohstoffe, 122 p.
Von Stackelberg, U., and Shipboard Scientific Party, 1990, FS Sonne cruise report SO67/2, Geoscientific investigations in the Lau basin (southwest Pacific Ocean): Hannover, Bundesanstalt für Geowissenschaften und Rohstoffe, 132 p.
Wallace, L.M., McCaffrey, R., Beavan, J., and Ellis, S., 2005, Rapid microplate rotations and backarc rifting at the transition between collision and subduction: Geology, v. 33, no. 11, p. 847–860, https://doi.org/10.1130/G21834.1.
Wallace, L.M., Ellis, S., and Mann, P., 2009, Collisional model for rapid fore-arc block rotations, arc curvature, and episodic back-arc rifting in subduction settings: G-Cubed, v. 10, articleQ05001, https://doi.org/10.1029/2008GC002220.
Wei, S.S., and Wiens, D.A., 2018, P-wave attenuation structure of the Lau back-arc basin and implications for mantle wedge processes: Earth and Planetary Science Letters, v. 502, p. 187–199, https://doi.org/10.1016/j.epsl.2018.09.005
Wetzel, L.R., Wiens, D.A., and Kleinrock, M.C., 1993, Evidence from earthquakes for bookshelf faulting at large non-transform ridge offsets: Nature, v. 362, p. 235–237, https://doi.org/10.1038/362235a0.
Wiens, D.A., Kelley, K.A., and Plank, T., 2006, Mantle temperature variations beneath back-arc spreading centers inferred from seismology, petrology, and bathymetry: Earth and Planetary Science Letters, v. 248, p. 30–42, https://doi.org/10.1016/j.epsl.2006.04.011
Wilkinson, B.H., and Kesler, S.E., 2009, Quantitative identification of metallogenic epochs and provinces: Economic Geology, v. 104, p. 607–623.
Wyman, D.A., 2013, A critical assessment of Neoarchean "plume only" geodynamics: Evidence from the Superior province: Precambrian Research, v. 229, p. 3–19, https://doi.org/10.1016/j.precamres.2012.01.010.
Wyman, D.A., 2018, Do cratons preserve evidence of stagnant lid tectonics?: Geoscience Frontiers, v. 9, p. 3–17, https://doi.org/10.1016/j.gsf.2017.02.001.
Wyman, D.A., Kerrich, R., Polat, A., 2002, Assembly of Archean cratonic mantle lithosphere and crust: Plume-arc interaction in the Abitibi-Wawa subduction accretion complex: Precambrian Research, v. 115, p. 37–62.
Zellmer, K.E., and Taylor, B., 2001, A three-plate kinematic model for Lau Basin opening: G-Cubed, v. 2, no. 5, article 1020, https://doi.org/10.1029/2000GC000106.
Zellmer, G.F., Annen, C., Charlier, B.L.A., et al., 2005, Magma evolution and ascent at volcanic arcs: Constraining petrogenetic processes through rates and chronologies: Journal of Volcanology and Geothermal Research, v. 140, p. 171–191, https://doi.org/10.1016/j.jvolgeores.2004.07.020.
Zhao, D., Xu, Y., Wiens, D.A., et al., 1997, Depth extent of the Lau back-arc spreading center and its relation to subduction processes: Science, v. 278, p. 254–257, https://doi.org/10.1126/science.278.5336.254.
Zhao, D., Maruyama, S., and Omori, S., 2007, Mantle dynamics of western Pacific and east Asia: Insight from seismic tomography and mineral physics: Gondwana Research, v. 11, p. 120–131, https://doi.org/10.1016/j.gr.2006.06.006.

Mark Hannington is a professor of economic geology at the University of Ottawa and former head of marine mineral resources at the GEOMAR Helmholtz Center for Ocean Research in Kiel, Germany. He obtained his PhD at the University of Toronto (1989) and spent 15 years as a research scientist in the Mineral Deposits Division of the Geological Survey of Canada before moving to the University of Ottawa in 2005. His research combines the study of active volcanoes on the ocean floor with ancient volcanic environments that host volcanogenic massive sulfide (VMS) deposits. He has participated on 30 research cruises and has conducted major research projects on VMS systems, including the giant Kidd Creek deposit and regional-scale hydrothermal alteration in the Noranda district. Mark was editor of the journal *Economic Geology* from 2001 to 2008.